Doctoral Dissertations   Graduate School

Spring 2000

Computational investigation of stress, contact conditions, and buckling of thin-walled pipe liners

Meihuan Zhu
Louisiana Tech University

Recommended Citation

INFORMATION TO USERS

This manuscript has been reproduced from the microfilm master. UMI films the text directly from the original or copy submitted. Thus, some thesis and dissertation copies are in typewriter face, while others may be from any type of computer printer.

The quality of this reproduction is dependent upon the quality of the copy submitted. Broken or indistinct print, colored or poor quality illustrations and photographs, print bleedthrough, substandard margins, and improper alignment can adversely affect reproduction.

In the unlikely event that the author did not send UMI a complete manuscript and there are missing pages, these will be noted. Also, if unauthorized copyright material had to be removed, a note will indicate the deletion.

Oversize materials (e.g., maps, drawings, charts) are reproduced by sectioning the original, beginning at the upper left-hand corner and continuing from left to right in equal sections with small overlaps.

Photographs included in the original manuscript have been reproduced xerographically in this copy. Higher quality 6" x 9" black and white photographic prints are available for any photographs or illustrations appearing in this copy for an additional charge. Contact UMI directly to order.

UMI®

COMPUTATIONAL INVESTIGATION OF STRESS, CONTACT CONDITIONS, AND BUCKLING OF THIN-WALLED PIPE LINERS

by

Meihuan Zhu

A Dissertation Presented in Partial Fulfillment
of the Requirements for the Degree
Doctor of Philosophy

COLLEGE OF ENGINEERING AND SCIENCE
LOUISIANA TECH UNIVERSITY

May 2000

UMI Number: 9963601

UMI®

LOUISIANA TECH UNIVERSITY

THE GRADUATE SCHOOL

<u>May 8, 2000</u>
Date

We hereby recommend that the dissertation prepared under our supervision by____Meihuan Zhu

entitled____COMPUTATIONAL INVESTIGATION OF STRESS, CONTACT CONDITIONS, AND

BUCKLING OF THIN-WALLED PIPE LINERS

be accepted in partial fulfillment of the requirements for the Degree of Ph.D. in

Engineering
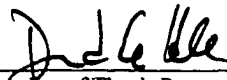
Supervisor of Thesis Research

Head of Department

Civil Engineering
Department

Recommendation concurred in:

Advisory Committee
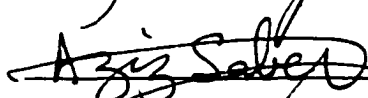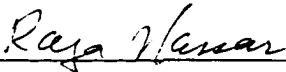
Approved:

Director of Graduate Studies

Approved:

Dean of the Graduate School

Dean of the College

GS Form 13
(1/00)

ABSTRACT

Thin walled polymeric liners are often used to rehabilitate deteriorated pipe lines. The host pipes into which these liners are installed are typically assumed to be structurally sound, and the liner is only expected to carry the external pressure exerted by the groundwater. This external pressure will induce creep deformation and radial deflections that may eventually result in collapse of the liner within the host pipe. The aim of this work is use computational modeling to better understand the evolution of conditions leading up to collapse so that improved liner design models can be developed. Emphasis is placed on a close examination of the contact forces, contact areas, displacements and stresses for short-term and long-term liner buckling. The contact force is seen to enhance the buckling resistance of the liners by inducing a reverse moment which decreases the deflections and stresses at the critical point in the liner. For pressure levels less than 30% of the critical pressure. the stresses at the critical point in the liner are dominated by compression. indicating that compressive material properties are most appropriate for liner design. The formation of inverse curvature at the liner buckling lobes indicates that failure is imminent, since the rate of stress relaxation can no longer keep pace with the rate of stress increase due to increasing curvature and deflections at the critical point. The liner tends to perform more like a beam rather than an arch after inverse curvature has occurred. The value of the applied pressure and the creep properties of the material are seen to have a tremendous effect on the expected lifetime of liner

systems. An improved short-term liner buckling model is developed that accounts for all of the couplings between the liner to host pipe gap, the diameter to thickness ratio, host-pipe ovality, and local intrusion imperfections. Three-dimensional finite element models are used to show that the critical length to diameter ratio for specimens used in liner buckling experiments around five. Finally, the effect of multiple local imperfections on the deformation history, short-term buckling pressures, and long-term buckling times are explored using an improved two-dimensional finite element model in which asymmetric deformation modes are permitted, allowing the liners to buckle in a natural way. These results indicate that any variations in material or geometrical parameters that induce scatter in short-term liner buckling tests are expected to induce much more scatter in long-term tests.

APPROVAL FOR SCHOLARLY DISSEMINATION

The author grants to the Prescott Memorial Library of Louisiana Tech University the right to reproduce, by appropriate methods, upon request, any or all portions of this Thesis. It is understood that "proper request" consists of the agreement, on the part of the requesting party, that said reproduction is for his personal use and that subsequent reproduction will not occur without written approval of the author of this Thesis. Further, any portions of the Thesis used in books, papers, and other works must be appropriately referenced to this Thesis.

Finally, the author of this Thesis reserves the right to publish freely, in the literature, at any time, any or all portions of this Thesis.

Author _Meihuan Zhu_

Date _May 16, 2000_

TABLE OF CONTENTS

LIST OF TABLES

LIST OF FIGURES

xv

ACKNOWLEDGMENTS

It was my privilege to work under the guidance of Dr. Hall. I express my gratitude for his expert guidance, generous financial support, and inspiring discussions during my graduate studies. Thanks are also given for his extended office hours and patience in correcting the manuscript of this dissertation. Also, I would like to thank Dr. Guice, Dr. Nassar, Dr. Saber, and Dr. Sterling for their support, encouragement. and service on my advisory committee. This acknowledgment could not be complete without acknowledging the financial support and assistance of the College of Engineering and Science, the State of Louisiana under Grant Number LEQSF (1995-98), Insituform Technologies, and the National Science Foundation through grant No. CMS-9872378.

I dedicate this thesis to my husband whose understanding, encouragement and support have made this work possible. Finally, the most thanks goes to my parents for their endless love and encouragement for making this work possible.

CHAPTER 1

INTRODUCTION

1.1   Pipeline Rehabilitation

Until recently, the common method of repairing deteriorated sewer pipelines was the open-trench method that often caused significant disruption of service, property damage, and inconvenience to the public. In recent years, however, the relining of deteriorated host pipes with polymeric liners has become increasingly popular. Cured-In-Place Pipe (CIPP) and Fold-and-Form Pipe (FFP) are two of the most popular relining methods. Such liners are often installed in structurally sound host pipes that lie below the water table and are consequently subjected to external hydrostatic pressure. This external pressure causes radial deflections of the liner within the host pipe, and as time passes, the inward radial deflections may reach critical levels resulting in the collapse of the liner within the host pipe. To prevent liner collapse, the thickness of a liner system must be chosen to resist this external pressure over the design lifetime of the liner system, which is most often taken as 50 years.

1.2   Background and Research Need

As a liner deforms, it will typically form two opposing lobes where the inward radial deflections are relatively large. Outward deflections at approximately 90° to the

1

lobes will also occur resulting in liner-host pipe contact, with the contact area increasing with pressure and time. Although it is well known that this contact between the liner and the host pipe greatly improves the collapse resistance of the liner, the details of the contact areas and forces associated with this support are not well understood.

The external pressure acting on the cylindrical pipe liner will give rise to a compressive hoop stress. Any deflection of the liner-whether due to prior bending, initial imperfection or load eccentricity-will cause an increase in the bending moment due to this compressive stress. As time passes, the effect of initial imperfections on the deflection and flexural stress will be amplified, resulting in liner buckling at a time which may be significantly less than the buckling time for a "perfect" liner. Understanding the effect of imperfections on liner deflection and stress evolution will allow designers to better anticipate potential problem areas and specify more reliable liner systems.

The variation of radial displacements around the circumference of the liner and the presence of liner-host pipe contact are accompanied by a corresponding variation in the stresses around the liner. The highest stresses that eventually develop as the pressure or time is increased occur at the lobes. After inverse curvature (Figure 1.1) occurs at a lobe, the flexural stress generally becomes dominant to compressive stress. The effect of the contact will restrain the flexural stress in the liner, especially when a region of inverse curvature has not formed. Since the flexural creep compliance of most polymeric materials is significantly greater than the compressive creep compliance, it is desirable to avoid the formation of inverse curvature during the design lifetime so that flexural stresses do not become highly dominant.

2

a. No inverse curvature formed   b.   Inverse curvature formed
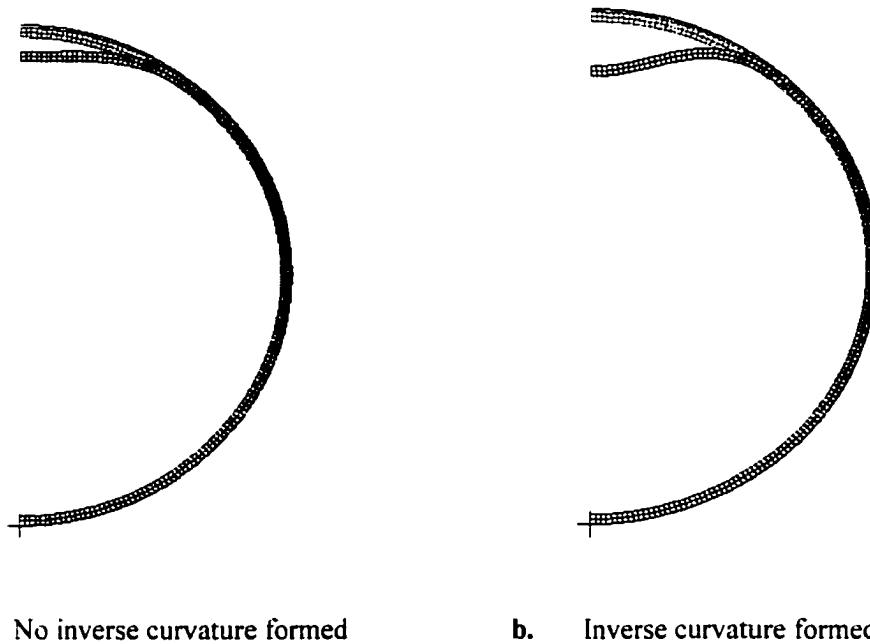
Figure 1.1   Definition of Inverse Curvature

Although creep-induced buckling has been observed to share numerous similarities with instantaneous buckling, including the identical buckling modes, it is still very necessary to study the deflection and stress evolution in both short-term and long-term cases. The nature and relative magnitudes of the stresses have important implications for liner material development and shed light on the choice of the appropriate material properties to use for liner analysis and design calculations.

The CIPP technique for pipeline rehabilitation was developed in the United Kingdom in the early 1970s and was transferred to the United States in the late 1970s. Current design practices for liners installed in structurally sound host pipes are guided by ASTM Designation F1216-93 which is based on the buckling equation for an unconstrained ring:

$$P = \frac{2KE_L}{(1-v^2)} \frac{1}{(SDR-1)^3} \frac{C}{N}$$

(1.1)

3

where P is the groundwater pressure applied over the service life, v is Poisson's ratio, SDR is the ratio of the outer diameter of the liner to the liner thickness, C is a reduction factor to account for host pipe ovality, and N is the factor of safety. The factor K is an enhancement factor to account for the increase in the buckling pressure due to the support provided by the host pipe, and a value no less than 7.0 is recommended for design purposes (Aggarwal and Cooper, 1984). Because creep deformation of the polymeric lining material may cause buckling at a pressure significantly lower than the critical short-term buckling pressure, a long-term modulus, E_L, is used in Equation (1.1). This modulus is typically taken as half the short-term flexural modulus of the liner material.

Since the basis of the ASTM F1216 design equation is a <u>short-term</u> buckling model for an <u>unconstrained</u> pipe, it is seen by many in the industry as an overly conservative equation that has been "patched up" to account for host pipe constraint and the effects of creep deformation. Moreover, the equation provides no means to account for local imperfections in the host pipe or for a gap between the host pipe and its liner. There are also questions about the validity of the ovality correction factor C. Finding improved design models for tight-fitting lining systems that produce safe and economical designs has been recognized as an important and challenging problem faced by the pipeline rehabilitation industry.

1.3 Objectives and Scope

The primary objectives of the proposed work are to develop an improved understanding of the forces, stresses, and deflections encountered as a pipe liner deforms within a rigid host pipe and to propose an improved short-term liner buckling model.

4

These contributions are needed to lay the theoretical groundwork for further development of design methodologies.

The research will also address a number of issues involving liner testing and design which have recently received considerable attention at technical meetings important to the pipeline rehabilitation industry. A computational approach based largely the results of the ABAQUS finite element software package (HKS, 1998) will be used to study liner systems with various geometric and material properties. The values of liner outer diameter to thickness ratio (SDR), host pipe ovality, gap between the liner and its host pipe, and local imperfections will be systematically varied to isolate their influence on liner response. The problems addressed here will be restricted to thin-walled liners with diameter to thickness ratios ranging from 30 to 60 installed in rigid host pipes with ovalities ranging from 0% to 6%. The ratio of the uniform gap between host pipes and its liner to the liner outer diameter will vary from 0.0% to 0.7%. The imperfections will be restricted to thickness variations in the liner wall and local imperfections in host pipes in the form of a smooth inward bulge. These imperfections will be assumed to be infinite in length. The material models employed will include linear elastic, perfectly plastic and power-law creep constitutive relations. Both two-dimensional and three-dimensional computational models will be constructed.

To accomplish these objectives, the finite element method will be used to complete the activities below:

- Study the evolution of contact forces, contact areas, deflections, and stresses for short-term and long-term loading of constrained polymeric pipe liners to provide a

5

clear understanding of how geometric and material properties influence liner response.

- Provide a basis for choosing either tensile, flexural, or compressive material characterization properties for use in liner design models based on an improved understanding of the evolving stress states in liners.

- Determine the length of host pipes that should be used in liner buckling experiments when clamped end conditions are employed so that existing experimental results can be appropriately interpreted.

- Simulate the response of pipe liners previously subjected to long-term tests at the Trenchless Technology Center using recently determined short-term and long-term mechanical properties to evaluate the utility of the finite element method in predicting long-term liner behavior.

- Develop an improved short-term liner buckling model that simultaneously accounts for all of the couplings between DR, gap, ovality, and local imperfections by extending Zhao's short-term model to include the effect of local imperfections.

- Qualitatively study the effect of multiple local imperfections on the short-term and long-term behavior of pipe liners.

CHAPTER 2

LITERATURE REVIEW

2.1 Introduction

The thin-walled cylinder is a widely used structural element that may fail due to structural instability. The relevant literature on the subject of buckling of thin walled cylinders can be classified as follows:

(1) buckling of free rings and cylinders;

(2) buckling of encased rings and cylinders; and

(3) creep induced buckling of cylinders.

The application of the theory of buckling of encased rings and cylinders relies heavily on the theory of free pipe buckling. Similarly, short-term (time-independent) buckling models for encased rings and cylinders are commonly used as the basis for long-term models, which can be used to design pipe liners to achieve a specified lifetime. Consequently, the relevant literature dealing with short-term and long-term buckling of free and encased cylinders is presented in this chapter.

2.2 Buckling Behavior of Free Rings and Cylinders

The subject of cylindrical tubes under external pressure was first investigated in the mid-1800s. Since then, many significant improvements have been achieved and

7

widely used in engineering applications. The critical failure mode of these cylindrical shells is a sudden loss of stability and inward collapse. The corresponding critical pressure is a function of the mean diameter (at the mid-surface of the shell) to thickness ratio (DR), as well as the type and magnitude of any possible initial imperfections of the shells.

Fairbairn (1858) first performed tests to investigate the behavior of cylindrical tubes under external pressure. He concluded that the length and wall thickness were important parameters of the pressure required for buckling. His results and predictions were, however, empirical.

Bresse (1866) was probably the first to derive an analytical solution to the buckling pressure by using small deflection theory, and the solution is still used today in design. The buckling pressure was expressed in terms of the elastic modulus, E, of the cylinder, the mean radius, R, of the cross section, and the moment of inertia, I, of the cross section:

$$P_{cr} = \frac{3 \cdot EI}{R^3} \tag{2.1}$$

Equation (2.1) is based on the plane-stress assumption and is appropriate for very short pipe designs.

Bryan (1888) gave a similar classical theoretical result based on the minimum potential energy theory for the critical buckling pressure as:

$$P_{cr} = \frac{2 \cdot E}{1 - v^2} \cdot (\frac{t}{D})^3 \tag{2.2}$$

where the effective modulus $\frac{E}{1 - v^2}$ indicates the assumption plane strain conditions associated with an infinitely long pipe. Here, t and D are the wall thickness and the

mean diameter of pipe, respectively. This equation can be modified to use the dimension ratio SDR (frequently used in industry to describe pipe wall thickness), and be written as:

$$P_{cr} = \frac{2 \cdot E}{1 - v^2} \cdot \left(\frac{1}{SDR - 1}\right)^3 \qquad (2.3)$$

where SDR is the Standard Dimension Ratio which is equal to the outside pipe diameter divided by the mean pipe wall thickness.

Timoshenko and Gere (1960) calculated the stresses in an elliptic ring under uniform load with an initial two-lobe deformation. It was suggested that failure of the ring be considered to have occurred when yield stress was reached in the outer fiber. They give the maximum stress in the liner as:

$$\sigma = \frac{P \cdot R}{t} + \frac{P \cdot R}{\frac{t^2}{6}} \cdot \frac{w}{\frac{P_{cr}}{P} - 1} \qquad (2.4)$$

where P is the applied pressure, P_{cr} is the critical pressure for the free standing round pipe, and w is the maximum out of roundness for an elliptical pipe as depicted in Figure 2.1. This stress is the combination of hoop stress and flexural stress.

The maximum flexural stress to hoop stress ratio (FTHR) can be induced from Equation (2.4) as following:

$$FTHR = \frac{3 \cdot DR \cdot w}{R \cdot \left(\frac{P_{cr}}{P} - 1\right)} \qquad (2.5)$$

where w represents a measure of the initial geometric imperfection commonly called ovality, P_{cr} is the critical pressure of the free pipe, and DR is mean liner diameter to liner thickness ratio (DR = SDR - 1). FTHR increases as any of DR, ovality and P/P_{cr} (PTCPR) increases.

They also provided the solution for the peak deflection in the elliptic ring under uniform load, as

$$d = \frac{w}{\dfrac{P_{cr}}{P} - 1}$$

(2.6)

So, the deflection is the function of degree of ovality and the pressure to critical pressure ratio (PTCPR).
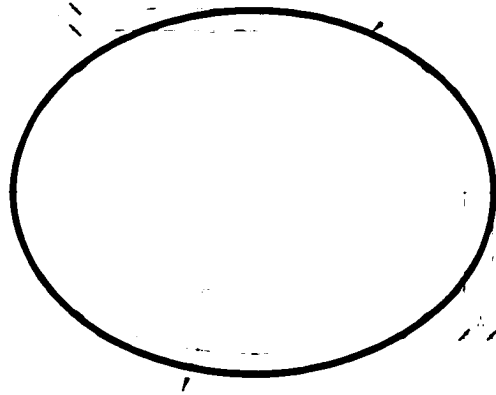
Figure 2.1   Schematic Defining Parameters Used by Timoshenko

Slocum (1909) noted that elliptical cross-sections and variation in thickness reduced the predicted failure pressure by comparing the physical test results with Bryan's theoretical work.

Cook in 1914, quoting experimental work by Carmen and Stewart and, using theoretical work proposed by Southwell, derived an empirical formula for critical length, of:

$$L_{cr} = 1.738 \frac{D^3}{t}^{\frac{1}{2}}$$

(2.7)

Carmen carried out his own experiments on short tubes and reviewed the relevant literature of his time. He concluded that Cook's formula was not valid for certain proportions of D/t and that the previously derived estimates of L_{cr} = 6D were more accurate.

Southwell (1913) introduced using ring stiffeners as a method of improving pipe strength without increasing the steel thickness, and assumed that the maximum deformation of the pipe occurred at the middle between the stiffeners. He noted that, depending on the distance between the stiffeners, the cylinder buckles into a different number of lobes, two being the minimum number which occurred for infinitely long tubes.

2.3   Buckling Behavior of Encased Rings and Cylinders

The design of constrained liners is still in its infancy and relies somewhat on the conventional theory of unsupported pipes subject to uniformly distributed external pressure. However, constrained liners show a tremendous increase in buckling resistance when compared to unconstrained liners with the same geometry. The increase in the buckling resistance of constrained liners is often accounted for by introducing an enhancement factor K which is defined as the ratio of constrained pipe liner's critical pressure to that of free-standing pipe.

2.3.1 Theory of Encased Ring Buckling

Several approaches to the analysis of a thin ring encased in a rigid cavity of constant size can be found in the literature. Amstutz (1969) presented a theory based on the assumption that failure occurs by one lobe indentation and when the yield stress in an outer fiber is first reached. He indicates that under practical conditions, the plastic behavior of steel will cause liner failure at a lower load.

Chicurel (1968) considered the shrink buckling of a thin elastic circular ring which is compressed by being inserted into a circular opening of smaller diameter than the outside diameter of the free ring. He modeled the buckled portion as an axially compressed curved beam.

Cheney (1971) used the linear small-deflections theory to study the stability of a circular ring buried in soil. The constraint effect from the surrounding soil was modeled as an elastic support with a modulus expressed as a function of the physical parameters of the soil.

Glock (1977), who gave the first theoretically sound model for constrained liner buckling, analyzed the stability problem of liners encased by a rigid circular wall by pre-assuming the deformed shape of the detached part of the liners. During his analysis, the radial deflection for the buckled portion was assumed to have the functional form

$$u = u_0 \cdot \cos^2(\frac{\pi \cdot \theta}{2 \cdot \phi}) \qquad (2.8)$$

in which 2ϕ represented the deflected region (Figure 2.2). He used a non-linear deformation theory and the principle of minimum potential energy to derive the solution for the critical load in a similar form to Timoshenko's equation. Glock's solution is given as

$$P_{cr}^G = \frac{E}{1-v^2} \cdot (\frac{t}{D})^{2.2}$$

(2.9)

This model does not take into consideration any initial imperfections of the liner wall, does not account for gap between the liner and its host pipe, and is applies to a perfectly circular host pipe (does not account for ovality). Conequently, it may overestimate the buckling resistance of imperfect liners.

Figure 2.2   Glock's Predefined Deflection Patterns

Based on analysis of experimental buckling pressure data obtained by Aggarwal & Cooper (1984), Lo *et al.* (1993), Guice *et al.* (1994), and Omara (1997) suggested that the critical pressure of a constrained liner can be related to D/t ratios as follows

$$P_{cr} = \frac{a \cdot E}{1-v^2} \cdot (\frac{t}{D})^{m}$$

(2.10)

The fitting parameters a and m, obtained by a regression analysis of Aggarwal and Cooper's data, were reported to be 1.07 and 2.17, which are close to 1.0 and 2.2 as in Equation (2.9). Zhao (1999) determined the constants for *a* and *m* based on as series of 27 finite element runs to develop a model that could simultaneously account for effects of DR, gap, and ovality on the buckling pressure. He used least-squares fitting to

determine nine pairs of a and m values that could be used along with Lagrangian interpolation to find the a and m corresponding to any arbitrary gap, ovality, and DR.

Boot (1998) developed Glock's solution further by modeling the annular gap between a liner and its host pipe and incorporating both symmetrical (two-lobe) and asymmetrical (one-lobe) gaps in their models.

Noting the constants and exponents used in the buckling models for constrained liners reveals trends in their values, as summarized in Table 2.1. It should be noted that there are consistencies in the exponents for the different models.

Table 2.1 Buckling Equation Parameters

Model	Coefficient, a	Exponent, m
Timoshenko Unconstrained	2.0	3.0
Chicurel's Shrink Buckling	2.76	2.2
Cheney's Encased Ring	2.55	2.2
Glock's Encased Ring	1.0	2.2

El-Sawy & Moore (1997) parametrically studied the effect of liner geometry and imperfections on liner buckling strength by using finite element analysis. The effects of initial liner imperfection (defined as a wavy intrusion), loose fitting (uneven gap) between liner and host pipe, and ovality were included, and empirical formulae for reduction factors accounting for various imperfections were proposed for practice. However, the effect of gap is not coupled with the other parameters in their model.

Moore (1997) suggested a reduction factor based on normalizing the wave amplitude with liner thickness. From his solution, the reduction factor is strongly related to the thickness of the liner, with the reduction factor increasing as the liner thickness

decreases. When the amplitude is equal to the thickness, the critical pressure is reduced by approximately 40%.

2.3.2 Modes for Encased Ring Buckling

With the exception of Boot's model (Boot, 1998), all of the above theories for the encased ring buckling are based on the one-lobe buckling mode assumption. However, most liner buckling tests conducted at TTC, Louisiana Tech University reveal a roughly symmetric two-lobe deflection pattern during pressurization followed by a single lobe collapse. The observed two-lobe deformation histories can be further divided into symmetrical and asymmetrical types as in Figure 2.3. Boot and Welch (1996) report a two-lobe deformation history leading to buckling; only one of their 14 specimens exhibited a one-lobe deformation history. And, some of their tests even showed a four-lobe mode as in Figure 2.4. Generally speaking, however, experimental results indicate that a restrained liner with an even surrounding gap will usually deform into a roughly symmetrical two-lobe shape and will contact the host pipe at diametrically opposite points and have maximum deflections at 90° to these contact points. The degree of symmetry of the lobes is seen to increase as the degree of ovality of the host pipe is increased, as discussed by Seemann et al. (2000).

Lo and Zhang (1993) derived an analytical expression for the critical pressure for clamped shallow arches under uniform load with one-lobe and two-lobe modes respectively (Figure 2.5). Zhao (1999) simulated the lobe transitions from two-lobe to one-lobe by FEM and found that the conventional one- and two-lobe buckling modes

correspond to the lower and upper bound critical pressures, respectively. Zhao's work

indicated a trend similar to the results of Lo and Zhang (1993) in Figure 2.5.
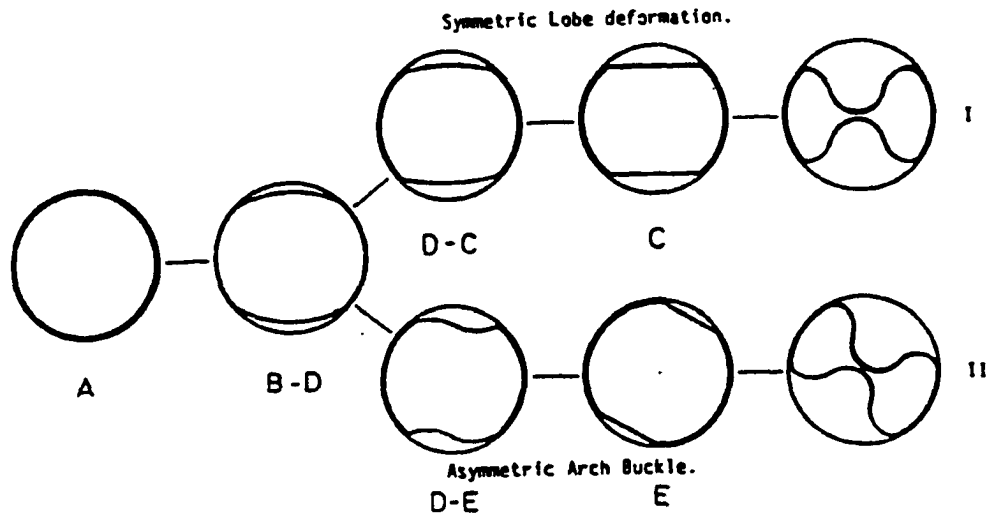
Figure 2.3   Two-lobe Deformation Mode for Constrained Liners
with Even Gaps (Welch,1989)
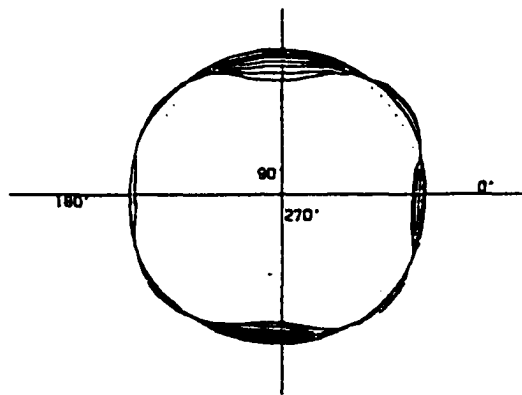
Figure 2.4   Four-lobe Deformation Mode Recorded by Welch (1989)

a. Asymmetrical mode

b. Symmetrical mode

c. A clamped circular arch model
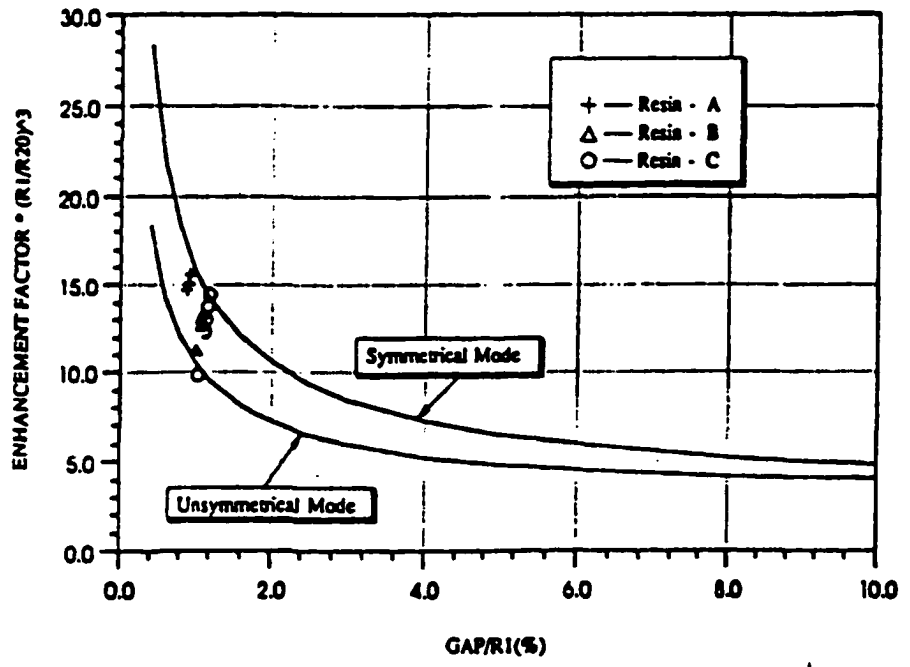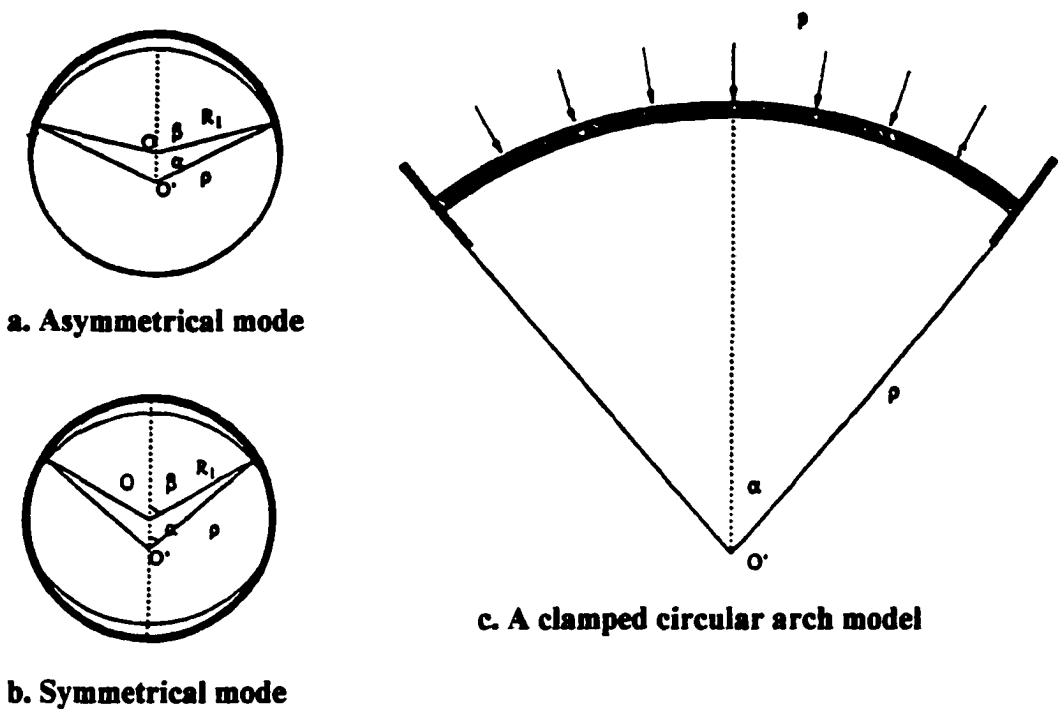
d. Predicted versus buckling test results

Figure 2.5   Schematic of Model Used by Lo and Zhang (1993)

2.3.3 Effect of Gap

Yamamoto and Matsubara (1981) introduced both gap and material nonlinearity into their finite element model for encased liner buckling analysis. They considered three typical gap distribution patterns: initial deflection (or, imperfection), even, and uneven gaps (Figure 2.6). They concluded that:

(1) The liner buckles in a one-lobe mode for the uneven gap and initial deflection cases, while it buckle in a two-lobe mode for the even gap case.

(2) For a given pipe, the enhancement factor K decreases with an increase gap.

(3) For a given pipe, the enhancement factor K increases with DR.

(4) The critical pressure for the two-lobe buckling mode is greater than that of one-lobe mode. So, predictions by using the one-lobe mode were proposed to be used for practical purposes.

Lo and Zhang (1993) concluded that the enhancement factor is simply a function of the gap size ratio, and is almost free from the geometry of the liner-pipe system.

(a) Assumed initial deflection (b) Uniform initial gap (c) Non-uniform initial gap
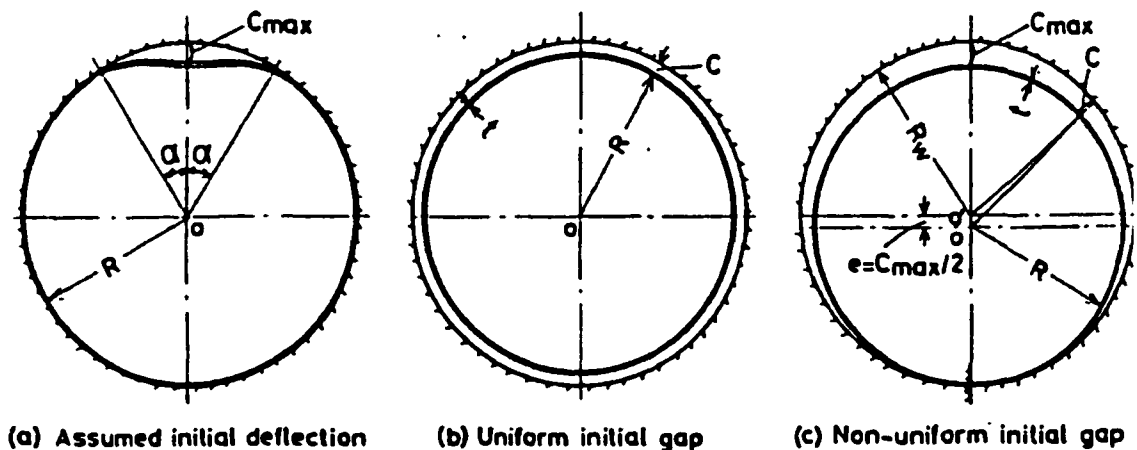
Figure 2.6   Schematic of Models Used by Yamamoto and Mastubara (1981)

2.4   Creep Induced Buckling of Cylinders

2.4.1   Creep Behavior of Plastics

Creep is the phenomenon whereby a solid body can change its shape or slowly deform as time passes, even when the stresses and applied loading are constant. Most structural materials will exhibit a significant amount of creep deformation when the temperature becomes high enough to activate molecular processes by which atoms or molecules move in a preferential direction within the solid. Most polymeric materials will show some level of creep even at room temperature.

As depicted in Figure 2.6, three distinct phases of creep deformation are apparent for most materials when examining a strain versus time plot. The decreasing strain rates of the primary (or transient) phase I is followed by the constant rate of the secondary (or steady state) phase II. Specimen failure usually occurs during the tertiary phase III, where the creep rate accelerates as the material starts to fail on a microscopic level.

The creep behavior can be modeled using the Norton-Bailey model as

$$\varepsilon^c = A \cdot \sigma^m \cdot t^n$$

(2.11)

where ε^c is the accumulated creep strain, σ is the stress, and t is time. The parameters A, m, and n are constants that are determined by fitting the results of creep deformation tests. The Norton-Bailey model above is known as a time-hardening model, since time is explicitly given in the constitutive relation. A strain-hardening form of this expression can also be written as

$$\frac{d}{dt}\varepsilon^c = A^{\frac{1}{n}} \cdot \sigma^{\frac{m}{n}} \cdot n \cdot \varepsilon^{c^{\frac{n-1}{n}}}$$

(2.12)

Such strain hardening forms are often employed in computational analyses because they are considered to give better results than the time-hardening form. Findley (1987) also indicated that strain hardening constitutive relations provide better long-term predictions than time-hardening relations. Strain hardening relations will be used for the long-term computational analyses completed in this research.

a. strain
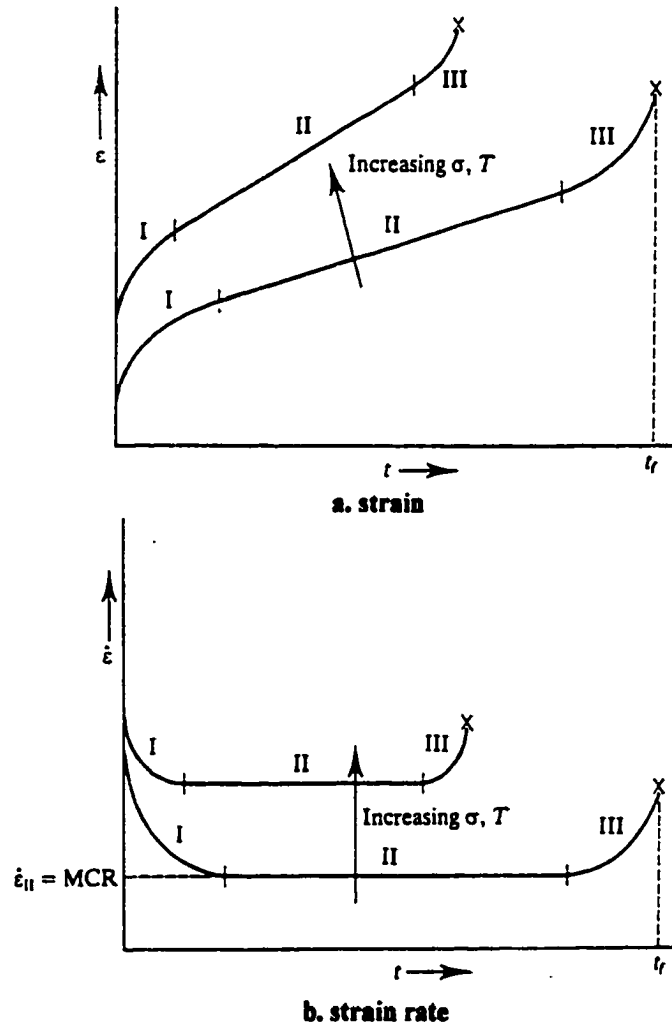
b. strain rate

Strain (a) and strain rate (b) vs. Time in a constant-stress creep test. The creep curve can be divided into three stages. In Stage I (transient creep), the strain rate decreases until it attains a steady-state, minimum value (Stage II). Tertiary creep (Stage III), characterized by an increasing strain rate, precedes fracture at t_f. Increasing stress and/or temperature raises the overall level of the creep curve and also results in higher creep strain rates.

Figure 2.7   Phenomenological Description of Creep (From Courtney (1990), Fig. 7.2)

2.4.2 Creep Induced Buckling

When creep deformation is involved, structural elements such as columns, beams, plates, and shells are susceptible to instability failure even when the pressures or loads are much less than their critical short-term (time independent) values. Therefore, it is important to be able to predict the lifetime, or critical time, of a component for a given loading. As polymeric materials find more and more structural applications, more emphasis has been put into the creep induced buckling of such structures, since plastics are known to creep even under normal temperature.

The study of Hoff (1959) was among the first analytical investigations towards creep buckling of cylindrical shells under uniform external pressure. The shell materials exhibit only secondary creep deformation. The deformation shape of the circular pipe is assumed to be two lobes. The shell construction is of the sandwich type, with concentric cylindrical membranes taking normal stresses and an annular core supporting shear without deformation. He concluded the following:

(1) A structural element will not buckle when no compressive load is applied

(2) A structural element will buckle when the critical load is applied

(3) When the applied compressive load is less than the critical load, the element will buckle after a finite time given that the load is continuous

(4) The larger compressive load will correspond to shorter critical time, and vice versa.

Nishiguchi (1990) made an improvement by allowing the incorporation of general creep laws with accompanying elastic material behavior into the buckling calculations. The growth of the displacement field is represented by the change of a

shape factor with time, as governed by an ordinary differential equation. Nonlinear stress distribution through the wall of tube is also allowed.

Another way to predict creep induced buckling is to incorporate a unified viscoelastoplastic constitutive relation into a finite element model to incrementally trace the evolution of stresses, strains, deflections and other important state variables. Zhao (1999) applied a simplified constitutive relation reflecting different creep strain rate dependency on stress state in his finite element models by means of a "composite" beam element, a combination of two standard beam elements. One of the elements is assumed to carry no tension while the other can carry no compression. The material properties used for the tensile and compressive elements are shown in Table 2.2. Zhao's work revealed good agreement between the finite element predictions and existing experimental data.

Table 2.2   Material Properties used in Zhao's Model (1999)

	E (psi)	v	σ_y	k	M	n
tension	650000	0.35	3500	3.5e-7	1.15	0.11
compression	650000	0.35	8000	4.2e-7	1.146	0.24

2.4.3 Liner Buckling Experiments

The short-term buckling resistance of CIPP liners was experimentally studied by Aggarwal & Cooper in 1984. Their 49 liner buckling experiments revealed that the enhancement factor K varied from 6.5 to 25.8 for DR ranging from 30 to 90, with K increasing with DR. These results showed that for a given host pipe inside diameter, thinner liners benefit more from host pipe support than thicker liners.

A number of time dependent material characterization studies on liner materials have been carried out since the late 1980s. Welch (1989) conducted a series of time-dependent material characterization tests for a CIPP material under constant uniaxial and bending stresses over a period of six months. A constitutive relation representing this material's behavior was incorporated into a finite element code to predict the critical pressure for a design lifetime of 50 years. The effects of material failure and water submergence were also taken into consideration. Similar tests for the Insituform UP resin were conducted by Lin (1995) under tension, compression, and bending conditions for 3,000 hours, and continued by Ravi (1996) to 6,000 hours under bending. It was observed that the materials crept at different rates under different stress states. As for the Insituform resin, the creep rates for a given stress decreased in the following order: tension, flexural and compression.

Instantaneous and creep buckling experiments were performed by Guice *et al.* (1994) on a number of commercially available CIPP and thermoplastic products in a series of 10,000 hour tests. These tests are commonly called the CPAR tests. The diameter to thickness ratio ranged from 30 to 70 for the products tested. The load ratio, which is the ratio of the sustained pressure to the critical pressure observed in the instantaneous test, was in the range of 40% to 90%. Results of linear regression analyses, which correlated the external pressure to the buckling time, suggested that the ratio of long-term (50-year) to instantaneous critical pressure would be in the range of 34% to 46%. This result was smaller than the value of 0.5 suggested by ASTM specifications. Liners made of PVC with large thickness showed very low scatter in the short-term

buckling tests. All liners tested showed a large amount of scatter in the buckling time for a given pressure level.

In the BORSF (Board of Regents Support Fund) tests performed by Straughan and Hall et al. (1999), 180 specimens of the Insituform Enhanced polyester resin were subject to long- and short-term tests. DR ranged from 40 to 70 for these tests. Six series of tests were conducted, including tests on 8-inch diameter 4.5-mm thick liners, 8-inch diameter 5.0-mm thick liners, 8-inch diameter 5.5-mm thick liners, 12-inch diameter 5.5-mm thick liners, 12-inch diameter 6.5-mm thick liners, and 12-inch diameter 7.5-mm thick liners. While the liners were allowed to carry the external pressure for a maximum of 10,000 hours, most of the liners buckled long before the 10,000 hour limit was reached. In another set of tests by Seemann et al. (2000), 15 – 12-inch diameter host pipes with ovalities of 0%, 3% and 5% were tested to determine the effect of host pipe ovality on the short-term critical buckling pressure. Liner deformation measurements were taken for these liners, revealing a two–lobe deformation history followed by a one–lobe collapse. This work also showed that determining the size of the annular gap by measuring the volume of water between the liner and its host pipe is accurate. However, the liner deformation measurements showed that the gap was not uniform around the circumference of the liner.

The tests above all have generated significant scatter in measured response, complicating efforts to develop design procedures that ensure liner stability.

2.5 <u>Summary</u>

The solution of the liner buckling problem is complex due to several sources of nonlinearity, including liner/host-pipe contact, structural instability, large displacements, and time-dependent material behavior. The problem is further complicated by host pipe ovality, gap, and the presence of imperfections. A complete, analytically based, closed-form solution to this problem is not possible. Computational techniques, which employ incremental load-time-deflection analyses, allow for the effects of geometrical and material parameters on liner behavior to be systematically explored and provide a mechanism by which improved liner design models can be developed.

The philosophy is to conduct numerical simulation to reveal the short-term and long-term structural behavior of encased liners subject to external pressure. After quantifying the effects of several factors discussed in this chapter, models for accurate and efficient prediction of liner life can be established.

CHAPTER 3

FINITE ELEMENT MODELING FOR CONSTRAINED LINER BUCKLING

3.1   Introduction

The general purpose ABAQUS/Standard finite element analysis software (HKS, 1998) was selected to simulate constrained liner buckling. The assumptions made in constructing the numerical analysis are presented first in this chapter and are followed by a description of the implementation of the finite element model. The features of ABAQUS which are employed are described where necessary. The two dimensional short-term and long-term models, as well as three-dimensional short-term model described here are the principle tools used to complete the studies presented in the later chapters.

3.2   Assumptions

The following sections describe the assumptions used in setting up the encased liner buckling finite element models.

3.2.1 Material Properties

There are a variety of pipe liner materials on the market corresponding to a wide range of mechanical properties. The computational results presented here inherently

26

assume that the liner materials are homogeneous and isotropic. These assumptions are typical for unreinforced thermoplastic products (such as PVC and polyethylene). The assumptions are believed to also apply to CIPP products made from non-woven fabrics injected with a thermosetting resin. This is particularly important since the computational results are often compared to the experimental results for a polyester felt impregnated with a polyester resin material. The non-woven nature of the felt results in mechanical properties that show little difference in the longitudinal and circumferential directions. It is possible that the mechanical properties in the radial direction may be significantly different than in the longitudinal and circumferential directions for CIPP materials due to the manner in which the polyester fibers are laid down during felt production. However, this difference should not result in significant error since the stresses in the radial direction are very small compared to the in-plane stresses.

It is well known that liner materials may exhibit a significant amount of creep deformation at room temperature, especially at stress levels that are a significant fraction of the material yield strength. Lin (1995) quantified the elastic and inelastic properties for a CIPP material. In particular, he studied the creep behavior of a CIPP material under tensile, flexural and compressive loading and found that the resulting properties were a strong function of loading state.

The results later in this thesis show that the flexural stresses are dominant for short-term buckling while compressive stresses are generally dominant for long-term buckling. For this reason, the flexural properties will be used for the short-term buckling simulations while the compressive properties will be used for the long-term buckling simulations which deal with understanding the stress evolution. For the long-term

simulations of the experimental results, a combination of compressive and tensile properties are used with a dual beam element model as described later, thus accounting for the differences in tensile and compressive behavior (and flexural behavior since flexure is a combination of tension and compression).

3.2.2 Loading Condition

According to ASTM F1216, the liner is designed to withstand only the hydrostatic pressure caused by the underground water which infiltrates through the cracks in the host pipe. The original soil and pipe system is assumed to be stable and strong enough to support the weight of soil as well as surcharging loads. And, the liner is assumed to interact only with the host pipe. Therefore, the only loads acting on the liner are the external groundwater pressure and the contact forces from the host pipe

3.2.3 2-D Configuration

The liner thickness is very small compared with the diameter of the liner, and the liner system can be simplified as a thin-walled circular cylinder. In a typical rehabilitation application, the length of a liner will be much greater than the diameter of the liner. Along the longitudinal direction, the contact condition between the liner segment and the sewer pipe would be expected to be roughly constant. To simplify the solution procedure, the original problem can be viewed as a ring configuration with the plane strain assumption, and the assumption of a single cross-section of the liner (with a length of unity) can be used to represent the whole liner.

3.2.4 3-D Configuration

When the length of the liner is not long enough to ignore the effect of ends, the simplified plane strain ring configuration can no longer represent the entire stress state in the liner. For this case, the pipe system should be simulated using three dimensional finite element analysis with the appropriate boundary condition.

3.3 The FEM Model

For the current study, the ABAQUS finite element software was used because it can solve a wide range of linear and nonlinear problems involving geometric nonlinearity, material nonlinearity, and boundary nonlinearity. Specifically, ABAQUS provides an extensive element library including contact elements and built-in creep constitutive models, and the results can be visualized using the ABAQUS post processor.

3.3.1 Definition of Geometric Parameters

The geometry of the pipe-liner system can be characterized by the liner dimension ratio, the annular gap between the liner and host pipe, the ovality of the host pipe, and by local imperfections. These parameters are defined below.

DR: DR is defined as the ratio of the mean liner diameter D (halfway between the liner ID and OD) to the thickness of a liner t as

$$DR = \frac{D}{t} \tag{3.1}$$

This equation is different from the definition of SDR (= OD/t where OD is the outside diameter of the liner) used in the current CIPP design equation.

DR levels of 30, 45 and 60 were chosen for this study because these values encompass the most common DRs used in field applications. These are also the values used by Zhao (1999).

Gap: Accurately simulating the gap between the pipe liner and the host pipe is very important and helps us to understand contact-force evolution between the pipe liner and the host pipe. A uniformly distributed gap g was used for two-lobe models while the total gap Δ was used for one-lobe models. The gap ratio, defined as the percentage of the gap size g to the liner mean diameter D in Equation (3.2), was varied from 0.0% to 0.7% for this study.

$$G\% = \frac{g}{D} \cdot 100 \qquad (3.2)$$

Note that the uniform gap is half of the total gap Δ, as expressed in Equation (3.3).

$$g = \frac{\Delta}{2} \qquad (3.3)$$

Ovality: As discussed in the literature review chapter, the elliptical shape of the host pipe will affect the liner's ability to resist collapse. In the present study, the initial ovality of the liner is always assumed to be the same as that of its host pipe.

$$G\% = \frac{D_{max} - D_{min}}{D_{max} + D_{min}} \cdot 100\% \qquad (3.4)$$

A very small ovality is imposed to calculate the peak stress evolution for perfectly round pipe liners to avoid the effect of the stress induced by an initial disturbing force. The ovality ratio of 0.17% was found to be satisfactory in this study. Different levels of ovality (0%, 3%, 6%) were simulated for developing an improved short-term buckling model.

Local Imperfection: Wavelike local imperfections commonly found in the field will be studied parametrically similar to the procedure used by El Sawy and Moore (1997) and by Zhao (1999). According to Figure (3.1), the imperfections can be defined by the relative local denting LI and the wave length ratio S as

$$LI\% = \frac{\Delta_0}{D} \cdot 100\% \tag{3.5}$$

$$S = \frac{L}{\pi \cdot R} \tag{3.6}$$

a. gap & ovality   b. local imperfection
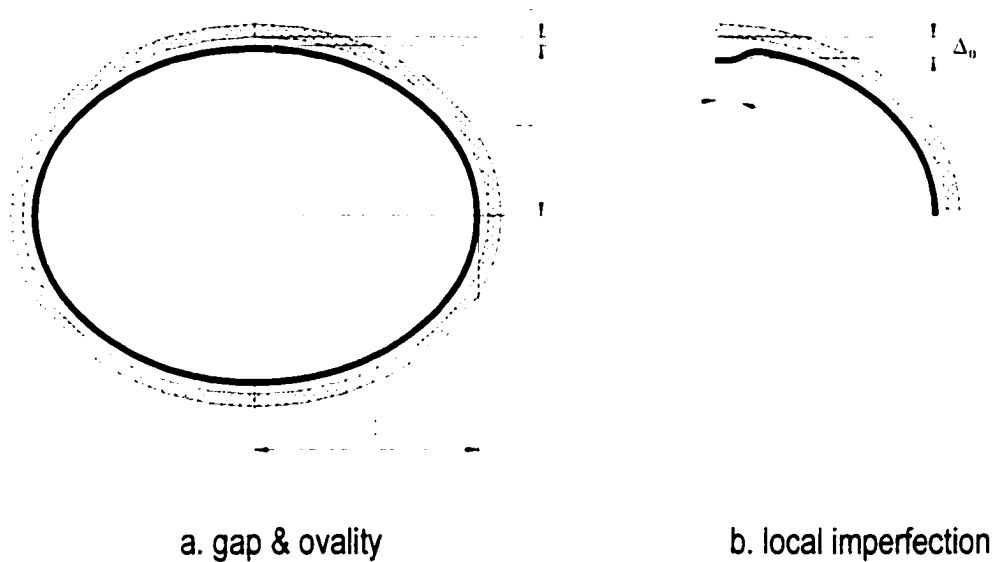
Figure 3.1   Schematic of Imperfections and Pipe Geometry

Note: R = (a+b)/2 and D = 2R.

3.3.2 Constraint from the Host Pipe

The encased liner deformation is always constrained within the confines of its host pipe. As the external pressure or time increases, interaction between the liner and its host pipe evolves with a changing contact size and contact pressure. This contact

evolution can be quantitatively explored using the surface contact capabilities of ABAQUS.

In this finite element model, the host pipe, assumed to be rigid, is modeled with a set of R2D2 (2-node two-dimensional rigid body) elements for the two-dimensional models, or with a set of R2D4 (4-node three-dimensional rigid body) elements for the three-dimensional models. The set is defined as fixed without any transition or rotation relative to a reference node. All the degrees of freedom of the reference node are inhibited to fully constrain the host pipe against any motion.

The surfaces of the contact area for the liner and host pipe are defined by the SURFACE DEFINITION command and the potential for contact is set up using CONTACT PAIR command.

During the calculation, any liner nodal displacement attempting to penetrate the rigid host-pipe surface will be cut back, and the finite element code will iterate until the liner no longer penetrates the host pipe (until the liner and the host pipe are in contact but do not penetrate one another). The contact pressure is positive at any node whenever the gap between the pair of surfaces is closed; otherwise. the contact pressure will remain zero. The exact contact information can be stored in the output ".dat" file by using CONTACT PRINT command with CFN option.

In ABAQUS, the flexible liner surface is allowed to slide along the rigid pipe surface and the relative sliding can be finite. The possible friction force can be assumed by defining an appropriate friction coefficient in the SURFACE INTERACTION command. The friction coefficient is usually defined as zero for the current study by assuming both surfaces are smooth. Only in Chapter 9 is the friction assumed to exist by

using the integrated model discussed in the following section when considering the effect of multiple local imperfections. The friction force can restrict the liner from transitioning from a higher to a lower deformation mode. The coefficient of static friction used in Chapter 9 will be taken as 0.2 which is about half of the 0.43 value obtained from dry friction testing at Tulane University (1996).

3.3.3 Model Setups

Three types of two-dimensional finite element models are used in this study for different purposes: one- and two-lobe models and integrated models. The one-lobe model is used to determine the buckling pressures for the short-term design model in Chapter 8 since it gives the lower bound for the critical pressure or time. The two-lobe model is used to analyze the liner stress, displacement and contact evolution since most liners deform into two-lobe shapes prior to one-lobe buckling. And, the integrated model allows the liner to buckle in any direction under the combined effect of a variety of imperfections. For simplicity, liners are assumed to buckle along the vertical axis for the one- and two-lobe models. A three-dimensional model is set up to simulate two-lobe bucking so that the critical specimen length to pipe diameter ratio can be studied. The two- lobe model is used to reduce the number of required elements, since single-lobe buckling would require a half-symmetry model.

One-Lobe Model

In this kind of model, the gap is assumed to be unevenly distributed, as in Figure 3.2(b). The radial displacement at the bottom node where the liner touches the host pipe is constrained for simplicity. One-half of the liner and host pipe is modeled due to its symmetric configuration.

Two-Lobe Model

This type of model is quite similar to the one-lobe model. The only difference is that the gap is uniformly distributed, and a quarter of the liner-pipe system is meshed as in Figure 3.2(a). This model will predict significantly higher buckling pressures than the one-lobe buckling model.

Integrated Model

The entire pipe liner system will be simulated in this model. The VISCOUS DAMPING command will be employed to overcome numerical convergence difficulties due to the sudden violation of contact constraints by allowing a viscous pressure to be transmitted between the contact surfaces as they come into contact or separate. The viscous contact pressure is proportional to the relative velocity between potential liner and host pipe contact points. This model will be applied in Chapter 9.

Three-Dimensional Model

One-eighth of the pipe-liner system was set up with symmetrical boundary conditions based on a two-lobe buckling mode assumption. Both clamped ends (end nodes fixed in all directions) and ends fixed in the longitudinal direction only were simulated separately. The application of this model will be discussed in Chapter 7.

a. Two-Lobe Mode   b. One-Lobe Mode
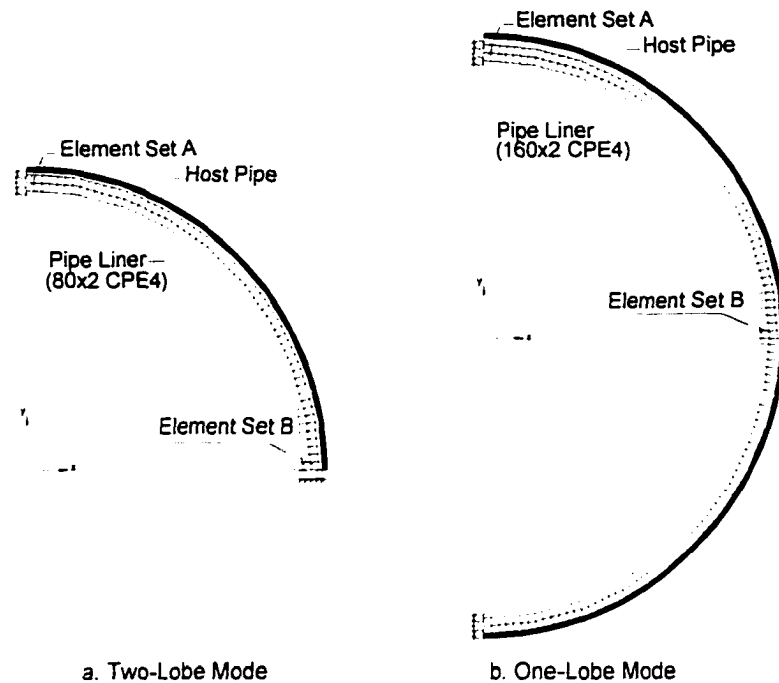
Figure 3.2 Finite Element Model

3.3.4 Solution Procedures

Short-term buckling will be modeled assuming rate-independent elastoplastic material behavior with a pressure that increases monotonically from zero to the buckling pressure. Long-term buckling will be modeled using time-dependent, visco-elastoplastic material behavior under constant pressure until the buckling time is reached. Two different solution procedures in ABAQUS can be used to simulate these two different processes: STATIC for time-independent loading, and VISCO for time-dependent creeping behavior. Both procedures can deal with the geometrical nonlinearity resulting from finite displacements of the liner during liner buckling.

ABAQUS allows the user to step through the loading or time history to be analyzed by dividing the problem into steps. For short-term analyses, a step is static

analysis where the pressure changes from one magnitude to another. For each step, the state of the model is updated throughout all non-linear analysis steps, and the effects of previous history are always included in the response in each new step.

In the creep-induced liner buckling model (the long-term model), the liner will deform elastically under applied external pressure. As time lapses, the contact surface between the liner and host pipe will be changed as the liner continues to deform due to accumulating creep deformation. To obtain convergence, the lifetime of the liner will be broken into a number of "time steps". Time steps will progress from "small" (near the beginning of an analysis when creep deformation accumulates rapidly), to "large" (as the rate of creep deformations decreases), to "small" (as buckling is approached and the liner geometry changes rapidly).

Short-term Buckling Solution Procedures

A typical finite element analysis of the short-term buckling of an encased liner includes one *STATIC* step: the uniformly distributed external pressure is applied on the liner and increased until the liner buckles.

Long-term Buckling Solution Procedures

A typical finite element analysis of the long-term buckling of an encased liner includes two steps. Besides the one static step described in short-term case, an additional *VISCO* step is included to incorporate the creep induced buckling problem. The solver can automatically assign appropriate time increments according to the error tolerance on creep strain defined by the user. The solution will stop when the liner collapses. At that point, any attempted time increment is less than or equal to the minimum time step.

3.4 Model Verification

3.4.1 Mesh Refinement

As explained previously, the liner was analyzed as a two-dimensional, plane-strain problem. The element type used is a bi-linear, four-noded, plane-strain element since it can provide a stress contour plot for the purpose of following the stress evolution. The finite element model used here is based on Zhao's (1998) model. From his mesh refinement study as in Figure 3.3 and Table 3.1, it is suggested that a 640 element model has a relatively small amount of error and acceptable computation times. And, Figure 3.4 shows that the elements used for the 640 element model have an aspect ratio that is near one. Since the stress distribution is very sensitive to the size of the elements in both directions, further mesh refinement analysis is performed here to find the minimum number of layers of elements. In Table 3.2, the relative change in the critical buckling pressure between the one-layer model (320 elements) and the two-layer model (640 elements) is 46%, while the relative change between the two layer model and the four-layer model (1280 elements) is about 5.7%. Furthermore, the four-layer model with 2560 elements was run with the result of 124 psi due to improve the consideration of aspect ratio of the four-layer model. The relative difference between this 2560 element four-layer model and the two-layer model (640 elements) is 2.5%. Consequently, using two layers of elements for a total of 640 elements is assumed to be acceptable to capture the trends in the stress evolution and to accurately determine the critical buckling pressures.
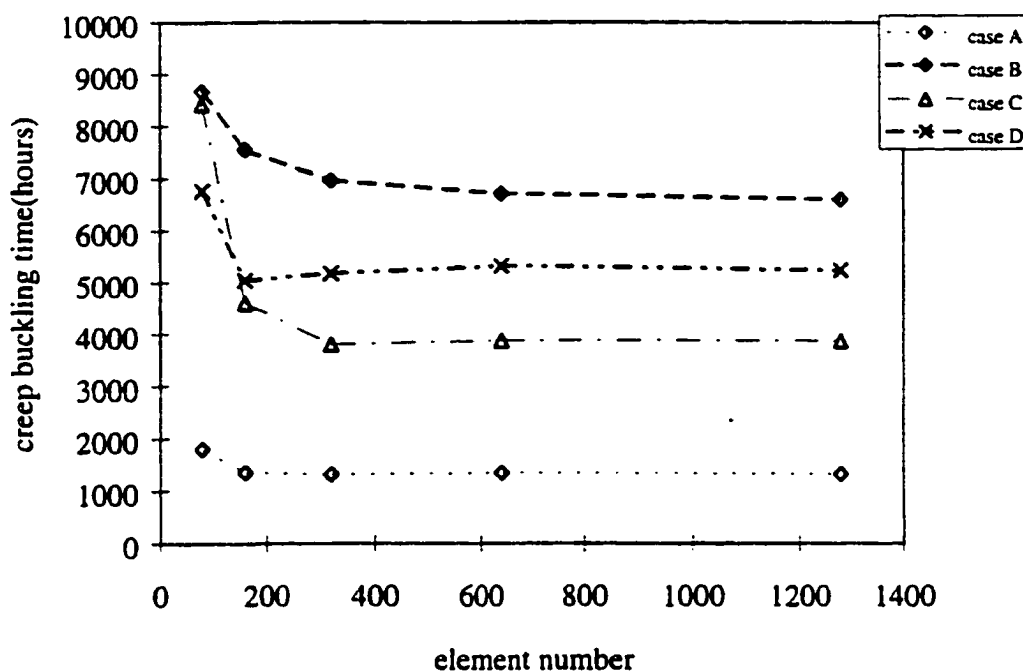
Figure 3.3 Finite Element Mesh Refinement by Zhao (1998)

Table 3.1 Relative Change in the Buckling Time for Different Numbers of Elements (Zhao, 1998)

Element number	160	320	640	1280
relative change for A (%)	25.00	2.74	2.59	1.96
relative change for B (%)	13.99	8.42	3.77	1.55
relative change for C (%)	45.36	17.39	1.81	.10
relative change for D (%)	25.49	2.86	2.75	1.50
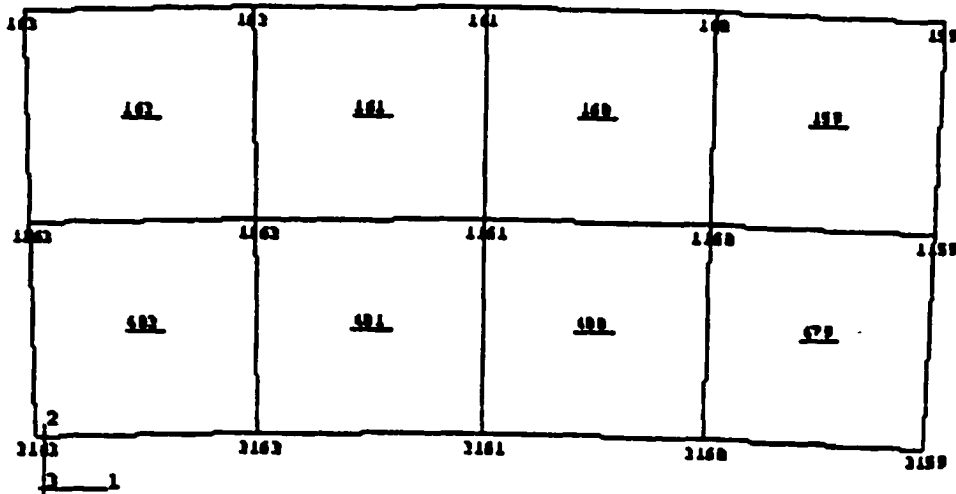
Figure 3.4   CPE4 Element Shape with 640 Elements

Table 3.2 Relative Change in the Buckling Pressure and Maximum Flexural Stress for Different Numbers of Elements

Number of Layer	Pressure (psi) or Flexural stress (psi)		Relative change
1	P_{cr}	65.3	46 %
	σ_{Flex}	6525	16 %
2	P_{cr}	121	0 %
	σ_{Flex}	7780	0 %
4	P_{cr}	128	5.7 %
	σ_{Flex}	8180	5.1 %

In the three-dimensional model, 32x2x8 triangular STR13 shell elements (8 elements in the longitudinal direction and 32 elements in the circumferential direction with two triangular elements per rectangular element) and 32x8 rigid elements were used for the one-foot-long pipe-buckling simulation following the mesh refinement study shown in Table 3.3. Notice that the shell elements appear to be stiffer than the two dimensional continuum elements which are slightly stiffer than the beam elements. From Table 3.3, the relative change in buckling pressure for the three-dimensional model is

3.3% from two-dimensional CPE4 model. This accuracy is believed to be sufficient for determining the critical length to diameter ratios in Chapter 7.

Table 3.3   Relative Change in the Buckling Pressure for Different Numbers of Elements for Three Dimensional Model

Element Type & Number	Critical Pressure	Relative Change
STRI3 8x2x4	101	12.2%
STRI3 16x2x8	94	4.4%
STRI3 32x2x16	93	3.3%
STRI3 32x2x8	93	3.3%
STRI3 32x2x4	93	3.3%
STRI3 64x2x8	92	2.2%
B21 72x2	91	1.1%
CPE4 80x2	90	0.0%

3.4.2   Verification of Finite Element Model

Glock's analytical model was used to evaluate the accuracy of the finite element models for perfectly round pipes. The critical pressure for Glock's model is 135.6 psi for a pipe with a DR of 41.97, an elastic modulus of 459,000 psi and a Possion's ratio of 0.3, while the critical pressure from the finite element model is 136.8 psi. The relative error is 0.9%. This finite element model is also used to simulate the Seemann's ovality test results (2000). Figure 3.5 shows that these finite element results compare with the lower values of the experimental results, which is not unexpected since the computational results correspond to one-lobe buckling models.

The viscoelastic material constitutive model (Equation (2.12)) used in this study is the same that used in Zhao's (1999) long-term model. Zhao demonstrated its

effectiveness in simulating the laboratory results of Lin (1995) by using his dual beam element model with tensile and compressive material properties to simulate the flexural response of the liner material. No repetition of this verification will be presented here.
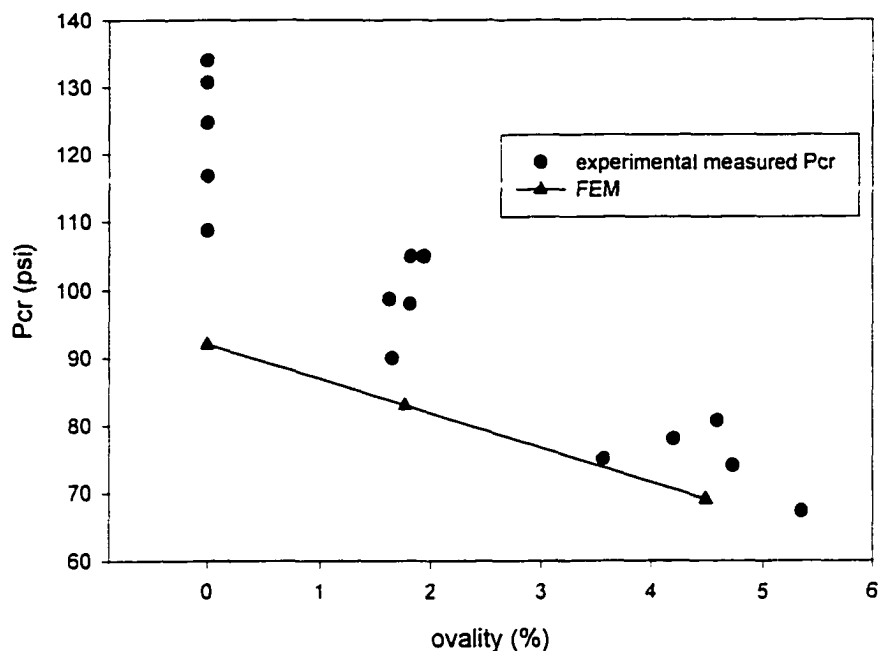
Figure 3.5   Simulation of Seemann's Test Results

3.5 Summary

Finite element models for both short-term and long-term liner buckling simulations were presented in this chapter. The geometry of the liner systems to be modeled were defined in terms of the DR, gap, gap distribution, ovality and local imperfections. The material properties to be used for these models were discussed along with some details required to implement the models in ABAQUS. The two- and three-dimensional models presented were verified using standard mesh refinement techniques and by comparison with analytical and experimental results.

CHAPTER 4

SIMULATION AND ANALYSIS OF
PREVIOUS EXPERIMENTAL RESULTS

4.1 Introduction

A number of researchers have experimentally studied the short-term and long-term behavior of pipeline rehabilitation liners. Laboratory measurements of liner buckling are an essential step in developing an understanding of the stability of the liners placed within rigid host pipes. Analysis of these test results gives an improved understanding of the structural mechanism of encased liner buckling for the future analysis and provides a basis for the numerical analysis in the following chapters.

Both CPAR and BORSF tests performed at the TTC (TTC) will be studied here and have the most complete test records for variables like DR, gap, ovality, hydrostatic pressure, and time as well as mechanical properties for both short-term and long-term material behavior. This chapter will focus on simulating the BORSF long-term test results using finite element analysis and fitting the constants which are required for Zhao's (1999) model. The finite element model employed here is identical to the one used by Zhao. Plotting the pressure versus time curves together with the experimental data for the six series will determine the utility of the finite element model for providing useful predictions of long-term liner behavior. This finite element model can be used as

42

the basis for developing more advanced long-term buckling models. The three constants in Zhao's analytical model will be evaluated for each of the six liner series. Trends in these constants will be studied to see if generalizations can be drawn across liner SDRs and host pipe sizes for the Insituform resin used in the liners.

4.2   Analysis of CPAR and BORSF Experimental Results

Two distinct sets (CPAR and BORSF) of long-term liner buckling experiments have been conducted at the TTC. For both the CPAR and BORSF studies, the liners were installed in steel pipes with clamped ends. The length of the steel pipes used was at least six times the pipe diameter to minimize the possible effects of the clamped ends. This critical specimen length is shown to be sufficient in Chapter 7. The long-term test pressures were chosen based on the short-term critical pressures.

4.2.1. Analysis of CPAR Results

The first set of experiments was known as the CPAR study (1994) and involved the testing of seven products referred to here as Nupipe, Insituform Standard, Insituform Enhanced, Paltem, Spiniello KM-Inliner, Inliner U.S.A, and Superliner. The primary control variables were pressure, time, and DR. Both short-term and long-term tests were conducted. In Table 4.1 and 4.2, analytical comparisons were made with the short-term results and in Table 4.3 and 4.4 with the long-term results. Theoretical buckling pressures were derived from the Glock's model (1977) as given in Equation (2.9). The average elastic moduli adopted in the calculations were taken from the material characterization results (three point bending) of the CPAR tests.

Table 4.1   Analysis of CPAR Short-term Buckling Test Results

Pipe No.	Dimension Ratio (D/t)	Flexural Modulus E(psi)	P_{test} (psi)	P_{Glock} (psi)	P_{Glock}/P_{test}
Product: InLiner USA					
L-01	40.30	292,740	53.0	94.5	1.786
L-13	45.55		46.0	72.23	1.563
L-25	44.53		55.0	75.9	1.39
Avg.	43.46		51.3	80.1	1.563
Product: Insituform Standard					
C-01	48.85	448,630	67.5	94.9	1.4
C-10	47.76		98.5	99.75	1.01
C-20	51.96		84.0	82.86	0.99
C-25	52.56		80.0	80.8	1.01
C-30	50.51		85.5	88.2	1.03
C-36	52.83		71.5	79.9	1.12
Avg.	50.38		81.2	88.7	1.09
Product: Insituform Enhanced					
D-10	53.20	538,620	88.0	94.46	1.07
D-20	52.04		97.0	99.15	1.02
D-30	52.54		83.5	97.09	1.16
D-40	54.52		96.5	89.5	0.93
Avg.	53.08		91.3	94.9	1.04
Product: NuPipe					
B-01	31.09	384,450	213.5	219.8	1.03
B-13	31.08		213.0	219.9	1.03
B-25	31.29		214.0	216.7	1.01
Avg.	31.15		213.5	218.9	1.025

Table 4.2   Analysis of CPAR Short-term Buckling Test Results

Pipe No.	Dimension Ratio (D/t)	Flexural Modulus E(psi)	P_{test} (psi)	P_{Glock} (psi)	P_{Glock}/P_{test}
Product: Paltem HL					
E-01	51.06	292,810	83.0	56.2	0.68
E-11	46.33		64.5	69.6	1.079
E-14	47.17		65.0	66.9	1.03
E-27	47.10		87.5	67.1	0.77
Avg.	47.89		76.5	64.7	0.85
Product: Spiniello KM-Inliner					
F-01	63.56	282,610	42.0	33.5	0.80
F-13	61.08		31.0	36.57	1.18
F-25	59.60		28.5	38.6	1.35
Avg.	61.41		33.8	36.14	1.07
Product: Superliner					
S-01	52.04	1,784,900	129.0	328	2.54
S-13	50.55		121.5	350.3	2.88
S-25	52.74		125.0	319.0	2.55
Avg.	51.78		125.2	332.2	2.65

From Table 4.1 and 4.2, it can be seen that the majority of the experimental results are less than the theoretical results except for the Paltem product. This difference occurs because the geometrical imperfections (particularly gap) have not been embedded in the theoretical model, since Glock's model does not account for gap. Although Glock's model is for a tight-fitting round pipe, it does give an upper bound of the critical pressure. Glock's model does not consider material failure, which may result in a further overestimation of the buckling pressures. On the other hand, a decrease in the buckling

pressure "could" be present in the analytical predictions since Glock's model is for one-lobe buckling, which corresponds to a lower critical pressure than two-lobe buckling.

In general, most of the reduction factors listed in the above two tables for the short-term test results are at the same order of magnitude. Notably, the test results for the NuPipe products are quite consistent with each other, perhaps due to the fact that PVC pipe products are pre-fabricated with less initial random and unpredictable geometrical imperfections. On the other hand, the thickness of the Nupipe product is much higher than in the other products. The thinner product is more sensitive to imperfections. The NuPipe is thicker and is consequently relatively inert to the imperfections, resulting in more predictable results.

Another factor to note from Tables 4.1 and 4.2 is that the reduction factor for the Superliner product is two times larger than the other products. One reason for the larger reduction factors may be that the stiffer liner (higher flexural modulus) is more sensitive to imperfections. These imperfections may cause a slight variation in the deformation pattern that may trigger buckling at a significantly lower pressure, since more pressure is required per increment in deflection for the other liners. The Superliner does show a greater buckling pressure than the other liners of similar DR, but the increase is just not proportional to the increase in elastic modulus.

A number of papers question the validity of the CPAR results due to the large amount of scatter in the long-term results which are summarized in Table 4.3. The long-term test pressures varied from 37% to 83% of the short-term critical pressures. The common trend for the tests is that the higher the external pressure, the shorter the liner life and the more scatter in the time-to-failure. Although the NuPipe product gave very

stable results in the short-term tests, it still had a large amount of scatter in the long-term test, perhaps due to its large gap ratio.

Table 4.3   Long-Term CPAR Buckling Test Summary

Product	Outside Diameter (inches.)	Thickness (inches.)	DR	Gap (inches)	P_{test} (psi)	P_{short} (psi)	P_{short}/P_{test}	Time (hours)
InLiner	11.92	0.273	43.76	0.031	20 ~40	51.3	39% ~78%	0.5 ~9276
Insituform Standard	11.93	0.232	51.40	0.046	30 ~65	81.2	37% ~80%	10 ~10000
Insituform Enhanced	11.95	0.221	54.05	0.044	45 ~75	91.3	49% ~82%	0.2 ~10000
NuPipe	11.85	0.380	31.19	0.165	100 ~150	213.5	47% ~70%	2 ~10000
Paltem	11.94	0.245	48.59	0.045	30 ~60	76.5	39% ~78%	1.5 ~10000
Spiniello	11.92	0.195	61.46	0.044	13 ~28	33.8	38% ~83%	0.5 ~10000

4.2.2. Analysis of BORSF Results

Another series of long-term liner buckling tests referred to as the BORSF tests were performed by Straughan et al. (1998) at the TTC. While the annular gap was measured with a "feeler" gauge in the CPAR tests, the gap measurements for the 12-inch diameter pipes was estimated by measuring the volume of water which occupied the annular space between a liner and its host pipe. This water volume was then used to estimate the uniform gap of the liner. Although no measurements were taken for the eight inch pipes (the feeler gage gap measurements were assumed to be invalid due to the uneven flow of resin at the end of the host pipe lining), the volume-based measurements for the 12-inch diameter pipes were used to estimate a gap of 0.018 inches for all 8-inch

diameter pipes. The outer liner diameter was computed as the host pipe inner diameter minus two times the uniform gap. The gap value for the 12-inch diameter liners in the BORSF tests with 5.5, 6.5, 7.5 mm liner thickness were measured using the volume technique as 0.024, 0.026 and 0.031 inches.

The short-term and long-term test results are summarized in Table 4.4. For the 8-inch diameter pipes, the averages of the short-term test results were all greater than Glock's analytical results, while the averages for the 12-inch pipes were generally smaller than predicted by Glock's model. The degree of variation of the buckling time for both sizes of pipe are similar and at similar levels as that of the CPAR tests. Thus, the problem of variation in long-term results was not solved with the BORSF tests.

Table 4.4   Short- and Long-term Buckling Tests Summary for BORSF

Type	Diameter (inches)	Thickness (inches)	SDR	P_{test}	P_{Glcok}	P_{Glock}/P_{test}	P	P/P_{test}	Time (hrs.)
8" 4.5inch	7.6766	0.1495	53.37	82.4	75.4	0.915	39~ 58	47%~ 70.4%	3.0~ 13220
8" 5.0inch	7.6393	0.1611	49.42	106.8	86.9	0.814	51~ 77	47.7%~ ~72%	0.1~ 13066
8" 5.5inch	7.6191	0.1770	45.05	117.8	106.5	0.904	56~ 87	47.5%~ ~74%	15~ 6819
12" 5.5inch	11.4606	0.2003	59.24	52.8	65.6	1.24	25~ 41	47%~ 77.6%	1.9~ 8070
12" 6.5inch	11.4263	0.2378	50.06	92.2	95	1.03	41~ 66	44%~ 71.6%	23.2~ 7088. 7
12" 7.5inch	11.3667	0.2624	45.32	123.8	118.3	0.956	56~ 90	45%~ 72.7%	41.8~ 10106

4.2.3. Comparison of Short-Term and Long-Term Results

A number of models for short-term buckling analyses have been developed to determine the effect of ovality, gap, imperfections, and DR on the short-term critical

48

buckling pressure of liners. For example, Boot (1999) incorporated the effects of gap into Glock's (1977) analytical model for determining the critical pressure as a function of the elastic modulus, Poisson's ratio, and DR for both single-lobe and two-lobe buckling. El-Sawy and Moore (1998) developed a model derived from numerical solutions to compute the critical pressure based on the elastic modulus, Poisson's ratio, DR, ovality, and imperfections for single-lobe buckling. Their model, based on using charts to select reduction factors, is perhaps the most complete short-term buckling model available, although the effect of gap cannot be accommodated for imperfect pipes. It is important that models that can accurately predict short-term response based on all of the relevant geometric variables be employed as the basis for predicting long-term response (until reliable long-term models are developed). Failure to incorporate the effects of these variables can cause unexpected results, as demonstrated by the calculations in this section.

The ABAQUS finite element model described in the previous chapter is used here to compute critical buckling pressures and times for liners installed in round and imperfect host pipes. The imperfect host pipes modeled here include an oval imperfection and a local imperfection, as shown in Figure 3.1. All the calculations correspond to a DR of 40 and a gap of 0.25%.

Table 4.5 shows that the P_{cr} for the round host pipe is 152 psi, while P_{cr} for the ovalized host pipe is 131 psi. Dividing P_{cr} for the round pipe by P_{cr} for the ovalized pipe results in a ratio of 1.16. Although it may seem that a similar ratio would apply to the long-term buckling times, the remaining columns in the table indicate otherwise. Notice that the ratio of long-term buckling time for ovalized pipes to round pipes is 3.35

(3.146e8 minutes / 1.054e9 minutes) for a pressure level of 0.2 P_{cr} (0.2 * 152 psi), while the ratio increases to 269 for a pressure level of 0.8 P_{cr}. The results are even more dramatic when the local imperfections are involved, as demonstrated by a ratio of 7.36 (1.433e8 minutes / 1.504e9 minutes) for a pressure level of 0.2 P_{cr}. The last two cells in Table 4.5 are left blank because 0.8 P_{cr} exceeds the short-term buckling load for the imperfect liner.

All the long-term results in Table 4.5 were computed using pressure levels that were 20%, 50% or 80% of the critical pressure of the _round pipe_. Table 4.6 shows the corresponding calculations for the case where long-term pressure levels are based on the critical pressure computed for the imperfect pipes. For example, the long-term pressures applied to the ovalized pipe correspond to 20%, 50% and 80% of the 131 psi short-term buckling pressure of the ovalized pipe. These lower pressures result in much longer lifetimes and buckling time ratios of the same order of magnitude as the critical pressure ratios.

Consequently, when short-term buckling pressures are used as the basis for liner design, it is very important to include the effect of all factors known to significantly decrease buckling pressure. Overlooking the effects of imperfections may result in system lifetimes much shorter than predicted when groundwater loading is a significant fraction of P_{cr}. The trends observed in Table 4.5 may also have some implications for liner testing. That is, if significant scatter is observed in experimentally determined P_{cr} values, this scatter is likely to be amplified in long-term liner buckling tests, resulting in significant variance of buckling time for a given external pressure, with the degree of

variance increasing as the applied pressure increases. Such trends are present in previous liner buckling experiments (Guice *et al.*, 1994).

Table 4.5 Reduction Factors in Buckling Pressures and Times Due to Oval and Local Imperfections Where Long-Term Pressure Levels are Based on P_{cr} of the Round Pipe (DR = 40, G = 0.25%)

Pipe Type	Short-Term Results	Long-Term Buckling Times and Buckling Time Ratios		
	P_{cr} (psi)	$0.2\,P_{cr}$ (min.)	$0.5\,P_{cr}$ (min.)	$0.8\,P_{cr}$ (min.)
Round Pipe	152	1.054e9	1.226e6	2.295e3
Oval Pipe oval = 3%	131	3.146e8	2.019e5	8.52
	1.16	3.35	6.07	269
Local Imperfection Pipe $\frac{\Delta}{R} = 2\%$ $\theta = 10°$	110	1.433e8	4.829e4	*
	1.38	7.36	25.4	*

* No results available since 0.8 P_{cr} of the round pipe is greater than the short-term buckling Pressure

** R = (a+b)/2

Table 4.6 Reduction Factors in Buckling Pressures and Times Due to Oval and Local Imperfections Where Long-Term Pressure Levels for Imperfect Pipes are Based on P_{cr} of the Imperfect Pipes (DR = 40, G = 0.25%)

Pipe Type	Short-Term Results	Long-Term Buckling Times and Buckling Time Ratios		
	P_{cr} (psi)	$0.2\,P_{cro}$ (min.)	$0.5\,P_{cro}$ (min.)	$0.8\,P_{cro}$ (min.)
Round Pipe	152	1.054e9	1.226e6	2.295e3
Oval Pipe oval = 3%	131	7.975e8	9.305e5	1.619e3
	1.16	1.32	1.31	1.42
Local Imperfection Pipe $\frac{\Delta}{R} = 2\%$ $\theta = 10°$	110	1.08e9	1.657e6	3.779e3
	1.38	0.98	0.74	0.61

*R = (a+b)/2

4.3   Other Relevant Experimental Results

Another series of tests involving fifteen short-term buckling experiments with nominal ovalities of 0%, 2% and 5% for CIPP liners was performed by Seemann *et al.* (2000) at the TTC. Five liners at each of the three ovality levels were tested. The evolution of the radial deflections were measured at 20 psi pressure increments for each of the fifteen liners using three displacement transducers mounted on a rotating shaft. They also gave a more accurate measure of the annular gap within pipe-liner system. The gap was not uniformly distributed around the circumference of the liner. The average test results are summarized in Table 4.7 along with analytical and finite element results.

All theoretical results from Table 4.7 are based on a flexural modulus of 459,000 psi and a Possion's ratio of 0.3.   Figure 4.1 shows a plot of the experimental results versus the analytical and finite element results.   All results are less than the predicted value from Glock's model since it does not account for ovality or gap. Figure 4.1 shows that El-Sawy and Moore's model (1997) overestimates the buckling pressure. This overestimation is due to the fact that their model cannot be used when ovality and gap are present at the same time.   The ASTM design equation and FEM results are both lower than the average of the test results. The FEM model is conservative and considers the effect of gap, ovality and the coupling between them. No gap effect is included in the ASTM model. The effect of ovality on the ASTM results is more conservative than both El-Sawy's model and the FEM results.

Table 4.7 Analysis and Summarization of Test Results for Seemann (2000)

Type	SDR	Oval (%)	Gap (in.)	P_test (psi)	P_Glock (psi)	P_ASTM (psi)	P_El Sawy (psi)	P_FEM (psi)
0% ovality	42.041	0	0.051	123.0	135.6	102.8	133.075	92
2% ovality	41.987	1.77	0.053	99.3	136.4	87.9	121.207	83
5% ovality	42.117	4.48	0.055	75.0	136.2	68.1	103.219	69
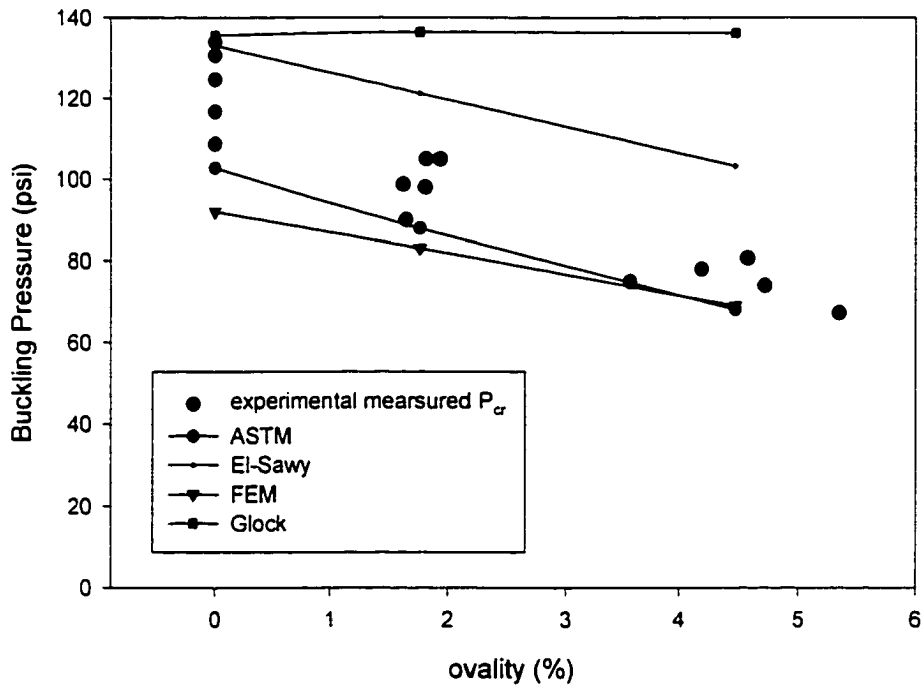
Figure 4.1 Comparison of Experimentally Determined Buckling Pressures with ASTM F1216, El-Sawy, Glock and FEM

4.4 Simulation of BORSF Long-Term Experimental Results

Zhao (1999) suggested the long-term buckling model in Equation (4.1) based on precisely controlled numerical tests similar to those conducted in the present study.

$$T_{cr} = \tilde{T}_0 (\frac{1}{P} - \frac{1}{P_{cr}})^n \tag{4.1}$$

By introducing the dimensionless pressure ratio PR = P/P_{cr}, the model be written as:

$$T_{cr} = T_0(\frac{b}{PR} - 1)^n \qquad (4.2)$$

This model accommodates the natural extremes of the problem by predicting a T_{cr} of 0 for a PR of 1 and a T_{cr} of infinity for a PR of 0. But the time constant T_0 is the nominal life of a certain constrained liner which is a function of critical pressure and depends on the DR, gap, ovality, and other imperfections. So, parameters T_0, n, and b depend on material properties and the liner/host-pipe configuration. Zhao's model has only been compared to the CPAR results. The results provided below evaluate the model for the BORSF test data.

The series of six long-term BORSF liner buckling experiments discussed in the literature review section will be simulated using finite element analysis. The finite element model will be identical to the model Zhao (1999) used in his study, in which 144x2 "composite" B21 beam elements were used. The composite beam elements consist of two standard beam elements connected at the ends, with one of the elements handling the tensile loading and the other handling the compressive loading. Both tensile and compressive elastic, perfectly plastic, power-law creep constitutive relations whose constants were determined based on material characterization results of specimens cut from the BORSF 8-inch 5.5-mm thick liner samples will be employed as listed in Table 4.8. The long-term mechanical properties of the five other BORSF liner series will be assumed to be identical to the BORSF 8-inch 5.5-mm thick liner series, since all six liner series were composed of the same resin and felt.

For each of the six pipe liner series, the average DR and gap were simulated resulting in the buckling times shown in Table 4.9. Seven FEM long-term runs for PR

ratios from 0.1 to 0.9 were performed following one short-term FEM calculation to decide the critical pressure. A total 48 FEM runs (6 liner series times 8 runs for PR equal to 0.1, 0.3, 0.5, 0.6, 0.7, 0.8 and 0.9 plus one short-term result) were completed and used to fit six sets of T_0, n, and b parameters as given in Table 4.10. Figure 4.2 shows a plot of the PR versus the buckling time for the 12 inch, 5.5 mm liners. The plots for the other liner series are given in Appendix C.

From Figure 4.3 – 4.8, it can be found that all the FEM results are less than the test data from the very beginning. One reason that may account for these lower results is the modulus value used. Since no compressive modulus is available, the flexural modulus is used to replace the compressive modulus, which will give conservative results. The final reason may be that the value of modulus is low (at least when compared to the CPAR modulus for the Insituform Enhanced product) and the predicted critical pressure is less than the test result. But, all of the finite element results have a good agreement with the Equation (4.2).

Table 4.8   Material Properties for the Long-term Buckling Simulations

	E (psi)	E´ (psi)	v	σ_y (psi)	$\sigma_y´$ (psi)	A $(psi^{-m} \cdot time^{-n})$	A´ $(psi^{-m} time^{-n})$	m	n
Tens.	453400	498242	0.3	3427	3766	7.83e-7	5.81e-7	1.0753	0.1991
Comp.	474083	520970	0.3	8541	9386	1.14e-7	0.85e-7	1.01	0.2921

Note:

(1) $E´ = E/(1- v^2)$

(2) $\sigma_y´ = \sigma_y/(1- v^2)$

(3) $A´ = A(3/4)^{(m-1)/2}$

Table 4.9 FEM Buckling Times for BORSF Long-term Test Simulations

PR	1255	1265	1275	845	850	855
0.90	4.68	6.24	7.17	4.93	4.44	3.28
0.80	1.42e2	175	178	121	100	65.5
0.70	1.47e3	1.799e3	1.737e3	1.277e3	1.035e3	734
0.60	9.60e3	1.1 54e4	1.071e4	7.833e3	6.717e3	5.039e3
0.50	5.20e4	6.129e4	5.55e4	4.154e4	3.634e4	2.848e4
0.30	1.61e6	1.826e6	1.603e6	1.236e6	1.12e6	9.433e5
0.10	2.33e8	3.259e8	2.136e8	2.188e8	2.075e8	1.786e8

Table 4.10 Fitting Constants for the Six Test Series Based on FEM Simulations

Type	n	T_0	b	P_{1h}	P_{10kh}	P_{50Y}
8" 4.5 inch	4.30356	36483.5	0.99902	56.978	35.592	22.267
8" 5.0 inch	4.04942	32375.8	0.999902	72.42	44.614	26.869
8" 5.5 inch	3.98269	39706.8	0.993652	87.29	54.707	33.037
12" 5.5 inch	3.90734	54685.7	0.981152	51.771	33.353	20.326
12" 6.5 inch	3.96186	62522.6	0.987402	66.969	43.626	26.985
12" 7.5 inch	3.84966	55420.3	0.987402	102.603	66.19	40.066
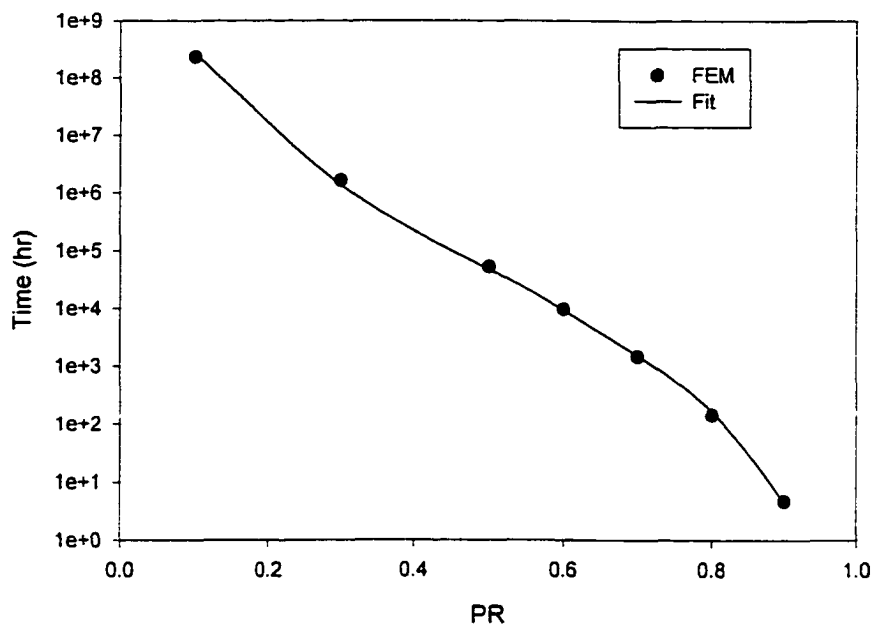
Figure 4.2   Typical Critical Time Pressure Ratio Fitting Curve for Simulation of BORSF Long-term Test Results (1255 series of pipe)
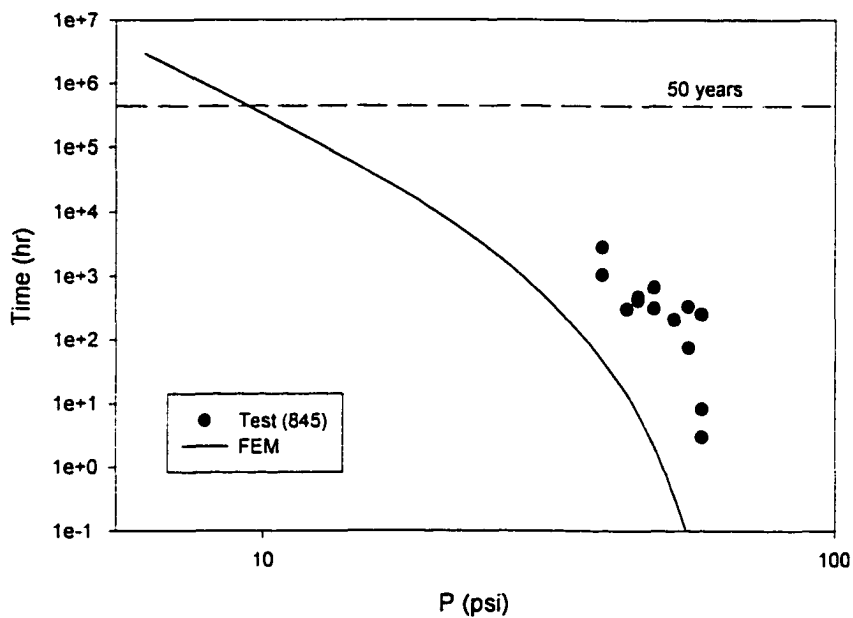
Figure 4.3   Comparison of Predicted and BORSF Test Results (845 series of pipe)
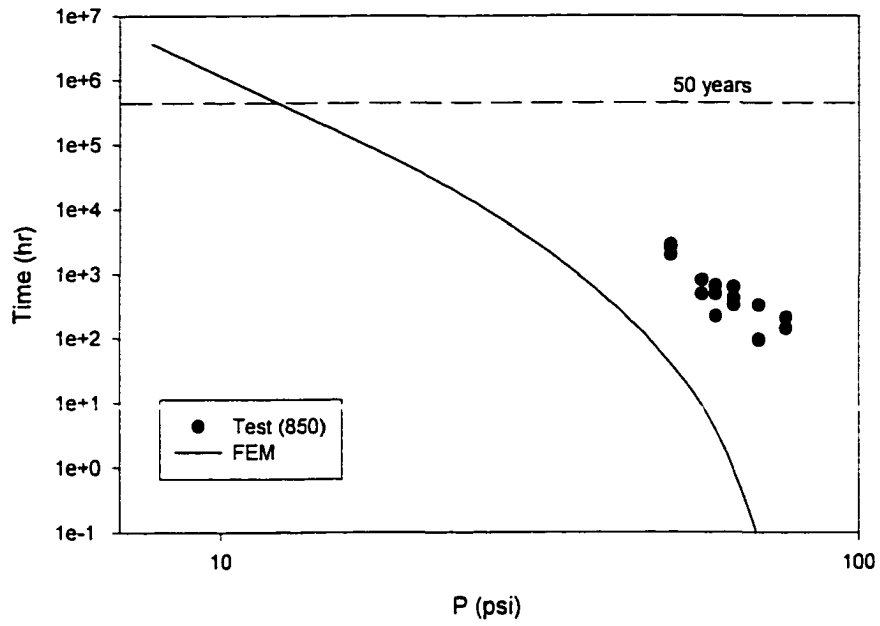
Figure 4.4   Comparison of Predicted and BORSF Test Results (850 series of pipe)
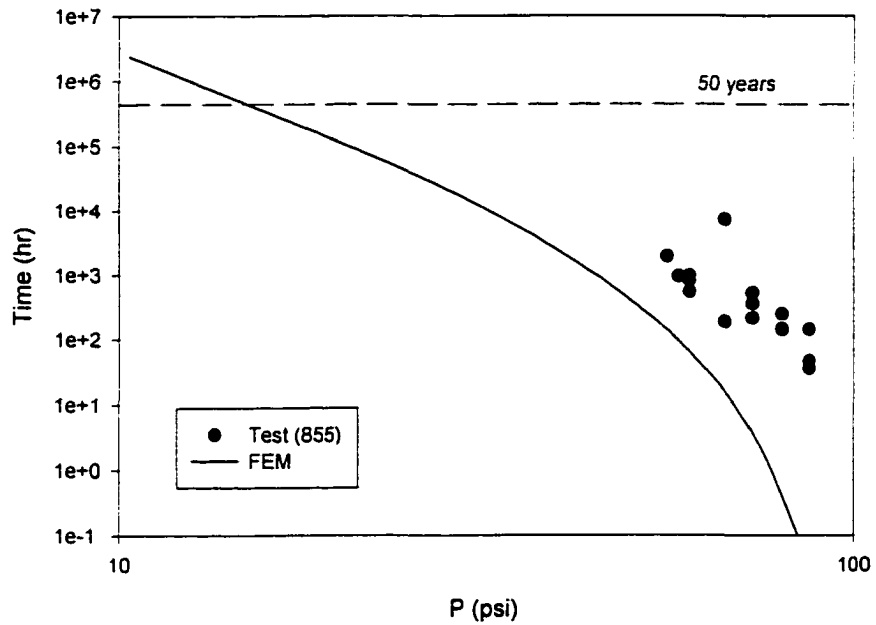
Figure 4.5   Comparison of Predicted and BORSF Test Results (855 series of pipe)
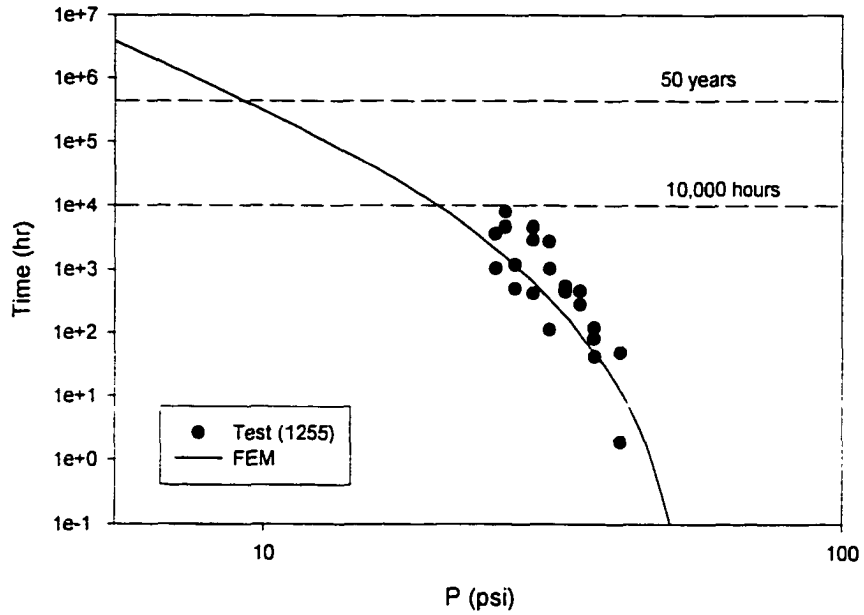
Figure 4.6　Comparison of Predicted and BORSF Test Results (1255 series of pipe)
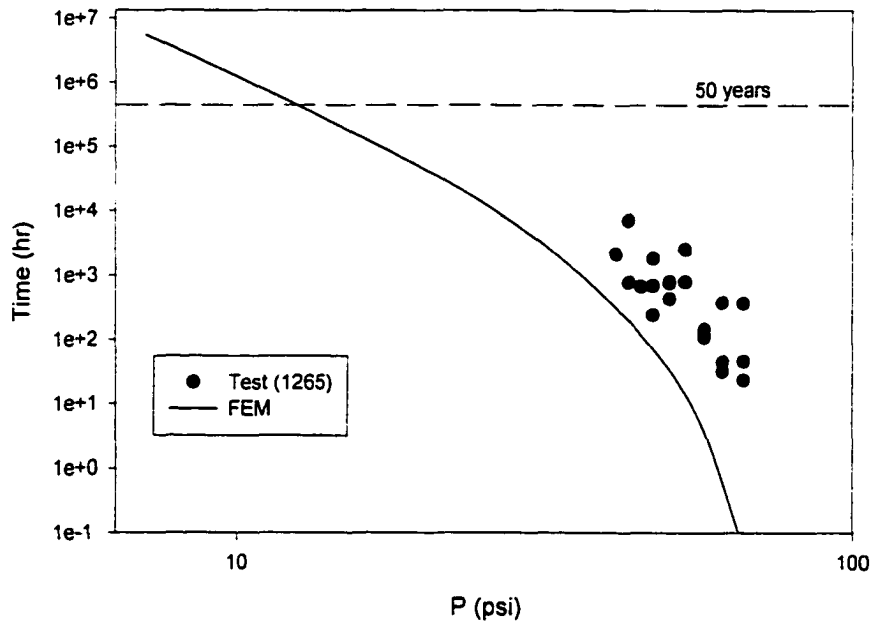
Figure 4.7　Comparison of Predicted and BORSF Test Results (1265 series of pipe)
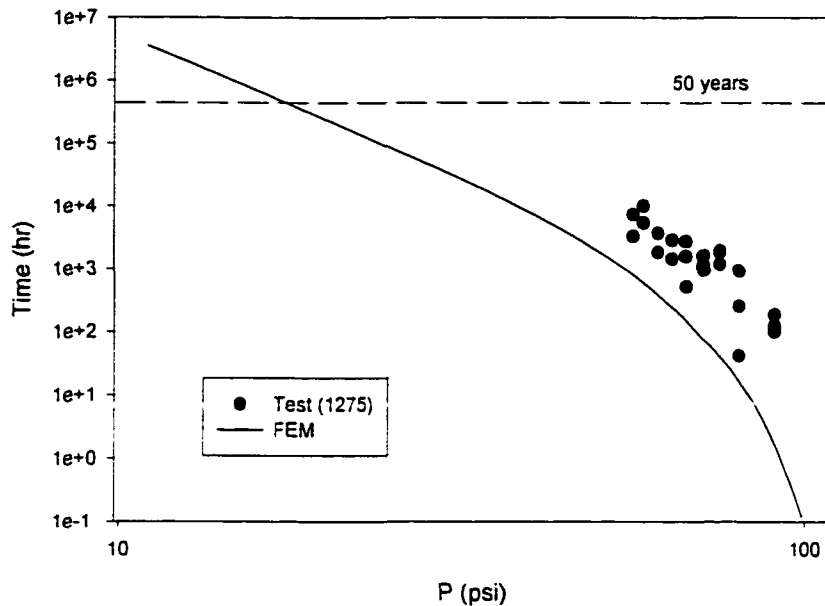
Figure 4.8 Comparison of Predicted and BORSF Test Results (1275 series of pipe)

4.5 Conclusions

Both experimental and numerical analyses are needed to quantify the factors which influence liner buckling. The experimental data provides a basis for the numerical data and more closely reflects the probable behavior of liners in the field, at least for the unrealistically high PR ratios used in the long-term testing. On the other hand, numerical analysis can isolate the effect of noise that cannot be avoided during testing, thus allowing the problem to be solved more systematically. The study presented in this chapter will provide a strong basis for the finite element analyses in the following chapters and serve as a gauge for the extent to which the results can be extended to field applications..

A number of factors with potential importance in pipe liner testing and analysis have been discussed, resulting in the following conclusions:

(1) Overlooking the effects of imperfections may result in system lifetimes much shorter than predicted when groundwater loading is a significant fraction of P_{cr}.

(2) Unaccounted-for factors which produce scatter in short-term buckling pressures may result in amplified scatter in long-term buckling times, where the amplification increases dramatically as the external pressure level approaches the critical pressure.

(3) Both the short- and long-term finite element models can effectively predict the liner buckling resistance for a given pressure when based on appropriate material properties and liner configurations. The finite element results appear to give conservative estimates of liner buckling pressure and lifetime.

(4) The long-term model suggested by Zhao (1999) as described in Equation (4.2) has a good agreement with finite element results.

CHAPTER 5

EVOLUTION OF STRESSES AND CONTACT CONDITIONS
IN SHORT-TERM BUCKLING

5.1 Introduction

There has been much debate in the industry over the type of material properties to use in the liner design models. While short-term flexural properties are currently used for design calculations in ASTM F1216, the use of short-term and/or long-term tensile, compressive, and flexural properties are also candidates for use in design models. Discussions at technical meetings indicate that there is a need to clearly understand the nature of the contact between a host pipe and its liner, liner deflections, and how the stresses vary around the circumference of a liner. While it is understood that the mechanical properties used for design purposes should be those which reflect the state of stress in a liner wall, the state of stress is not well understood.

The evolving contact forces, contact areas, deflections and stresses as a function of DR, ovality, and gap will be studied here by employing a finite element model based on an assumed two-lobe deformation mode, since two-lobe deformation histories are most commonly observed in experiments. The evolving conditions in the liner will be plotted versus the pressure, showing how the condition of the liner depends on ovality, gap, and DR. The distribution of the contact forces over the evolving contact area will be

62

shown, and nature of the enhancement in buckling pressure gained from this contact will be explained.

The stresses in the wall of the liner will be decomposed into flexural and compressive components, and the ratio of these two components will be plotted versus pressure and time. The ratio of these stresses will be used as a basis for selecting the material properties to use in design. The premise to be used is that the stress state at the most critical point that is dominant over the majority of the life should be used for design. For example, when the ratio of compressive to flexural stresses is equal to 1.0, then all of the stresses across the wall of the liner are in compression, indicating that compressive properties may be most relevant. The short-term results presented here provide a basis for material property selection for short-term liner buckling experiments and lay the essential groundwork for understanding long-term creep-induced liner buckling.

The mechanical properties corresponding to the Insituform Enhanced product tested in the CPAR program (Guice *et al.*, 1994) are used in the calculations here since both short-term and long-term material characterization tests have been performed for this material. However, the trends revealed in present study on this material are considered applicable to other isotropic polymeric liner products. In this chapter which deals with short-term liner behavior, an elastic, perfectly-plastic material model will be employed with a flexural Young's modulus of 538,621 psi, a Poisson's ratio of 0.35, and a flexural yield limit of 8405 psi.

5.2 Effect of Contact on Encased Pipe Liners

Equation (2.4) shows that the maximum flexural stress in the free pipe is strongly related to the radial deflection of the pipe through w. On the other hand, the radial

deformation of a constrained liner is restrained by the host pipe, thus limiting the deflection and the flexural stresses. The increase in the buckling resistance of a liner due to the support of the host pipe can be studied by considering the evolution of contact force and contact area around the circumference of the liner. This study of the contact evolution will also provide a better understanding of the evolving displacements and stresses discussed later in this chapter.

The state of the contact force on a liner varies with the position around the liner. As the liner begins to deform in response to the external pressure, it will usually form two lobes where the inward radial deflections are largest. Outward deflections at approximately 90° to the lobes will also occur resulting in liner-host pipe contact. Therefore, the largest contact pressure is at these two points at the very beginning. As the external pressure increases, the contact area is increased due to the increased deformation of the liner. Figure 5.1 gives the definition of the contact area in terms of the angle ø.

The distribution of the contact pressure is not uniform across the contact area. The largest contact pressure occurs near the location where the liner departs from the host-pipe (four points of high contact force exist for two-lobe bucking). As the external pressure increases, the contact area increases, and the location of the maximum contact pressure moves upward (when looking at the top half of the liner). In Figure 5.2, this phenomenon is plotted using finite element results. Notice that the peak force occurs at a higher angle as the pressure is increased and that the contact force is relatively small except near the point where the liner departs from the host pipe. Also notice that the total contact force and area both increase with increasing external pressure.

Figures 5.3 and 5.4 show that the total contact force and the contact area are higher for a given pressure level for thinner liners (liners with a higher DR) than for thicker liners. Figure 5.3 indicates that the total contact force on thinner liners at buckling is smaller than that on thicker liners, since the thinner liners have a lower buckling pressure. However, the thinner liners are more flexible and consequently have a larger contact area throughout the loading history, even under the same pressure to critical pressure ratio (PTCPR) as shown in Figure 5.5.

Liners with larger contact areas also have smaller lobes. Since a lobe can be idealized as a beam, the span of a lobe will decide the magnitude of the deflection, which is a function of fourth power of its span under uniform loading. Thus, the longer the span, the larger the deflection and the flexural stress in the liner for a given DR and pressure level. When the flexural stress exceeds the flexural strength or the deflection exceeds a critical value, the liner will become unstable and buckle.

The horizontal contact force on the liner plays another important role. From Figure 5.6, the peak moment at the middle of crown is reduced by the reverse moment induced by the contact force. The smaller moment produces a smaller deflection and stress level at the crown. The contact between the host pipe and the liner not only constrains the deformation in horizontal direction, but also reduces the deformation in vertical direction. This effect will further increase the liner's ability to resist collapse.

Again, thinner liners have a larger contact area and contact force for a given pressure, meaning that host pipe contact improves the buckling resistance of thinner liners more than thicker liners. This is the reason that the enhancement factor K increases with increasing DR.

The existence of gap and ovality in the pipe liner system is inevitable due to the construction method and the existing shape of the host pipe. Although a liner with a larger gap will have a larger contact force for a given pressure, as shown in Figure 5.7, the contact area between the host pipe and liner will be reduced as shown in Figure 5.8. Therefore, the larger gap will increase the length of the lobe. Since the moment in the beam is a function of square of its span under uniform loading, the gap will increase the moment, the stress, and the deformation in the liner, thereby reducing its buckling resistance. This can also explain why liners with a non-uniform gap buckling in a one-lobe mode have a lower critical pressure than those with a uniform gap buckling in a two-lobe mode.

In Figure 5.9, it also can be found that the liner with higher level of ovality will receive more support from the host pipe for the same external pressure. However, the contact areas at buckling for liners with different ovalities are almost identical, as shown in Figure 5.10. The enhancement factor K relative to a liner installed in a round host pipe is still reduced due to ovality as shown in Table 5.1, even though the contact force is higher for higher ovality levels. This reduction can be rationalized by understanding that the major and minor diameters of the oval liner result in a larger effective lobe span and a reduced resistance to buckling.

Table 5.1   Reduction Factor and Enhancement Factor K in Buckling
Pressures Due to Ovality

		Oval 0%	Oval 3%	Oval 6%
DR = 40 Gap = 0.25%	P_{cr}	152	132	114
	Reduction Factor	0	0.868	0.75
DR = 40 Free Pipe	P_{cr}	17.2	15.6	14.1
	Reduction Factor	0	0.907	0.82
Enhancement Factor K		8.83	8.46	8.085
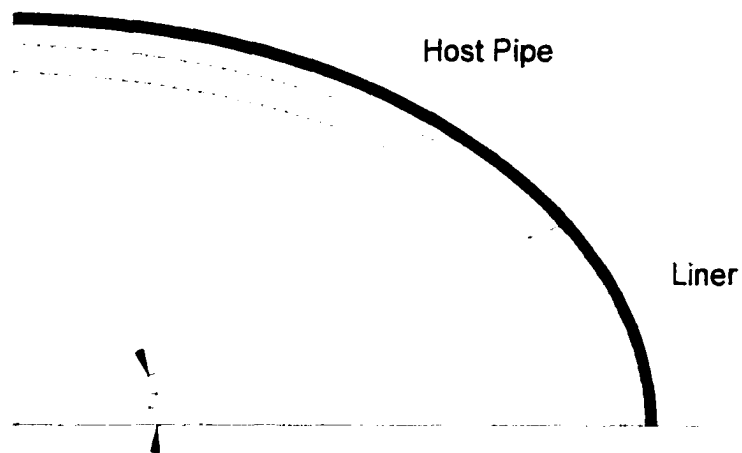
Host Pipe

Liner

Figure 5.1   Angle $\varnothing$ Defines the Contact Area between the Host Pipe and the Liner
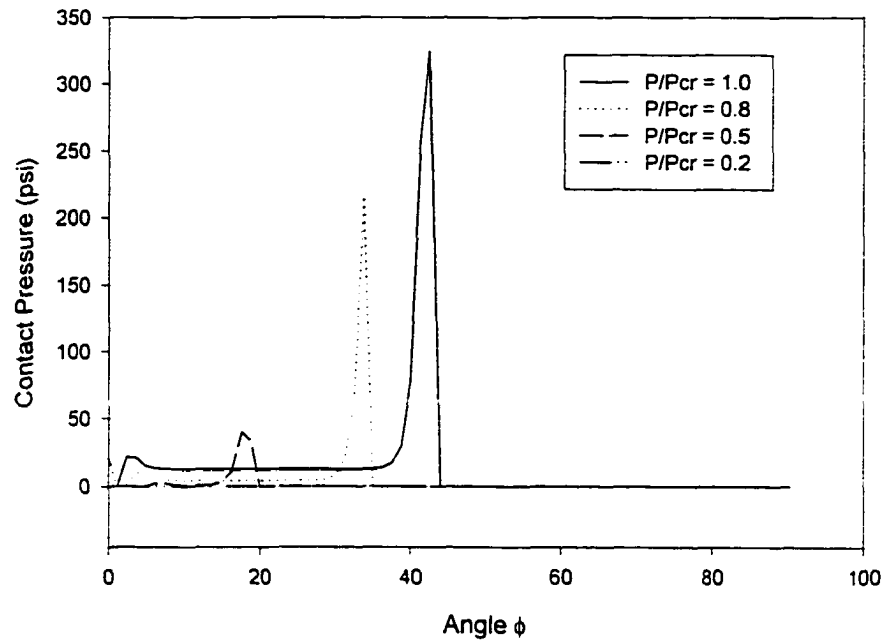
Figure 5.2   Contact Pressure Evolution (DR = 40, Oval = 0%, Gap = 0.25%)
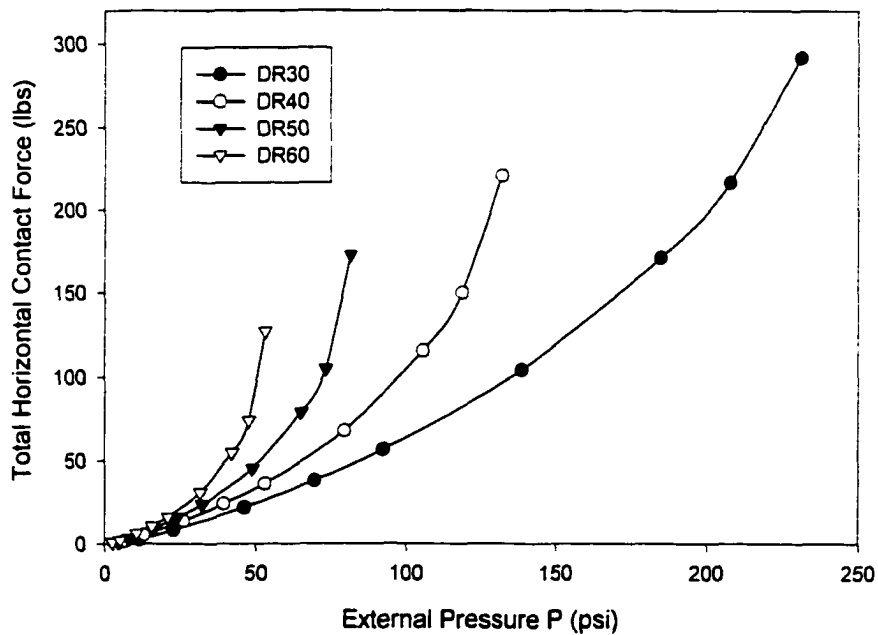
Figure 5.3   Contact Force Evolution under the Effect of DR
(Oval = 3%, Gap = 0.25%)
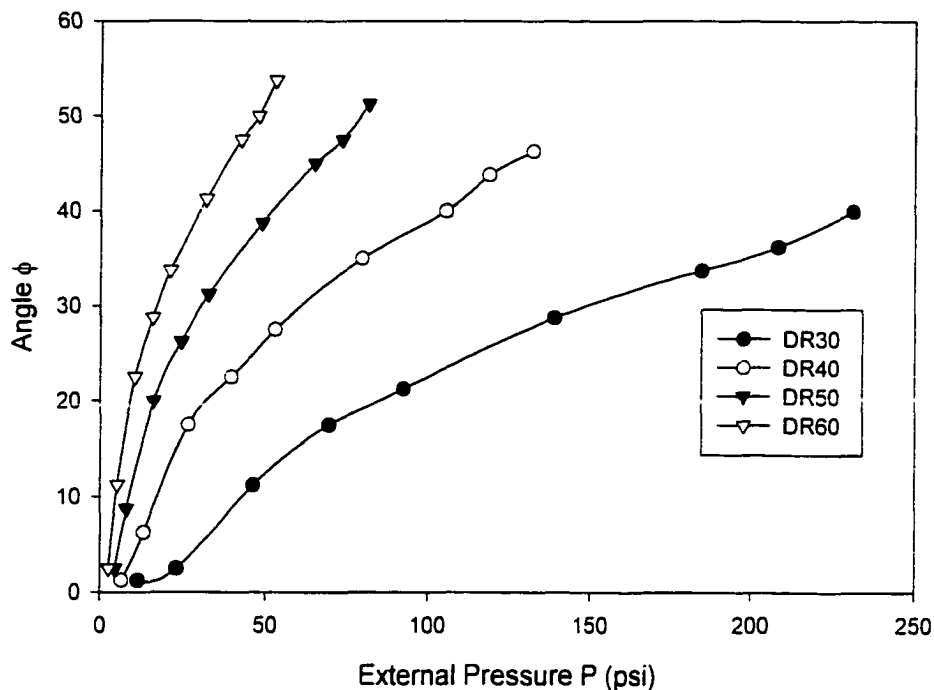
Figure 5.4   Contact Area Evolution under the Effect of DR
(Oval = 3%, Gap = 0.25%)
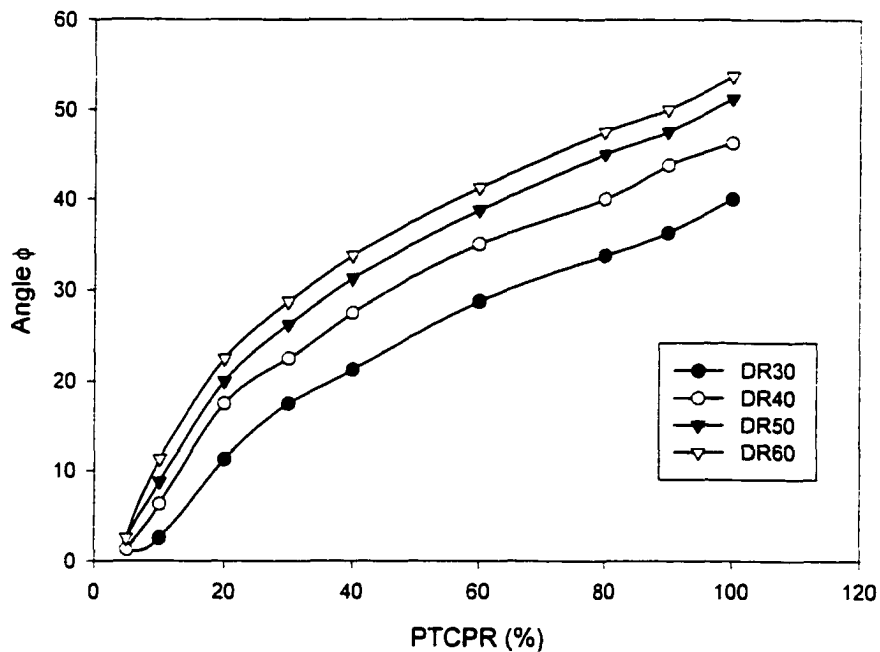
Figure 5.5   Contact Area Evolution under the Effect of DR
(Oval = 3%, Gap = 0.25%)

(a) Effect of Pressure on the Internal Moment

(b) Effect of Contact Force on the Internal Moment

(c) Combined Effect of Pressure and Contact Force
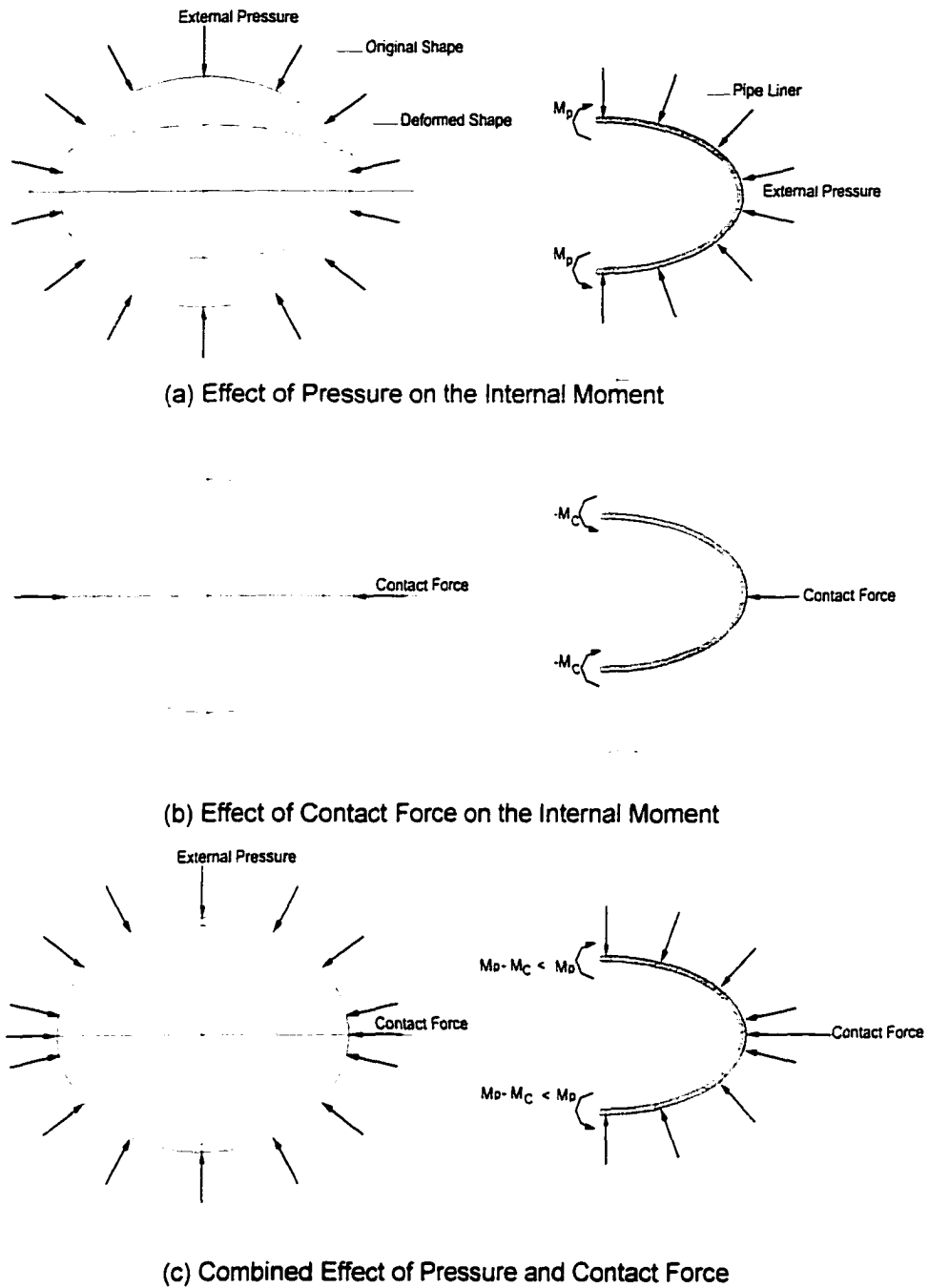
Figure 5.6   Effect of Contact Force on the Moment at the Middle of the Crown
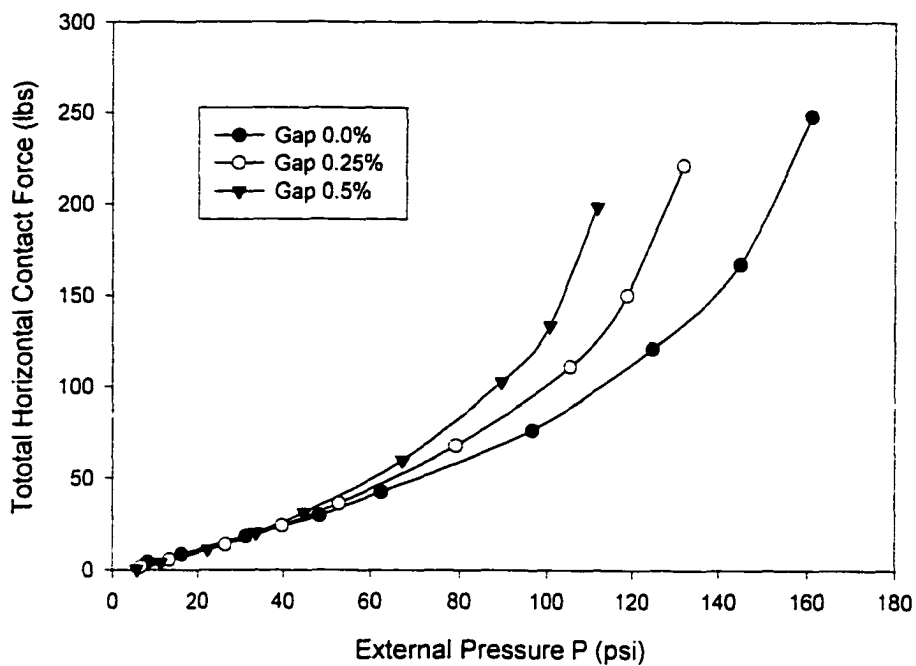
Figure 5.7 Contact Force Evolution under the Effect of Gap
(DR = 40, Oval = 3%)
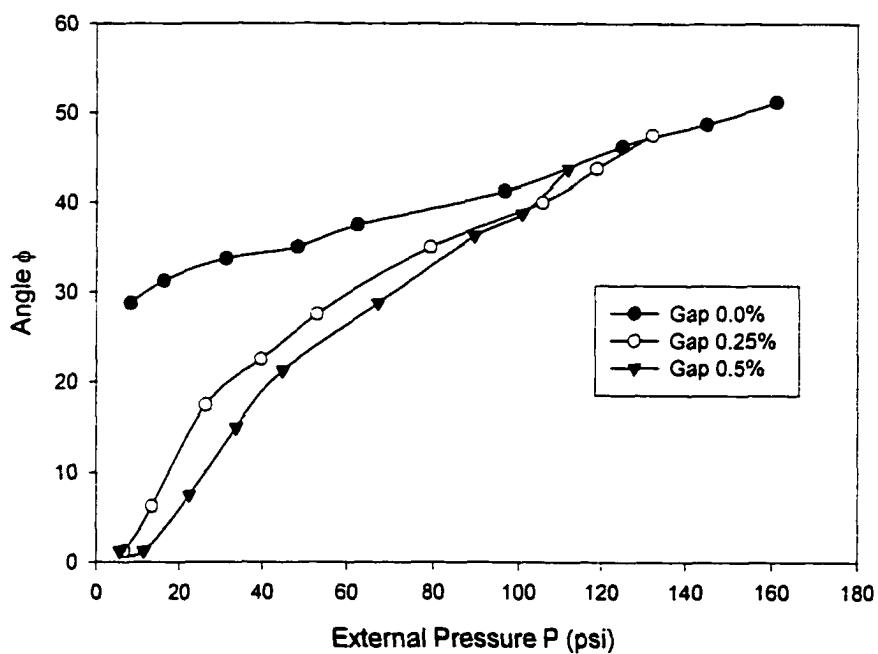
Figure 5.8 Contact Area Evolution under the Effect of Gap
(DR = 40, Oval = 3%)
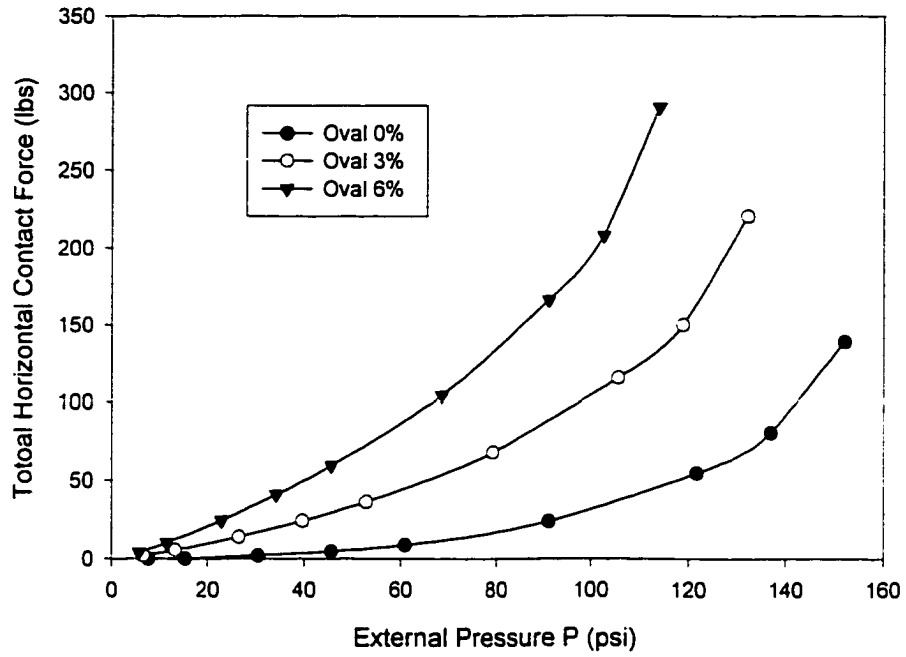
Figure 5.9   Contact Force Evolution under the Effect of Ovality
(DR = 40, Gap = 0.25%)
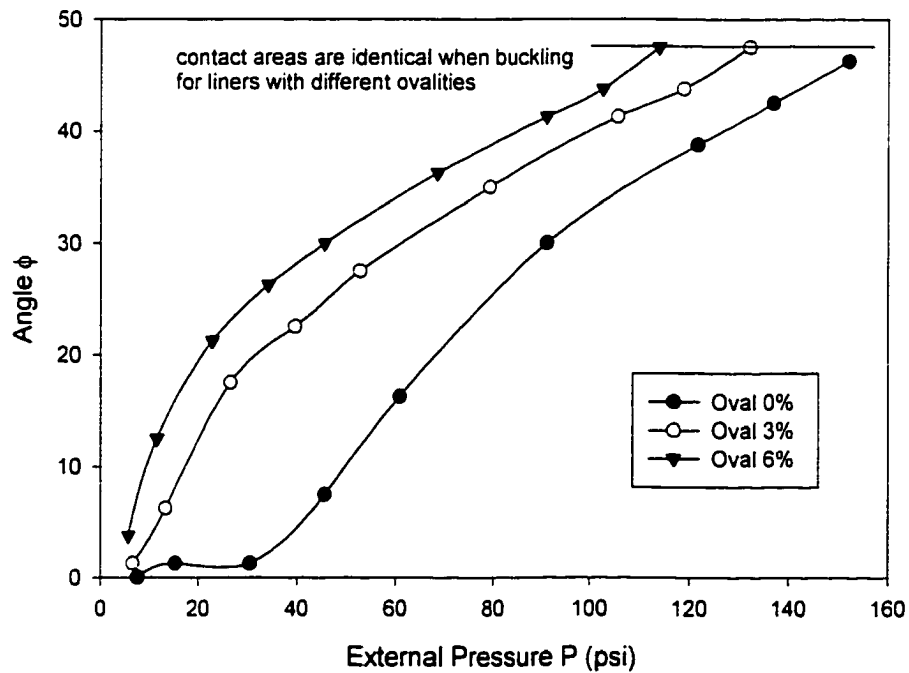
Figure 5.10   Contact Area Evolution under the Effect of Ovality
(DR = 40, Gap = 0.25%)

5.3   Effect of Imperfections on Deflection Evolution

The deformation of a liner depends on the external pressure, the shape of the liner and its stiffness. Thicker liners have less deformation than thinner liners for the same pressure, and the magnitude of the deformation increases with increasing pressure, gap, and ovality.

From Equations (2.4) and (2.6), it is evident that the flexural stress and the deflection d are related to the out-of-roundness w in a similar way for a free standing pipe. However, when liner/host-pipe contact is present, the deformation and the flexural stress no longer have such a simple relationship. The flexural stress in the pipe liner is still a function of the local curvature, which is strongly related to the deformation of the liner. The improved understanding of the deflection evolution presented in this section will aid in the understanding of the stress evolution presented in the next section.

The maximum deflections at the middle of the crown under different external pressure levels are recorded for DRs of 30, 40, 50 and 60, a gap ratio of 0.25%, and an ovality of 3% in Figure 5.11. The magnitude of the maximum deflection in the liner increases nonlinearly with the external pressure due to large deflections and contact. The deformation in the thinner pipe is much larger than the thicker pipe for the same external pressure level, with the rate of deflection per unit pressure increasing as buckling is approached. The deformation of a pipe with a DR of 60 is about twice as large as the deformation of a pipe with a DR of 30 for a pressure of 25 psi, while the ratio is increased to three for an external pressure of 50 psi. However, notice from Figure 5.12 that the deflections as a function of the pressure to critical pressure ratio (PTCPR) are independent of DR. The peak deflections at buckling are roughly equal for all of the

liners, implying that the liners with a given host pipe geometry and material stiffness lose stability suddenly when they reach a critical displacement. The dependence of the peak deflection on the pressure ratio is similar for a free pipe, since Equation (2.6) depends on PTCPR and not on DR. Even though free pipes undergo more deformation prior to buckling as shown in Figure 5.12, keep in mind that the critical pressures are much larger for encased liners.

The peak deflection is also a strong function of geometric imperfections including gap and ovality, as seen in Figures 5.13 and 5.15 for encased liners and in 5.14 for a free standing pipe. It can be seem that the deflection lines are almost parallel for encased liners when considering the effect of PTCPR only, with the level of deformation increasing with increasing gap and ovality. Comparing Figures 5.13 and 5.15 indicates that gap has a greater effect on deflections than ovalities for the ranges of gap and ovality commonly encountered in field applications. This is supported by Figure 5.14 which shows that the deflection increases substantially for free pipes when compared to encased liners, since the effect of a very large gap is to drive the behavior more toward free pipe behavior due to the loss of contact area.

Comparing the Figures 5.14 with Figure 5.15, we see that the deformation of the free pipe is about 12 times that of constrained liner for an ovality of 6%, while the factor drops to 6.5 times for an ovality of 3%. Thus, liners with a larger ovality receive much greater enhancement due to encasement than liners with smaller ovalities when the enhancement factor is based on the behavior of free standing ovalized pipes (not on the behavior of a free round pipe). Since the final contact areas are almost the same for the

liners with different ovality levels, the final deflections of the encased liners are very close in Figure 5.15, which is much different from the free pipes in Figure 5.14.
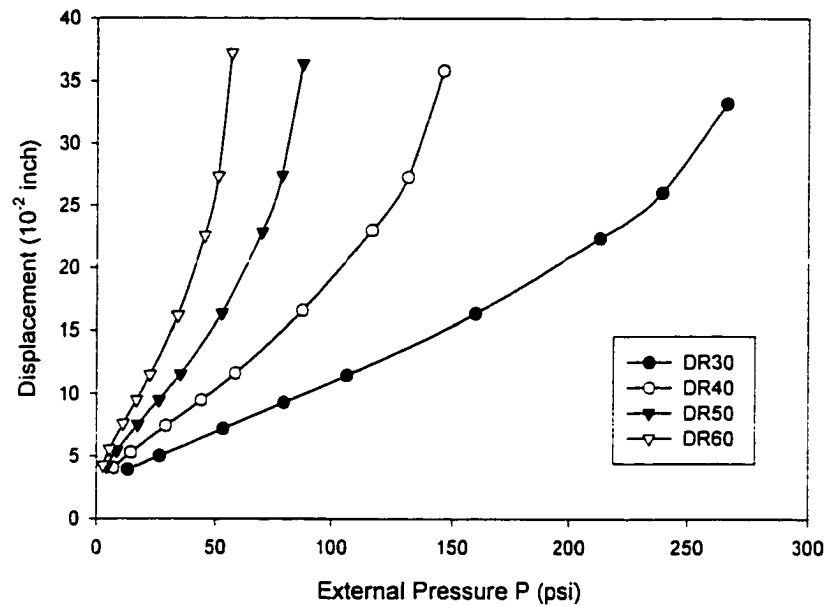
Figure 5.11   Displacement Evolution Under the Effect of DR
(Oval = 3%, Gap = 0.25%)
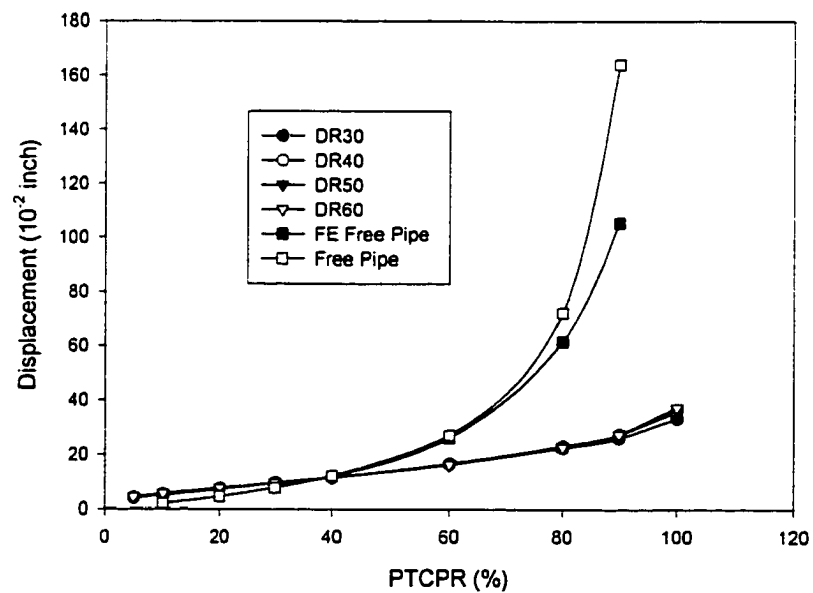
Figure 5.12   Displacement Evolution Under the Effect of DR
(Oval = 3%, Gap = 0.25%)
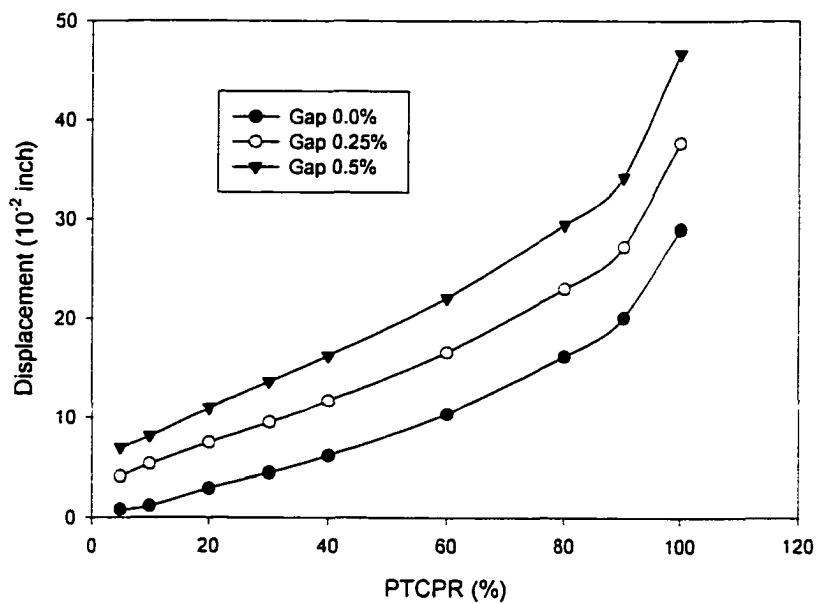
Figure 5.13 Displacement Evolution Under the Effect of Gap
(Oval = 3%, DR = 40)
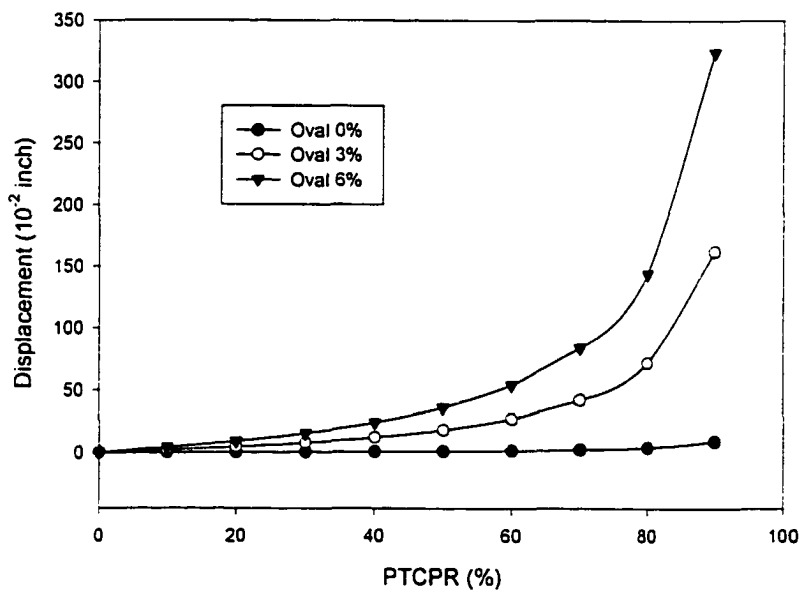
Figure 5.14 Displacement Evolution for an Unsupported Pipe under the Effect of Ovality
(Gap = 0.25%, DR = 40)
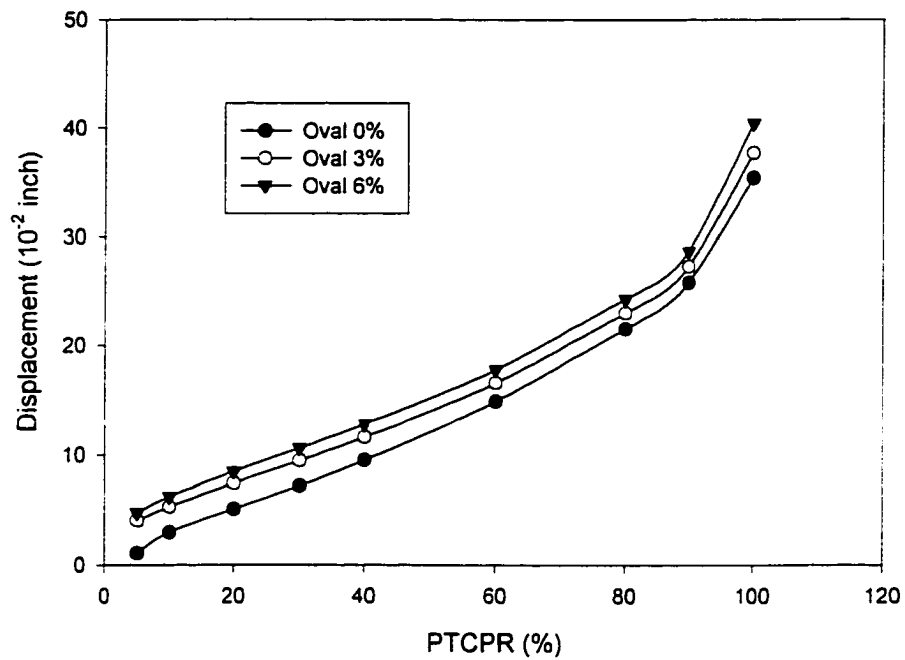
Figure 5.15 Displacement Evolution Under the Effect of Ovality
(Gap = 0.25%, DR = 40)

5.4 Stress Evolution

The stress evolution under short-term pressure loading can be understood by considering both the compressive hoop stress due to external pressure loading and the flexural stress associated with a curvature change at the lobe. For an elliptical free pipe, the peak flexural stresses are at the middle of crown of the pipe and will be increased as the pressure increases. The flexural stress to hoop stress ratio (FTHR) monotonically increases as the pressure to critical pressure ratio (PTCPR) increases, as shown in Figure 5.16. For a given PTCPR, the FTHR is higher for thinner liners due to their larger deflection and curvature. For free pipes, the flexural stress is dominant over the hoop stress for a majority of the pressure history, which can be seen by examining Figure 5.16.
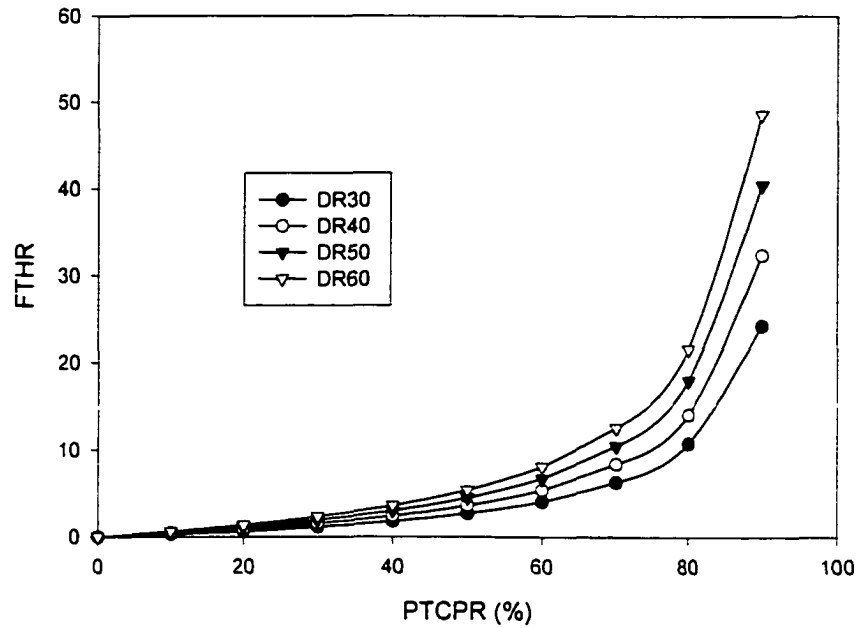
Figure 5.16   FTHR Evolution For Unsupported Elliptical Pipe
under the Effect of DR (Oval = 3%)

The stresses for element set A in the constrained pipe liner shown earlier in Figure

3.2 can be decomposed into (almost) pure bending and pure compression. Figure 5.17(a)

shows a contour plot of the stress across the thickness of the liner at element set A, where

the stress varies from 3,640 psi in compression at the outer fiber to 612 psi in

compression at the inner fiber. This stress distribution can be approximated by

superimposing the flexural and compressive components of stress, as depicted in Figure

5.17(b).
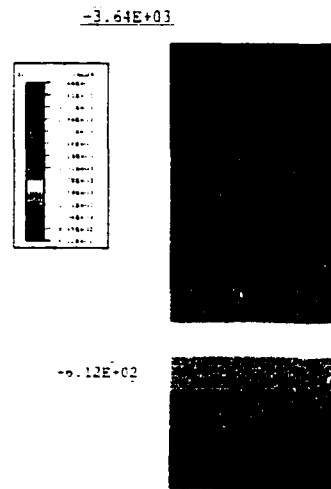
a. Contour Plot for Element Set A

Flexural Stress   Hoop Stress

b. Superposition for Element Set A

Figure 5.17   Stress Decomposition for Element Set A

As pressure is increased from zero, the thinner liner quickly touches the host-pipe and begins to receive sidewall support. The contact forces associated with this sidewall support induce a reverse moment, as described earlier, which reduces the moment at the crown and thus results in a reduction of the flexural component of stress at the crown.

This decrease in flexural stress corresponds to a decreasing FTHR with increasing pressure in Figure 5.18. However, as the pressure is further increased, the decrease in flexural stress due to increasing contact force begins to lose out to the increase in flexural stress due to increasing pressure, partly due to the decreasing moment arm associated with the peak contact force. This results in a FTHR that then begins to increase monotonically until collapse. Notice from Figure 5.18 that the minimum value of FTHR occurs at a lower external pressure for thinner liners. The thinner liners also reach a higher value of FTHR prior to failure.

Using the simple formula for the flexural stress in a beam (My/I) and the expression for hoop stress (PR/t), the FTHR can be written as

$$FTHR = \frac{\dfrac{6 \cdot M}{t^2}}{\dfrac{P \cdot R}{t}}$$

(5.1)

The ratio of the FHTR for a DR of 30 to the FTHR for a DR of 40 (under same pressure) can be reduced to

$$\frac{FTHR_{40}}{FTHR_{30}} = \frac{M_{40}}{t_{40}} \cdot \frac{t_{30}}{M_{30}}$$

(5.2)

For liners with DRs of 30 and 40 as in Figure 5.18,

$$\frac{M_{40}}{M_{30}} < \frac{t_{40}}{t_{30}} = 0.75, \qquad \text{before A}$$

$$\frac{M_{40}}{M_{30}} = \frac{t_{40}}{t_{30}} = 0.75, \qquad \text{at A}$$

$$\frac{M_{40}}{M_{30}} > \frac{t_{40}}{t_{30}} = 0.75, \qquad \text{after A}$$

This means that $FTHR_{40}$ will be less than $FTHR_{30}$ before A, equal to FTHR at A, and greater than FTHR after A. Figure 5.18 reflects this crossover of FTHR ratios before and after point A.

The results are Figure 5.18 are replotted in terms of the PTCPR ratio in Figure 5.19, showing that thinner liners always have higher FTHR ratios than thicker liners for a given PTCPR ratio. When the thickness of pipe is large, as for a DR of 30, the liner will only be in compression since FTHR is less than 2. Note that for a FTHR less than two, the stresses at all points through the cross section are compressive, as described in Chapter 6.

From Figure 5.20, it is evident that the shape of FTHR evolution curves as a function of ovality for unsupported pipes are very similar to the deformation evolution curves for unsupported pipes shown in Figure 5.14. But, the shape of the FTHR curves in Figure 5.21 for constrained liners is significantly different from the deformation history shown in Figure 5.15 due to the effect of contact. The FTHR curve for the constrained pipe is reduced about 36 times for an ovality of 6% when compared to the curve for free pipes. For constrained liners, increasing ovality will result in an increasing FTHR value, thus reducing the constrained liner buckling resistance.

Figure 5.22 shows that an increasing gap corresponds to an increasing FTHR value. The gap appears to cause a larger increase in the FTHR than ovality due to the decreasing contact area and increasing the span of the lobe, as described earlier.

Figure 5.23 shows the variation of the FTHR value around the circumference of the liner for a PTCPR of 0.50. Notice that the stress is almost pure compression for the portion of the liner that contacts the host-pipe. However, the flexural component

becomes important as the liner departs from the sidewall and reaches a peak at an angle

of 42° to 50° at the middle of reversed lobe. Notice that the length of the lobe is smaller

for higher DR as reflected by larger angles where the peak occurs (more contact occurs

for thinner liners). The peak magnitude of stress occurs at the center of the lobe as

expected. The FTHR evolution of element set B described in Figure 3.2 is shown in

Figure 5.24. The FTHR tends to zero after the pipe liner touches the host pipe, indicating

a stress state which is almost pure compression.
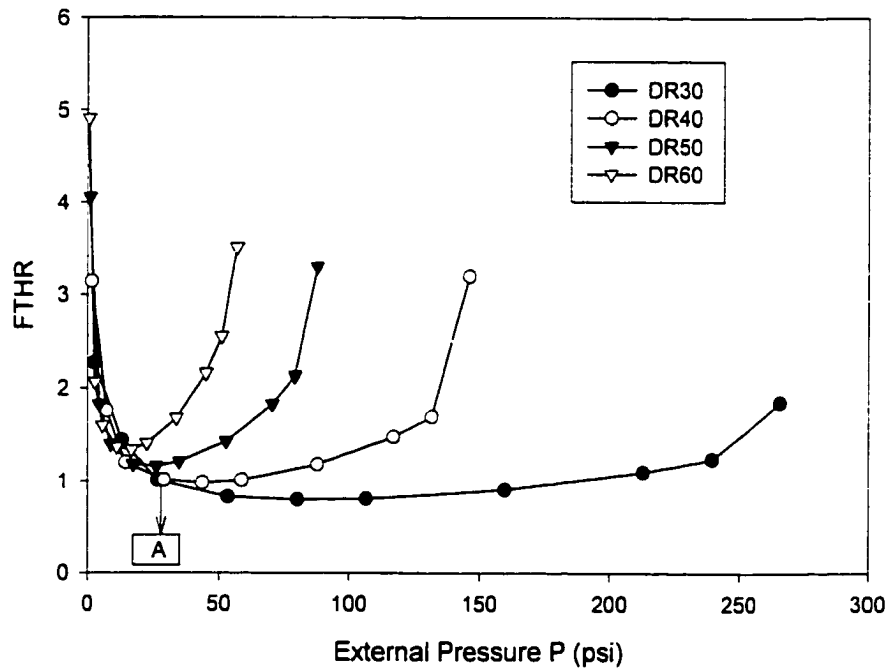
Figure 5.18   FTHR Evolution under the Effect of DR at Element Set A
(Oval = 3%, Gap = 0.25%)
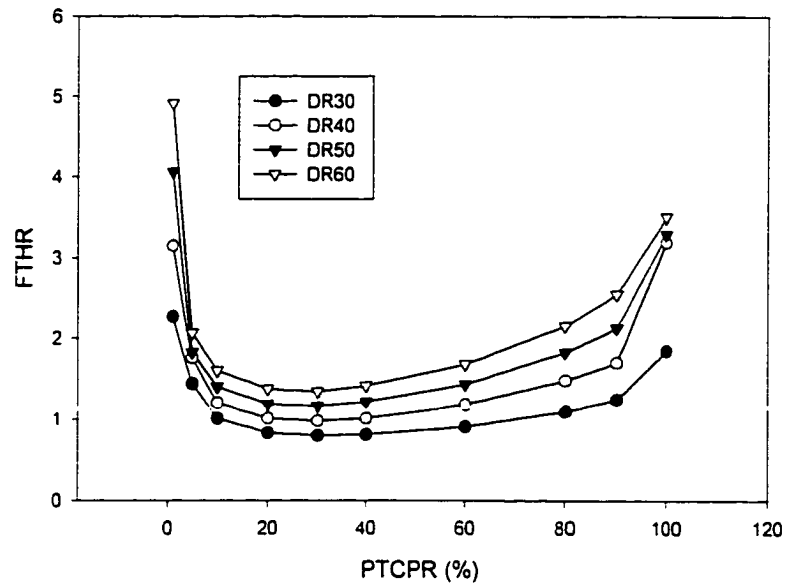
Figure 5.19   FTHR Evolution under the Effect of DR at Element Set A
(Oval = 3%, Gap = 0.25%)
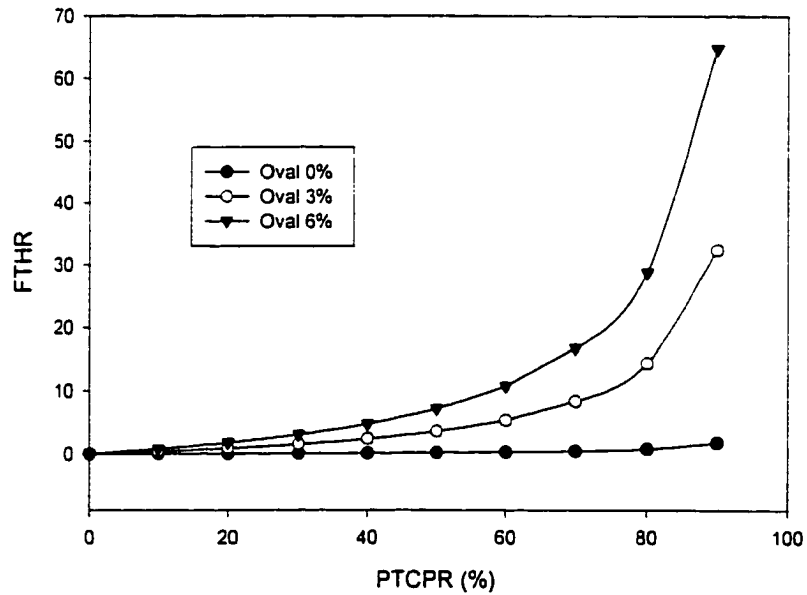
Figure 5.20   FTHR Evolution for Free Pipe under the Effect of Ovality
at Element Set A (DR = 40)
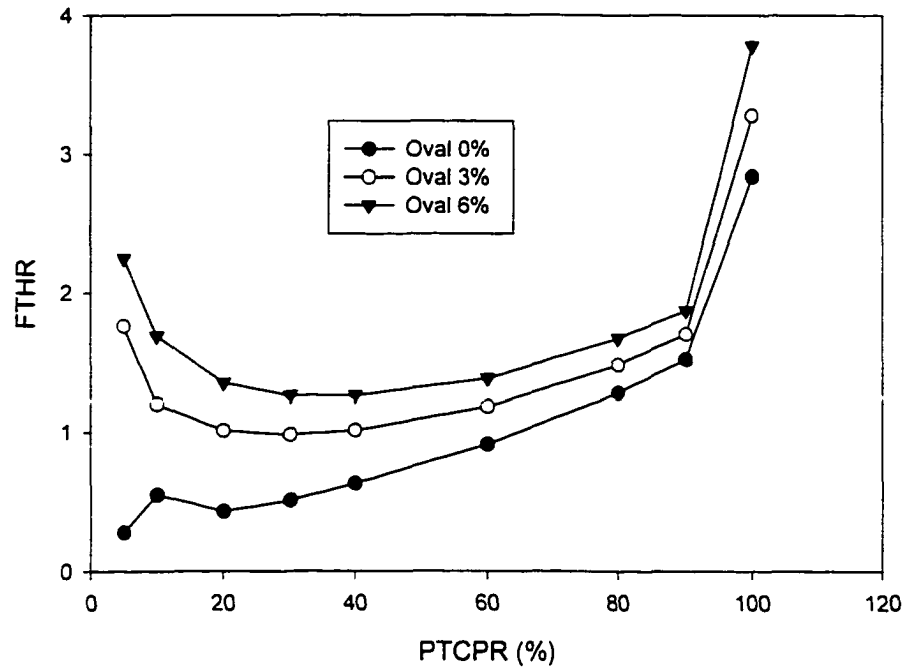
Figure 5.21   FTHR Evolution Under the Effect of Ovality at Element Set A
(DR = 40, Gap = 0.25%)
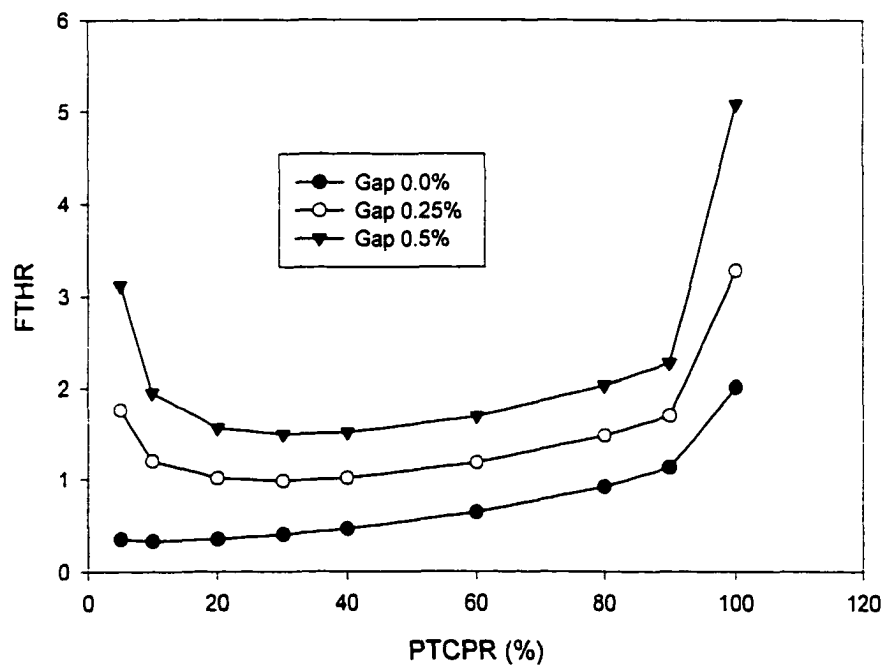
Figure 5.22   FTHR Evolution Under the Effect of Gap at Element Set A
(DR = 40, Oval = 3%)
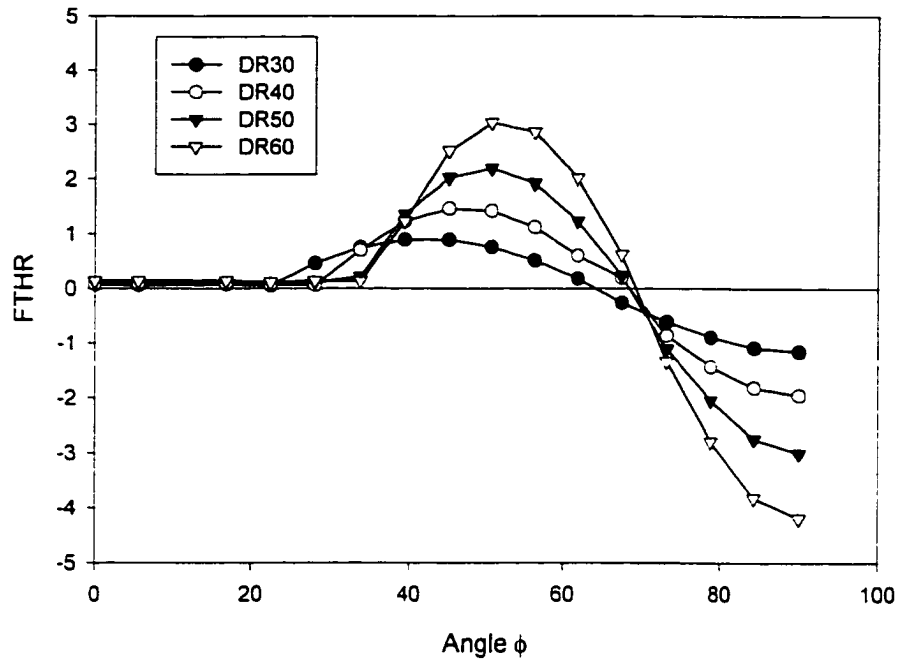
Figure 5.23   FTHR Evolution along the Pipe Liner Circumference under the Effect of DR (Oval = 3%, Gap = 0.25%, PTCPR = 0.5)
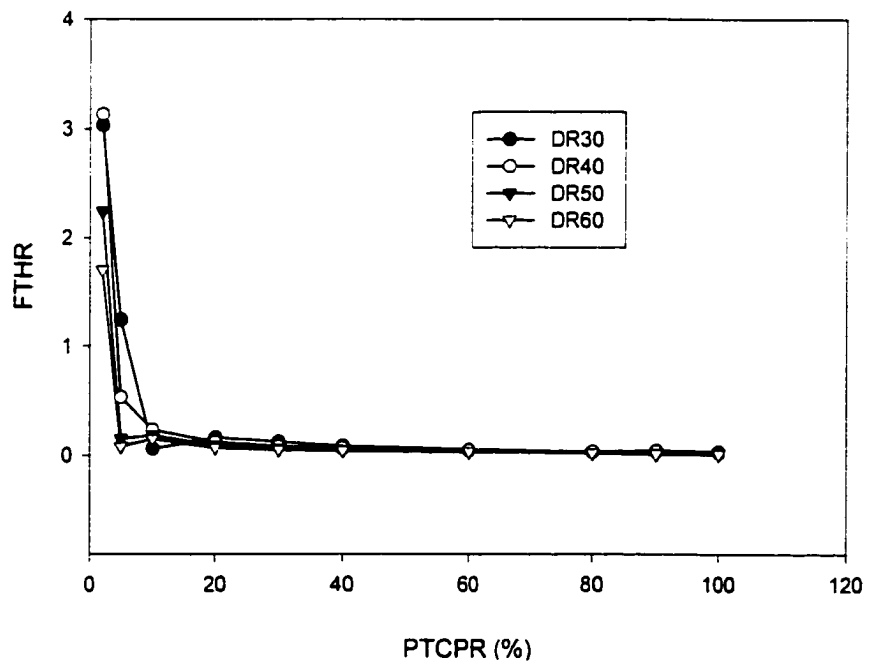
Figure 5.24   FTHR under the Effect of DR at C (Oval = 3%, Gap = 0.25%)

5.5 Observations

Conclusions for the evolution of contact conditions, deformations, and stresses in encased liners under short-term loading conditions are given below:

Contact Condition Evolution:

- The contact pressure varies with position around the liner, with the peak pressure occurring at the location where the liner departs from the host-pipe.

- For a given liner, the magnitude of the total contact force increases with increasing pressure.

- The total contact force is higher for thinner liners at a given pressure, while thicker liners eventually develop larger contact forces due to their higher buckling pressures. Consequently, for groundwater pressures which are a small fraction of the buckling pressure, thinner liners will receive more benefit due to host-pipe contact.

- Thinner liners have larger contact areas than thicker liners.

- The total contact force and area decrease with increasing gap.

- The total contact force increases with increasing ovality, while the contact area is roughly independent of ovality when the liner approaches buckling.

- The contact area appears to have a more important effect on buckling than the contact force.

Deformation Evolution:

- Thicker liners have less deflection than thinner liners for the same pressure, and the magnitude of deflection increases with increasing pressure, gap and ovality.

- The peak deflection at buckling is roughly independent of DR.

Stress Evolution:

- It is possible to approximately decompose the stress state in the wall of the liner into compressive and flexural components.

- The stresses in the area where the liner contacts the host pipe is dominated by compression.

- Two regions of high stress occur in the liner. The first region is between where the liner departs from the host-pipe and the center of the lobe (referred to as the reversed lobe above). The second region is at the center of the lobe, where the magnitude of the stress is highest. This is the critical point of the liner.

- Flexural stress is dominant at the critical point for pressures that are small compared to the critical pressure. As the pressure is increased, the FTHR (flexural to hoop stress ratio) decreases due to sidewall contact until a minimum value is reached where compression is dominant. Further increases in pressure cause the FTHR to increase, with flexural stresses becoming dominant as buckling is approached.

- The flexural stresses in a liner increase with increasing DR (thinner liners), ovality and gap.

Overall Conclusions:

- The larger contact force and area associated with thinner liners is associated with the higher enhancement factors (K) that have been observed experimentally. The larger contact area for thinner liners results in a shorter span for the lobe, thus decreasing deflections and stresses and increasing the buckling pressure.

- The contact force results in a reverse moment that decreases the stress level at the lobe, especially prior to the time that inverse curvature at the lobe is formed.

- Gap appears to result in larger decreases in the critical pressure than ovality for conditions likely to be experienced in the field, since the available contact area decreases significantly with increasing gap.

- Flexural stress is dominant at the time of buckling for short-term tests, indicating that flexural material properties should be used for short-term buckling predictions.

CHAPTER 6

EVOLUTION OF DISPLACEMENTS AND STRESSES
IN LONG-TERM BUCKLING

6.1 Introduction

There has been much discussion regarding the appropriate material properties to use in liner buckling analysis and design models (Whittle and Schrock, 1999). In general, the material properties used for analysis purposes should be measured under similar loading conditions that a body will encounter during service. For example, if compressive stresses are dominant during the life of a part, the compressive material properties should be used for analysis purposes. This chapter will examine the evolution of the stresses at the critical point in the liner so recommendations can be put forth regarding the most appropriate mechanical properties to used for long-term liner design.

Many of the characteristics of the evolution of contact conditions, displacements and stresses for short-term buckling can be directly extended to long-term buckling. For example, the critical point on the liner for long-term buckling is also at the center of the lobe(s), and the stresses can still be decomposed into flexural and compressive components. Moreover, the mechanisms by which the displacements and stresses are restrained due to liner/host-pipe contact remain unchanged.

89

However, the presence of time-dependent creep deformation can lead to some interesting and possibly unexpected results. Creep-induced buckling may occur at pressure levels that are significantly less than the critical pressure, and the stress state at the critical point may be significantly influenced by stress relaxation. It will be seen that applying different pressure levels to liners can result in major changes in the character of the stress and deformation histories. For this reason, it is especially important to understand the behavior of liners at pressure levels expected in field applications (usually 20% of Pcr or less). At these low pressures, it will be demonstrated that radial deflections significant enough to form inverse curvature at the lobes may not accumulate within the design life (usually 50 years).

To date, most of the long-term liner buckling tests have been performed at relatively high pressures which may result in material behavior that differs significantly from that expected in normal use. Most polymeric materials have much different material properties for different stress states, and the relationship of the stress level to the creep rate of a material may be nonlinear, particularly at lower stress levels. Choosing the appropriate material properties to apply in design calculations can lead to a more predictable and economical liner system.

All liner simulations in this chapter will assume a two-lobe deformation mode to reflect experimental observations. Host pipe ovality will be varied from 0% to 6%, the gap ratio will be varied from 0% to 0.7%, and the DR will be varied from 30 to 60. These ranges are representative of what is expected in field applications. The definition of ovality and gap is the same as what has been described in Chapter 3. The material properties associated with the Insituform Enhanced product of the CPAR tests will be

used, with a flexural modulus E of 538,621 psi, a Possion's ratio v of 0.35, a flexural strength σ_y of 8,405 psi, a creep coefficient A of 1.00788e-8 $\text{psi}^{-m} \text{time}^{-n}$, creep stress exponent m of 1.14585, and creep time exponent n of 0.24. These properties will be embedded in the ABAQUS FEM model. The trends revealed here are extendable to other similar polymeric materials.

6.2   Evolution of Liner Deflections

The evolving conditions in the liner are also a strong function of the external pressure level and the creep properties of the material, as discussed in the following sections.

6.2.1   Effect of External Pressure

The pressure level at which a liner is loaded is perhaps the single most dominant variable in long-term buckling analysis, with the exception of material properties. The time-deflection curves for various pressure levels (i.e., PR = 0.1, 0.3, 0.5, 0.6, 0.7, 0.8, 0.9) illustrated in Figure 6.1 show that the critical time and the peak deflection increase as the external pressure level decreases. This result indicates that the peak deflections associated with liner buckling tests will be significantly smaller than the peak deflections of liners in the field, since most field loading is less then 20% of the critical pressure.

Figure 6.2 shows that DR is of secondary importance when considering the effects of pressure level on long-term buckling, since the plots for different DRs are grouped together for a given pressure level. As the pressure ratio increases, the rate of deformation accelerates with passing time. This rate of deformation becomes very high after inverse curvature occurs at the lobes, indicating that failure is imminent.
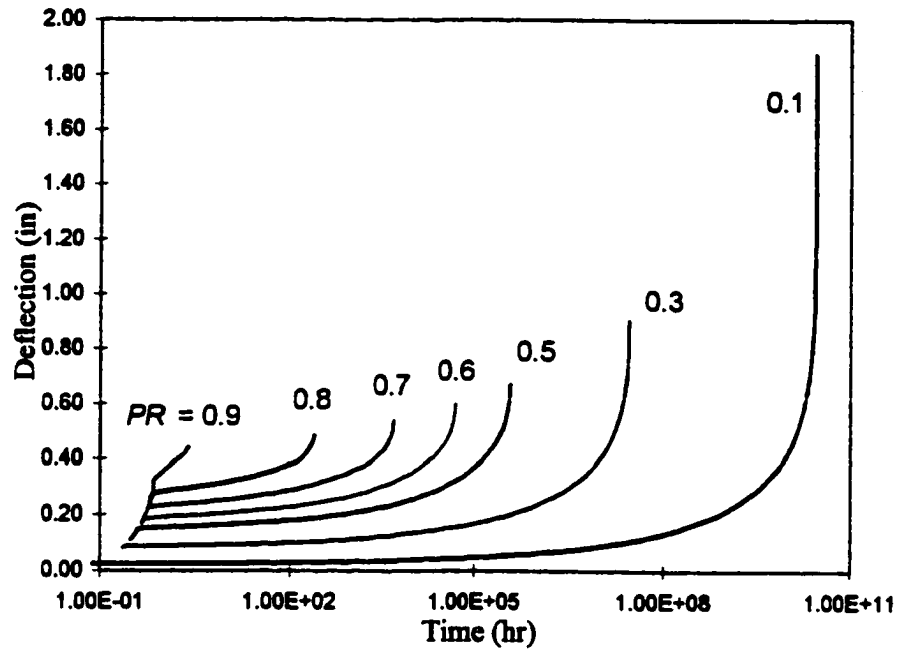
Figure 6.1   Typical Time-deflection Curves for Various Pressure Levels (Zhao, 1999)
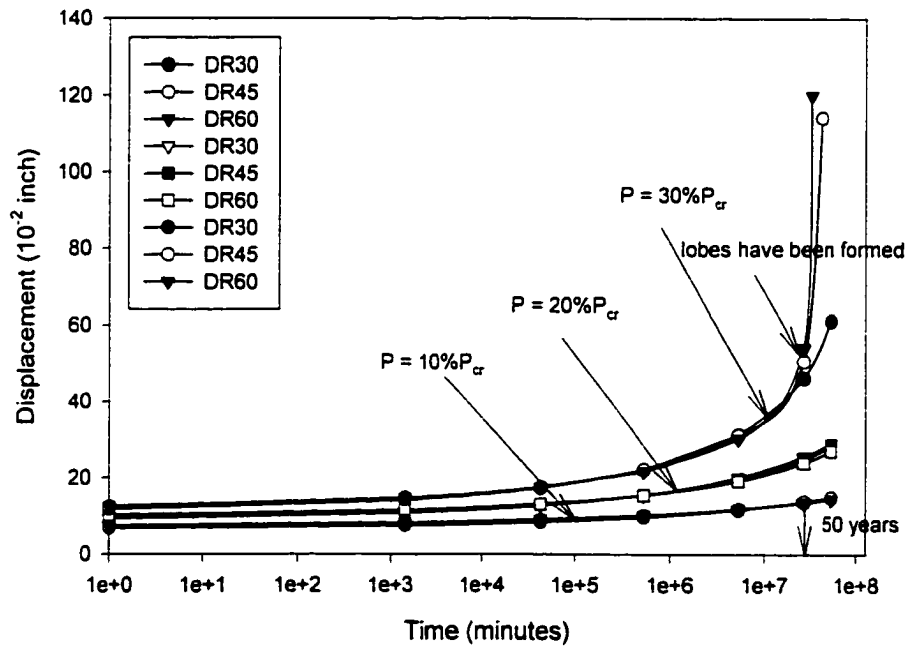
Figure 6.2   Effect of External Pressure on the Displacement Evolution
(OV = 3%, G = 0.4%)

6.2.2 Effect of Creep Constants

The material properties play a more important role in long-term buckling than in short-term buckling. Any small change in the values of the creep properties (A, m and n) will lead to quite different results. Figure 6.3 shows that deformation of a liner increases four fold over a one year period when the creep coefficient is increased by a factor of five. This increase in A results in a liner lifetime that is cut by a factor of 10. The creep time exponent has even more influence as indicated in Figure 6.4. Here, the deformation is increased by a factor of 3 in 1 month when n is doubled, and the life is shortened by more than 100 years.
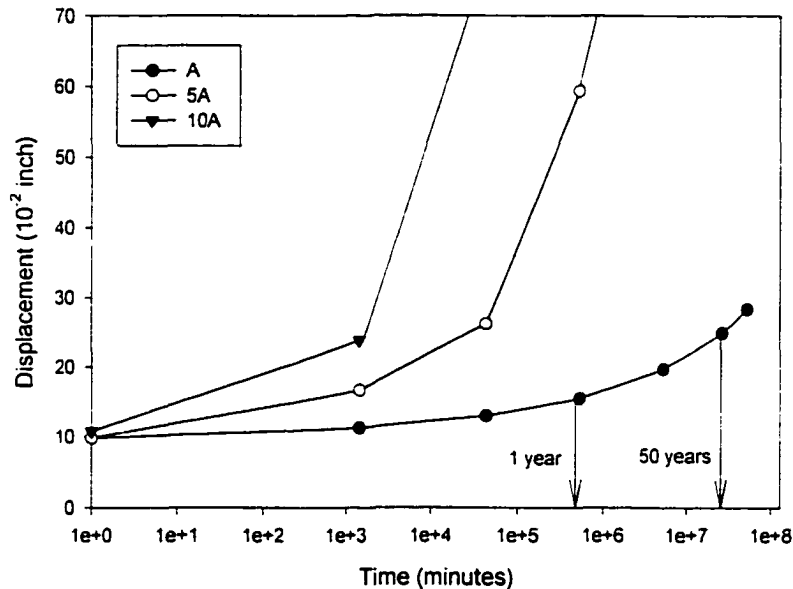
Figure 6.3 Effect of Creep Coefficient A on the Displacement Evolution
(P = 20%P_{cr}, DR = 45, OV = 3%, G = 0.4%)
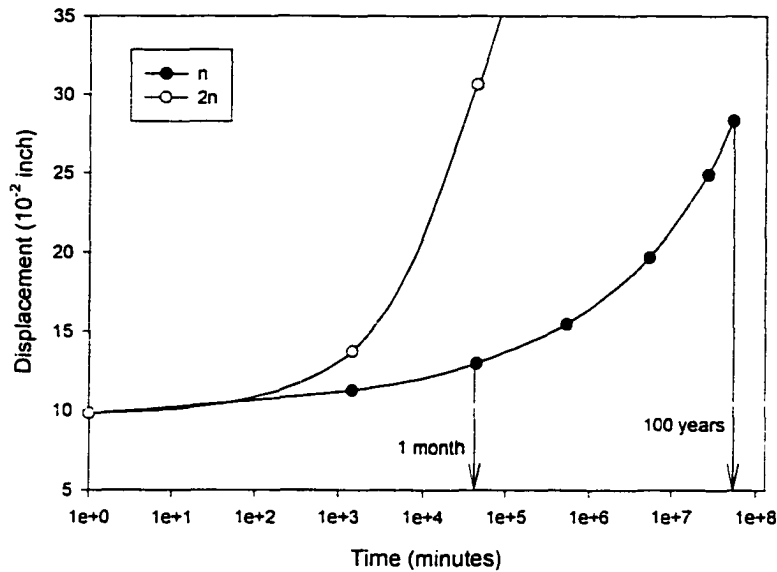
Figure 6.4   Effect of Creep Exponent n on the Displacement Evolution
(P = 20%P_{cr}, DR = 45, OV = 3%, G = 0.4%)

6.3   Evolution of Stresses

The stress at any point around the liner can be approximately decomposed into compressive and flexural components, as described in Chapter 5. By dividing the flexural component of the stress by the compressive component, it is possible to determine whether flexural or compressive stresses are dominant at any point and at any time throughout the liner lifetime. The effect of DR, external pressure level, gap, ovality, and material properties on the evolution of stresses will be studied here.

6.3.1   Effect of DR

Under an external pressure of 12 psi (which is larger than most hydrostatic pressures the liner will experience in field), all of the liners in Figure 6.5 have flexural stress to hoop stress ratios (FTHR) less than 2 for the majority of their lifetimes (which are more than 50 years). Notice that the pipe with a DR of 30 has a FTHR that is initially greater than 2. This initially high FTHR is due to the fact that the liner is too stiff to

initially have substantial contact with the host-pipe. It therefore has very little contact force which can produce a reverse moment to reduce the flexural stress in the liner, as discussed in Chapter 5. But, as the time passes, the thicker liner's stress relaxation combats the bending deflection, and its FTHR value decreases much faster than the other two thinner liners.
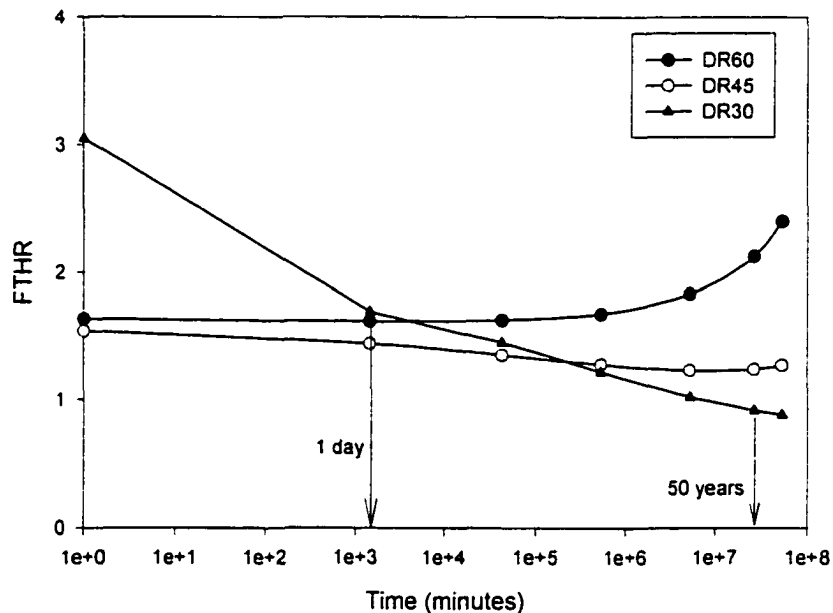
Figure 6.5   Effect of DR on the Stress Evolution
(P = 12 psi, OV = 3%, G = 0.4%)

6.3.2   Effect of External Pressure

Figures 6.6 through 6.8 show the variation of FTHR for pressures of 10%, 20% and 30% of Pcr, respectively. Notice that FTHR is less than two for the majority of the lifetime in all cases. As time passes, FTHR may decrease somewhat, especially for low pressure levels, due to accumulating creep strain which causes the stresses to relax through the thickness. Alternatively, this decrease in FTHR may be due to low contact

forces between the liner and its host pipe, as described earlier. As creep deformation continues to accumulate, the rate of inward deflection at the critical point will eventually begin to accelerate resulting in a corresponding increase in the stress level. Eventually, the rate of stress relaxation loses its ability to keep pace with the increasing deflections, resulting in increasing values of the FTHR. This increasing FTHR will eventually lead to liner instability. In Figure 6.8, the pipe liners with DRs of 45 and 60 form inverse curvature within 50 years and lose stability within 100 years under 30% of their critical pressures.
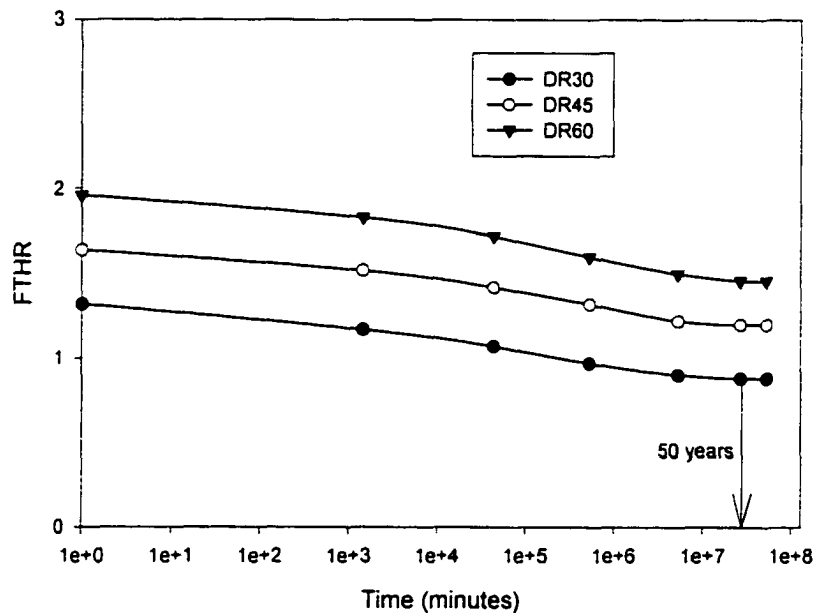
Figure 6.6   Effect of External Pressure on the Stress Evolution
(P = 10% P_{cr}, OV = 3%, G = 0.4%)
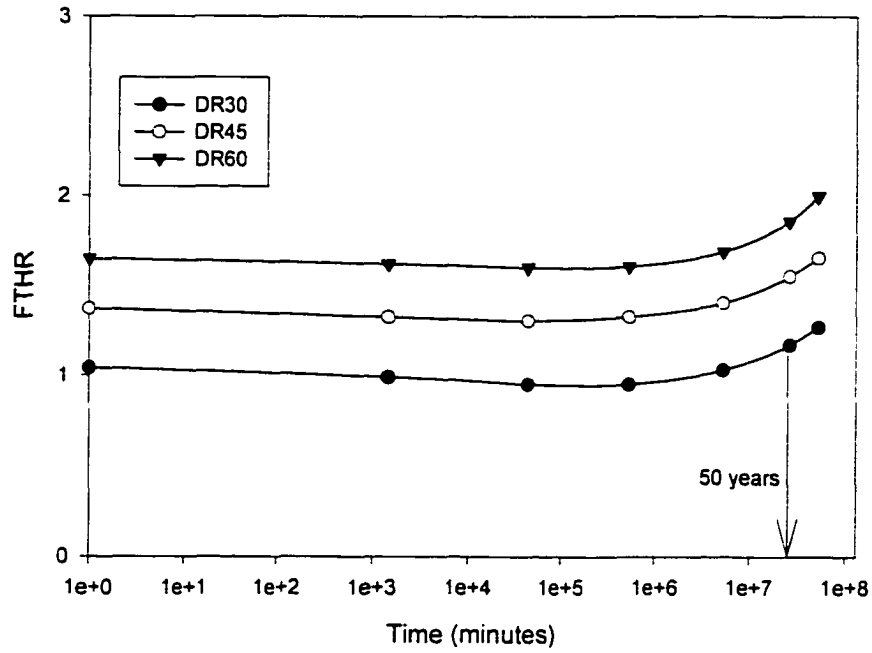
Figure 6.7   Effect of External Pressure on Stress Evolution
(P = 20% P_{cr}, OV = 3%, G = 0.4%)
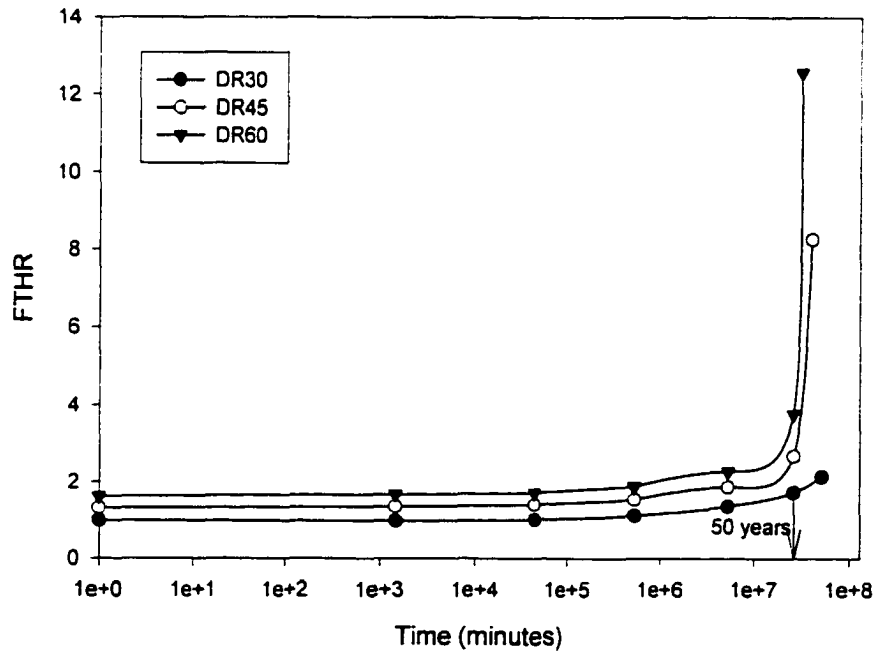
Figure 6.8   Effect of External Pressure on Stress Evolution
(P = 30% P_{cr}, OV = 3%, G = 0.4%)

6.3.3 Effect of Gap and Ovality

Both gap and ovality will produce a higher initial bending moment in the liner. This observation means that the gap and ovality will initially increase the FTHR value in the liner, as seen in Figures 6.9 and 6.10. However, the differences in the FTHR induced by the gap or ovality decrease as the time lapses, with the effect of ovality being diminished faster than the effect of gap. The pipe with larger ovality always has the larger contact force and contact area. This contact acts to decrease the increasing rate of the flexural stress in the liner for pipes with larger ovalities. The effect of gap is also somewhat diminished in the long-term loading case for a similar reason. The gap has a greater tendency to shorten the life than ovality due to the increased likelihood of forming inverse curvature at the critical point.
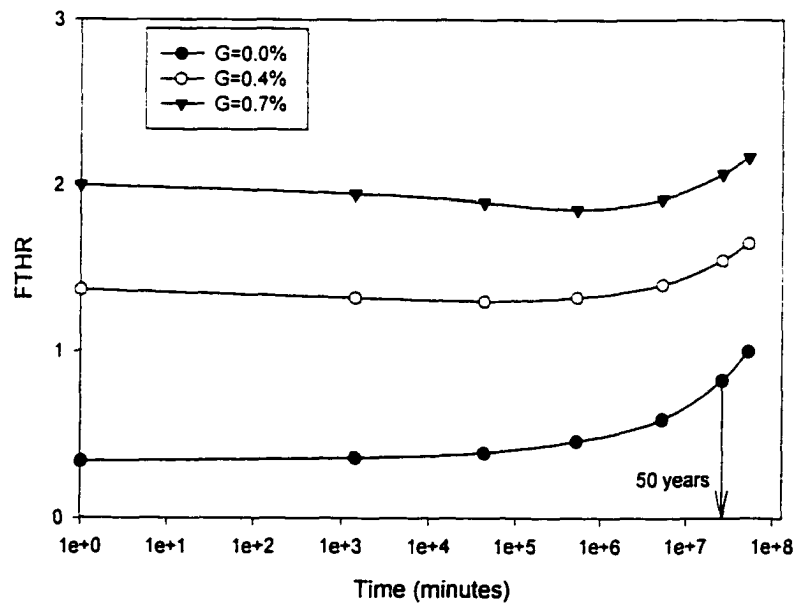
Figure 6.9   Effect of Gap on Stress Evolution
$(P = 20\% \; P_{cr}, \; DR = 45, \; OV = 3\%)$
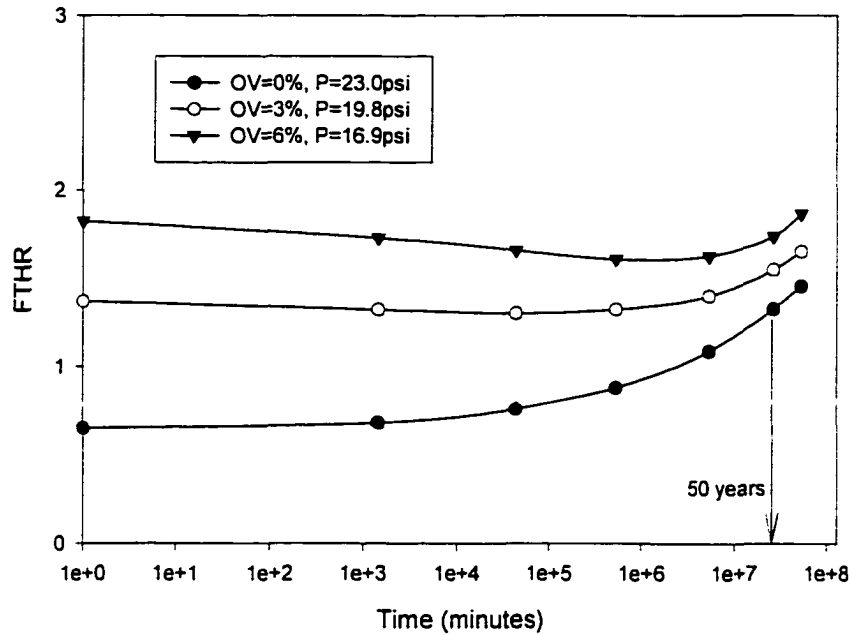
Figure 6.10   Effect of Ovality on Stress Evolution
(P = 20% P_{cr}, DR = 45, G = 0.4%)

6.3.4   Effect of Creep Rate

Figure 6.6 presented the long-term behavior of liners with DRs of 30, 45 and 60 at 10% of the critical pressure for a creep coefficient of A. Figure 6.11 shows that for a pressure level of 10% of the critical pressure and a creep coefficient of $5A$, a liner with a DR of 30 will not form inverse curvature within 50 years. However, the liners with DRs of 45 and 60 will form inverse curvature within 50 years and will buckle within 100 years when a creep coefficient of $5A$ is used. Comparing Figures 6.6 and 6.11 indicates that the liner lifetimes are greatly shortened by increasing the creep coefficient from A to $5A$.

Figure 6.12 shows that the FTHR is increased by more than a factor of two at one year for a liner loaded at 20% of the critical pressure when its creep rate A is five times larger. The corresponding lifetime is shortened by more than 10 times. If A is increased by a factor of 10, the design life can be shortened by more than 1000 times. Figure 6.29

shows that the creep exponent has an even larger impact on lifetime. By increasing the exponent from n to $2n$, the design lifetime can be reduced by more than 100 times. Figures 6.12 and 6.13 emphasize the need for accurate material properties, since slight variations in properties can lead to large difference in liner lifetimes.
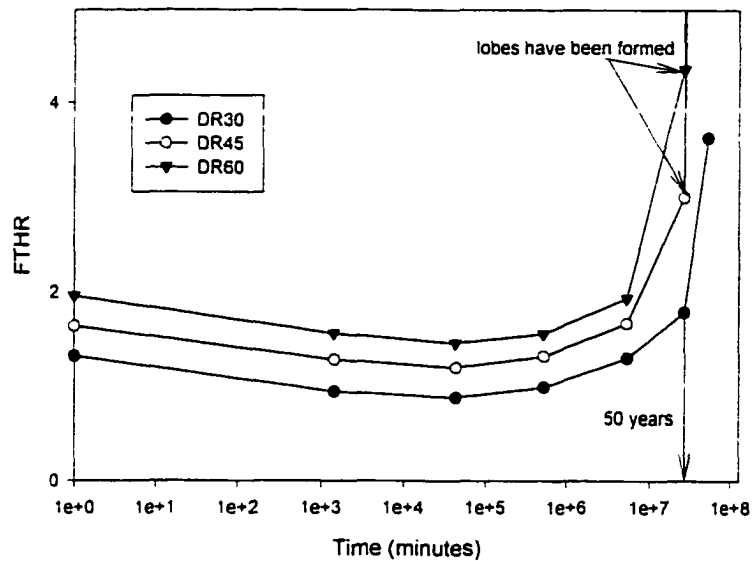
Figure 6.11   Effect of Creep Coefficient of 5A on Stress Evolution
(P = 10%Pcr, OV = 3%, G = 0.4%)
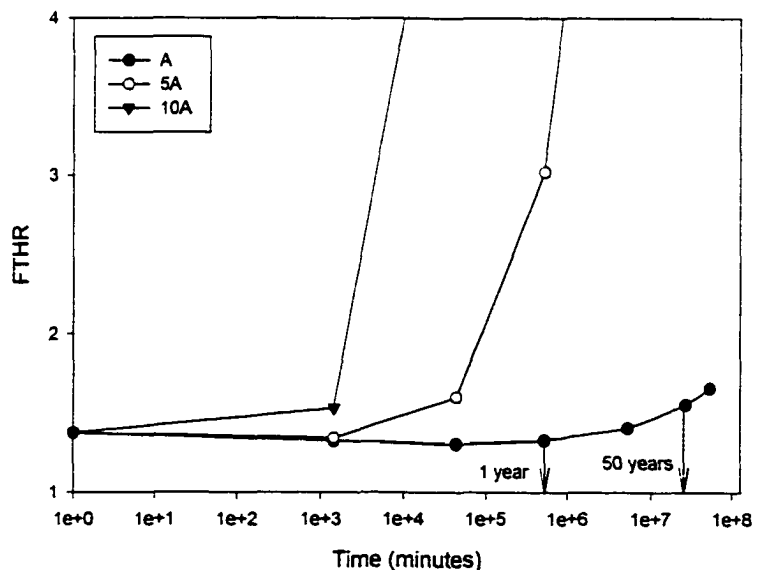
Figure 6.12   Effect of Creep Coefficient A on Stress Evolution
(P = 20%Pcr, DR = 45, OV = 3%, G = 0.4%)
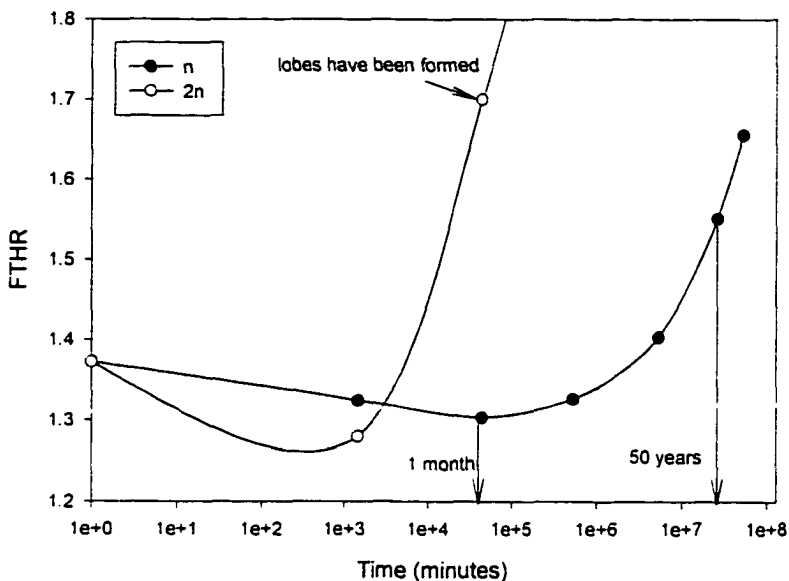
Figure 6.13 Effect of Creep Exponent n on Stress Evolution
(P = 20%Pcr, DR = 45, OV = 3%, G = 0.4%)

6.4 Design Implications

Table 6.1 lists the minimum percent of the critical pressure at which the pipe

liners will form lobes (inverse curvature) within 50 years for the material whose

properties were listed earlier in Table 2.2. The %P_{cr} values vary from 27% for a DR of

60 to 35%Pcr for a DR of 30. All of the pipe liners listed in this table will buckle within

100 years since they formed lobes during the first 50 years of their lifetime. Most of the

flexural to hoop stress ratios become greater than 2 only after the pipe liners have formed

lobes, with the exception of liners without gaps which currently do not exist in practice.

Compressive stresses are assumed to be dominant when the FTHR is less than or

equal to 2.0. Figure 6.14 shows that a value of h equal to 0.25 corresponds to a FTHR of

2.0. Thus, 25% of the cross sectional area is subjected to tensile stresses and 75% is

subjected to compressive stresses when the FTHR is equal to 2.0. When h is equal to

zero, the entire cross section is under compression, corresponding to a FTHR less than or equal to one. Consequently, when the flexural to hoop stress ratio is less than 2, inverse curvature has not been formed, the liner works more like an arch rather than a beam and the compressive stress is dominant to the flexural stress. This suggests that compressive material properties should be used when the FTHR is less than or equal to two, which can roughly be assumed to apply over the majority of the liners' lifetime at the critical point when the pressure level is less than 30% of Pcr.

The above paragraphs support the case for using compressive properties for liner design calculations and avoiding situations in liner design where the groundwater presure exceeds 30% of Pcr. The choice of material properties has important implications for liner design, since plastics are generally more resistant to elastic and creep deformation under compressive loading than under flexural or tensile loading. Basing the design of a liner system on flexural or tensile material properties may lead to overly conservative designs when accurate design models are employed. By choosing a small enough DR for a given application (a large enough thickness), the formation of inverse curvature and liner buckling within the 50-year design life can be prevented.

Table 6.1 Summary of FEM Results

			P_{cr} (psi)	P (psi)	FTHR	Disp. (10^{-1} inch)	Buckling Time (yrs)
DR 30	OV 0%	G = 0.0%	343	35%Pcr = 119.6	1.99	5.931	64.42
		G = 0.4%	269	35%Pcr = 94.15	2.18	6.373	74.54
		G = 0.7%	233	34%Pcr = 79.22	2.28	6.425	93.02
	OV 3%	G = 0.0%	308	33%Pcr = 101.9	1.93	5.669	67.32
		G = 0.4%	234	33%Pcr = 77.22	2.09	5.863	88.74
		G = 0.7%	202	33%Pcr = 66.6	2.51	6.682	89.65
	OV 6%	G = 0.0%	271	31%Pcr = 84.01	1.74	4.838	83.73
		G = 0.4%	212	30%Pcr = 63.6	2.09	5.577	100
		G = 0.7%	174	30%Pcr = 52.2	2.35	5.807	100
DR 45	OV 0%	G = 0.0%	162	31%Pcr = 50.22	2.01	4.033	69.38
		G = 0.4%	115	30%Pcr = 34.5	2.37	4.548	93.23
		G = 0.7%	94.8	30%Pcr = 28.44	2.92	5.429	94.82
	OV 3%	G = 0.0%	142	30%Pcr = 42.6	1.91	3.804	74
		G = 0.4%	99	30%Pcr = 29.7	2.68	5.054	78.6
		G = 0.7%	81.2	29%Pcr = 23.55	3.13	5.503	99.75
	OV 6%	G = 0.0%	123	30%Pcr = 36.9	2.03	4.032	67.1
		G = 0.4%	84.7	29%Pcr = 24.56	2.7	4.467	85.4
		G = 0.7%	69.1	28%Pcr = 19.35	3.27	5.515	100
DR 60	OV 0%	G = 0.0%	92.9	30%Pcr = 27.87	2.05	3.26	68.17
		G = 0.4%	59.5	29%Pcr = 17.25	2.79	4.177	87.23
		G = 0.7%	47.3	29%Pcr = 13.72	3.76	5.205	87.44
	OV 3%	G = 0.0%	81	30%Pcr = 24.3	2.23	3.551	61.22
		G = 0.4%	51.4	29%Pcr = 14.91	3.13	4.571	76.41
		G = 0.7%	40.7	28%Pcr = 11.4	3.81	5.217	96
	OV 6%	G = 0.0%	69.9	29%Pcr = 20.27	1.98	3.06	71.99
		G = 0.4%	43.5	28%Pcr = 12.18	3.04	4.369	88.05
		G = 0.7%	34.3	27%Pcr = 9.26	3.86	5.144	100
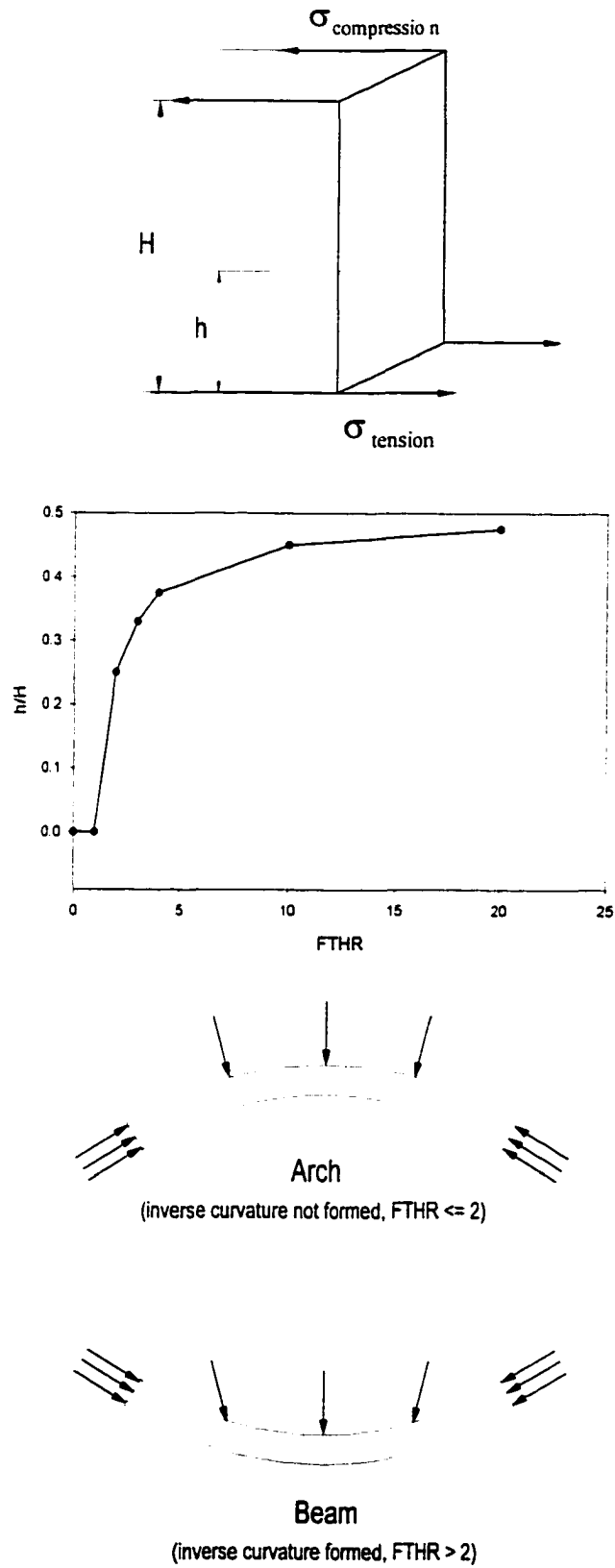
Figure 6.14 Schematic Defining the Physical Meaning of the FTHR

6.5 <u>Conclusions</u>

The stress-state is a function of DR, external pressure levels, material properties, global imperfections gap and ovality. The stress evolution in this study has not taken the effect of local imperfections (intrusion and thickness variations) into account, and the following conclusions may not suitable for liners containing local imperfections.

Most of pipes' flexural stress to compressive stress ratios are less than 2 within their 50-year design life in this study when the external pressure level is less than 30% of the critical pressure. After the study of stress evolution, the following conclusions can be made:

(1) The compressive stress is dominant to the flexural stress over the lifetime for applied pressures less than 30% of Pcr. When the flexural stress to compressive stress ratio is less than or equal to 2, the lobes have not been formed in most of the liners, and the liners work more like an arch rather than a beam. The compressive material properties will be appropriate for design and analysis.

(2) Using flexural or tensile material properties in design may lead to designs that are overly conservative.

(3) By choosing an appropriate DR during design, such that the groundwater pressure is less than 30% of the critical pressure, will allow inverse curvature and buckling to be prevented during the first 50 years of a CIPP liner's life.

(4) If a CIPP liner forms inverse curvature within 50 years, it will buckle within 100 years. The deformation, contact force, and flexural stress will increase much faster after the formation of inverse curvature.

(5) It is common to find stress relaxation when the external pressure is small. When the rate of stress relaxation cannot keep pace with the rate of inward radial deflections, the formation of inverse curvature is imminent and liner tends to lose stability.

(6) The gap and ovality imperfections will increase the deformation and flexural stress in the liner and will increase the likelihood of inverse curvature before the design lifetime is achieved. The gap has more effect on liner performance than the ovality does.

CHAPTER 7

THREE-DIMENSIONAL ANALYSIS OF LINER BUCKLING

7.1 Introduction

Specimen length can have a significant effect on measured buckling pressures if the ends of the sample are clamped to the host pipe. Most of the pipeline rehabilitation liner buckling tests in the past two decades were carried out using clamped ends to prevent leakage between a liner and its host pipe. Only the series of tests by Welch (1989) allowed the liners to freely deform at the ends. For the tests performed to date, the specimen's length to diameter ratio (L/D) has varied from 2.1 to 10. Since these buckling tests often yield buckling pressures that are higher than those from analytical or numerical predictions, questions have been raised regarding the appropriate pipe length to be used for buckling tests. If the pipe lengths being used for the existing tests are too short, it is clear that the buckling pressures obtained from the tests will be higher than those predicted for liners in the field. This chapter addresses the length to diameter ratio issue through two- and three-dimensional finite element analyses of short-term liner buckling.

107

7.2   Critical Length of the Specimen

Both short-term and long-term liner buckling tests involving 8-inch and 12-inch host pipes have been carried out at the TTC. When performing these tests, the external pressure is applied to each test specimen through a pre-tapped hole in the bottom of the steel pipe. Pressurized water enters this hole and works its way through the annular space between the host pipe and the liner to simulate the effect of groundwater pressure on a liner in service. To prevent leaking at the ends of the liner and host pipe, a system consisting of an o-ring, a tapered steel stiffener, and a power seal are installed at the end before testing, as described by Guice *et al.* (1994).

The 8-inch ID host pipes have a length of 5 feet for a pipe length to diameter ratio of 7.5, and the 12-inch pipes have a length of 6 feet for a ratio of 6.0. It is clear that the longer the host pipe, the more closely the system will resemble field conditions. However, to make the testing feasible for a large number of samples, a host pipe length that is manageable but that minimizes the effects of end conditions is desirable.

Moore (1998) pointed out that three-dimensional finite element solutions were needed to explore the effect of clamped ends (such as those in the TTC tests) and host pipe length on liner buckling pressure. To address this need, a number of 1/8 symmetry three dimensional finite element simulations of short-term liner buckling in various length host pipes were completed. The models were run using the ABAQUS finite element code using STRI3 shell elements to model the liner material and R3D4 contact elements to model the host pipe, which was assumed to be perfectly rigid. An elastic perfectly plastic constitutive relation was used based on the flexural properties listed for

the Insituform Enhanced product by Guice, *et al.* (1994) in Table D-2 of the report. That is, an elastic modulus of 538,621 psi, a yield strength of 8,405 psi, and a Poisson's ratio of 0.35 were used. A DR (outer liner diameter to liner thickness ratio) of 55 and an annular gap between the liner and the host pipe of 0.4% of the diameter was assumed for all calculations.

"Short" host pipes where the liner and host pipe are clamped together at the ends will lead to higher buckling pressures than "long" host pipes with clamped ends. With this in mind, it is reasonable to conclude that some critical host pipe length to diameter ratio (L/D) exists beyond which the presence of clamped ends no longer influences the buckling pressure. This critical L/D can be determined by plotting the decreasing critical pressure versus the host pipe length for a given diameter and noting the length at which the critical pressure no longer decreases significantly with increasing length, as described by Moore (1998).

Figures 7.1 and 7.2 show plots of the deformed and undeformed finite element meshes for a "short" pipe with L/D equal to 1.0. The deformation pattern corresponds to the development of six lobes (regions of large inward radial deflection) around the circumference and a critical pressure of 141 psi. As the host pipe length increases, this six lobe deformation pattern transitions to a two lobe pattern as shown in Figures 7.3 and 7.4, where L/D is 4 and the buckling pressure is 93 psi. Continuing to increase the length shows that the buckling pressure converges to approximately 92 psi.

The buckling pressure for this three-dimensional model can be normalized with respect to the two-dimensional plane-strain solution for identical DR and material properties. Plotting this normalized pressure versus L/D gives Figure 7.5. Notice that the

2D and 3D buckling predictions become very close to each other for L/D greater than about four, as indicated by the convergence of Pcr(3D) / Pcr (2D plane strain) to approximately one. The 2D solution shown here was constructed using ABAQUS with B21 elements as outlined by Zhao (2000).

The physical significance of the plane-strain model can be understood by considering the finite element model shown in Figure 7.6. For this model, displacements at the ends are constrained in the longitudinal direction but are free in the radial direction. The plot of the critical pressure ratio versus host pipe length that results from this model is shown to be independent of L/D in Figure 7.5. This model is effectively the same as the 2D model for all pipe lengths. The boundary conditions used for this model are similar to those used in the experimental work of Welch (1989).

The correspondence of the two 3D shell element models discussed above with the 2D plane strain beam element model helps to validate these numerical results. No attempt was made to quantify the effect of DR, host pipe ovality, or annular gap on the critical length, although these parameters are expected to have a "second-order" effect for the ranges commonly encountered for thin walled pipe liners.

Both 3D analyses inherently assumed that the buckling occurs at the midpoint of the liner/host pipe system. Any attempt to numerically force buckling at any point other than the midpoint using perturbation loads will result in the formation of a lobe which will spread to the midpoint. However, experimental tests at the TTC show that buckling is a local phenomenon (i.e., does not extend the full length of the pipe) and can occur at various locations along the length of the liner/host pipe system. Buckling at any point other than the center could be caused by several factors. First, the clamped ends could be

causing a <u>decrease</u> in critical buckling pressure rather than an <u>increase</u> for the L/D used. That is, local stress variations and deformations at the end induced in the clamping process could make the clamped end the weak part of the system. Second, local imperfections or material property variations could result in failure at a location other than the center. Third, the host pipes used in the testing are significantly longer than the critical value of L/D. That is, liners much longer than the critical L/D would not necessarily buckle in the middle. None of these three possible situations leads to the conclusion that clamped ends result in non-conservative estimates of the critical buckling pressure for L/D ratios greater than 5.

Original Shape

Deformed 6-Lobe Shap
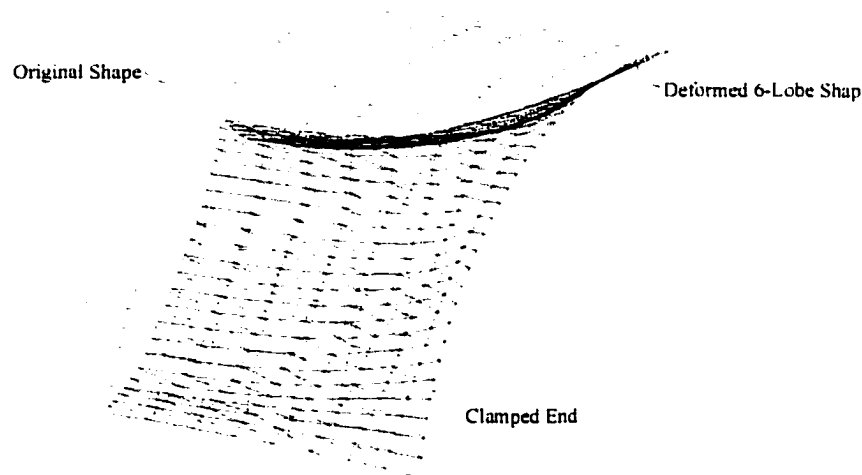
Clamped End

Figure 7.1   Three-Dimensional View of Deformed and Original Mesh for a Liner with Clamped End (Pipe Length = 1 ft., P_{cr} = 141 psi)
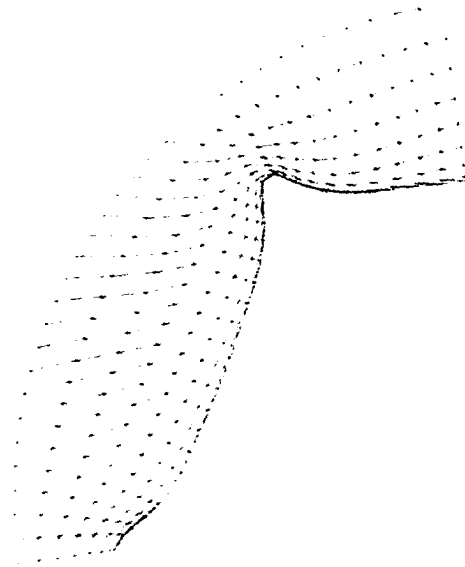
Figure 7.2   Two-Dimensional End View of Deformed Mesh for a Liner with Clamped End (Pipe Length = 1 ft., P_{cr} = 141 psi)

Original Shape

Deform 2-Lobe Shape
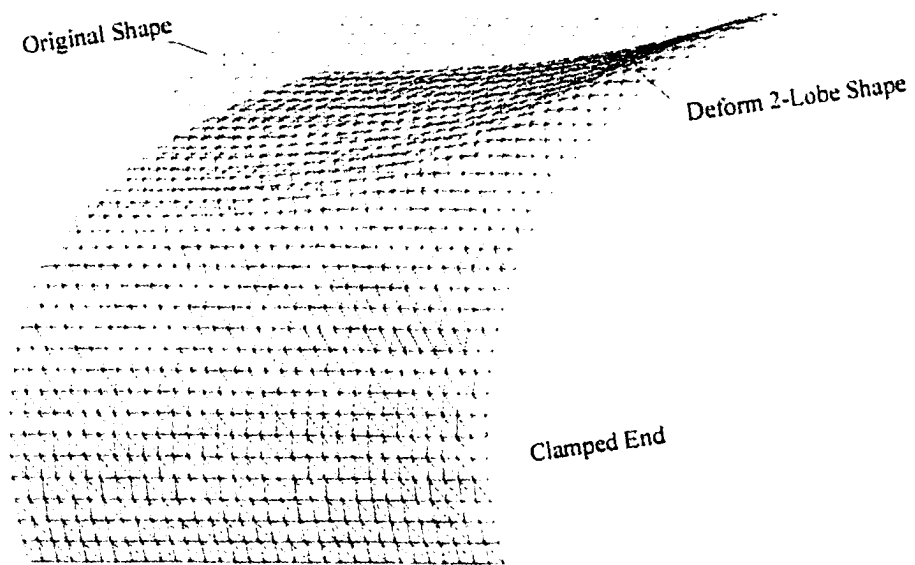
Clamped End

Figure 7.3   Three-Dimensional View of Deformed and Original Mesh for a Liner with Clamped End (Pipe Length = 4 ft., P_{cr} = 93 psi)
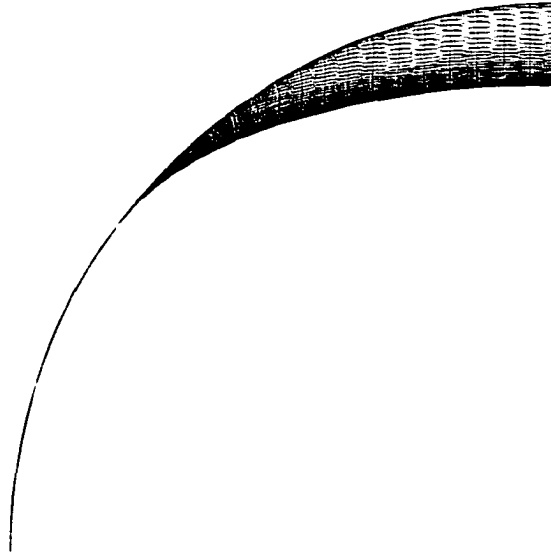
Figure 7.4   Two-Dimensional End View of Deformed Mesh for a Liner with Clamped End
(Pipe Length = 4 ft., P_{cr} = 93 psi)

3D Model with Clamped Ends

3D Model with Fixed Longitudinal
and Free Radial Displacement
Boundary Condition
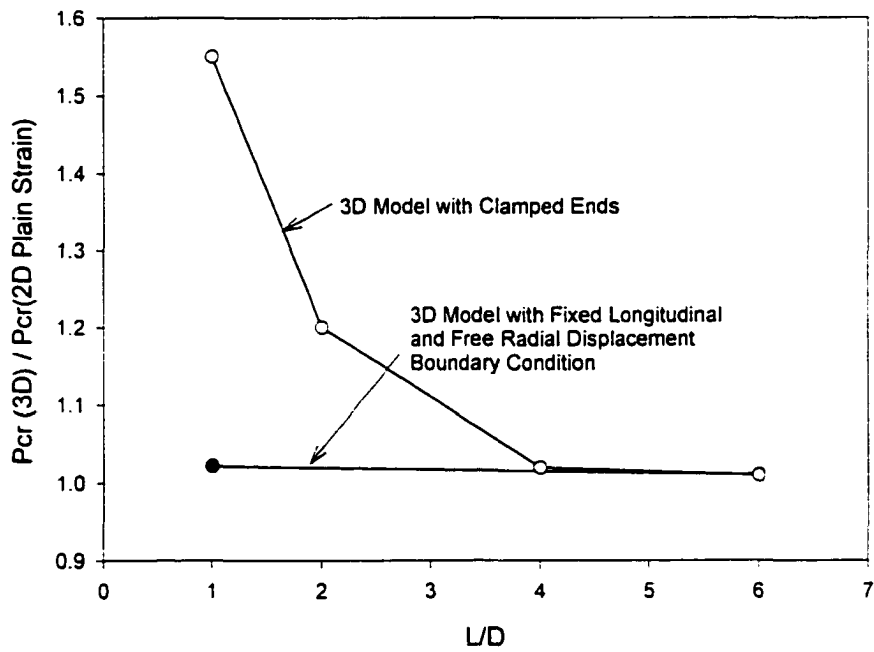
Figure 7.5   Normalized Pressure versus L/D Ratio

Original Shape

Deformed 2-Lobe Shape
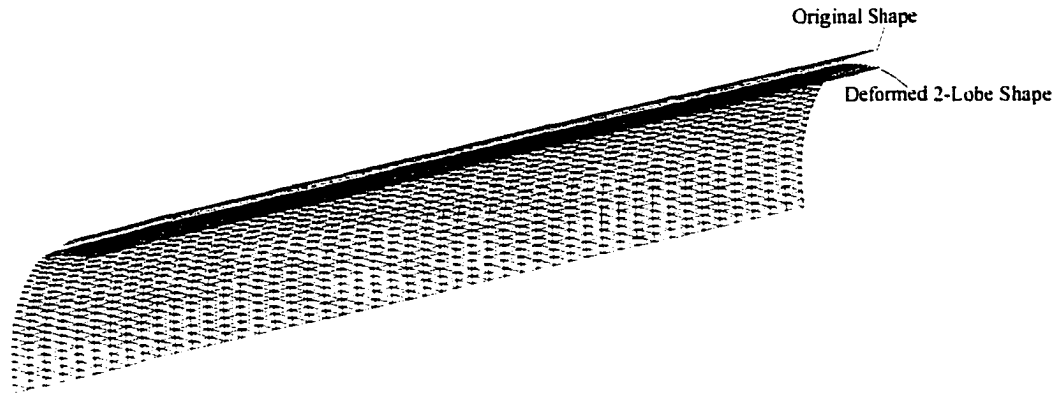
Figure 7.6 Three-Dimensional View of Deformed and Original Mesh for a Liner
with Fixed Longitudinal and Free Radial Displacement Boundary Condition
(Pipe Length = 6 ft., P_{cr} = 92 psi)

7.3 Conclusions

A number of factors with potential importance in pipe liner testing and analysis

have been discussed. resulting in the following conclusions:

(1) Three-dimensional finite element results for a liner with clamped ends show that end

effects become unimportant after L/D ratios of approximately 5.

(2) Since L/D values of six or more were used for all liner buckling tests at the TTC, with

the location of buckling varying along the length and frequently occurring near a

clamped end, the clamped ends used in the liner buckling tests at the TTC are

believed to result in conservative estimates of the critical buckling pressure.

CHAPTER 8

INFLUENCE OF IMPERFECTIONS ON CIPP LINER DESIGN

8.1 Introduction

Currently, no short-term liner buckling model simultaneously includes the effects

of SDR, ovality, gap, and local imperfections on liner buckling. The model developed

here will be similar to that of Zhao (1999), except that the effect of imperfections will

also be included. This new model will be based on the 81 finite element runs for all

possible combinations of each of three levels of DR, gap, ovality, and local

imperfections. Regression analysis will be used to determine the slope and intercept for

each combination of gap, local imperfection, and ovality for each DR, resulting in 27

separate regression analyses and 27 separate pairs of constants. These 27 pairs of

constants will be embedded into a Lagrangian interpolation scheme, identical to the

method that the shape function of a 27-node brick element uses for interpolating

displacements and stresses in the finite element analysis. All of the 27 shape functions

will be evaluated resulting in two polynomial expressions with 27 constants, which can

be used to predict a and m in Equation (2.10).

The resulting short-term model could be used in much the same way as the ASTM

F1216 design equation for design applications, where the elastic modulus would be

replaced with a long-term modulus. Of course, this new model would account for gap and local imperfections, whereas ASTM F1216 does not.

8.2 Effect of Imperfections on Buckling Pressure

Since the buckling resistance of an encased liner is enhanced due to the effect of contact, any factor which causes a certain change (or degradation) from the ideal fitting between a liner and its host pipe may lead to a reduction in the enhancement, and hence a reduction in the liner's buckling pressure. The effect of each factor can be determined by a parametric study.

8.2.1 Influential Parameters

The dimension ratio (DR) is the first parameter to be included in the study, which is essential to any pipe design where buckling is involved. In the context of constrained pipe liners, the most influential factors are the geometric imperfections of the liner-pipe system as a whole, most important of which is the gap (annular spacing) between a liner and its host pipe. When the deteriorated pipe loses its original circular shape, the ovality of the host pipe should be considered. It is very common to find 2% - 5% ovality existing in the host pipe in practice. Another kind of imperfection considered in this study is a local wavy intrusion into the liner. These four factors (DR, gap, ovality and intrusions) are considered essential for accurate prediction of buckling pressure and will be included in the following study to develop an empirical model for liner design based on a short-term buckling criterion.

Of the parameters, DR and host pipe ovality are dimensionless. To enhance the applicability of the model and the ability to compare its results with those available in the

literature, an effective gap parameter, the ratio of the total gap to the mean diameter of the liner, is used. The definition of local imperfection is based on the work of El-Sawy & Moore (1997), which includes the length of the wave imperfection and the depth of the intrusion. Figure 3.1 shows these types of imperfections and will be studied here.

Because of the thermal contraction after the curing process, a gap between a liner and its host-pipe cannot be avoided in the liner-pipe system. In Seemann *et al.* (2000), the gap was estimated using the "volumetric method," which involves measuring the volume of water between the liner and the host pipe, and the "deflection method," which estimates the gap based on the results of LVDT measurements. The volumetric method gives slightly better consistency than the deflection method but does not account for the nonuniformities that can be estimated using the deflection method. According to the volume measurement data, an effective (uniform) gap size g can be determined by averaging the volume uniformly over the whole outer area of the liner. A dimensionless gap parameter G is defined as the ratio of uniform gap size g to the liner mean diameter D.

Based on the study of Lo *et al.* (1994) and Zhao (1999), the one-lobe mode can be used to give a lower bound on prediction of critical pressure of an encased pipe liner. Therefore, in this chapter, gap is assumed to be unevenly distributed along the circumference, which implies that one-lobe mode will be used. In the one-lobe model, the gap size is 2g at the crown, while there is no gap between the liner and its host pipe at the invert.

To model local imperfection, the shape of the dented cross-section is assumed to follow Equation (8.1),

$$u = \Delta_0 \cdot \cos^2 \left(\frac{\pi\theta}{2\phi} \right)$$

(8.1)

with 2ϕ being the range of the dented part.

Table 8.1 shows that length ratio of local imperfections has little effect on the buckling pressure, while the depth ratio has a significant effect. In this study, only the change of depth ratio of the dent will be considered, and the length ratio will remain fixed.

Table 8.1 Comparison of Length Ratio vs Depth Ratio Effect of Dent on Critical Pressure

type	P_{cr} (psi)	Relative change
S = 0.1, LI = 2.25	54	0.0%
S = 0.05, LI = 2.25	54.2	0.4%
S = 0.1, LI = 4.5	45.5	15.7%

The range of interest of the dimensionless parameters are defined as follows and summarized in Table 8.2:

(1) <u>Dimension Ratio (DR)</u>: This parameter is defined as the ratio of the mean diameter (measured at the middle surface) to the thickness of a liner. Three levels (30, 45, and 60) were chosen over a moderate range of DR, to ensure that meaningful empirical formulas can be derived.

(2) <u>Dimensionless Gap (G)</u>: Three levels for even gap ratio G were chosen as 0.1, 0.4% and 0.7%, based on test conditions considered representative in real applications.

(3) <u>Host Pipe Ovality (OV)</u>: The ovality levels of 0%, 3%, and 6% were selected to compare with experimental data, in which nominal ovality values of 2% and 5% were used. An elliptical shape for the host pipe and the liner were assumed.

(4) <u>Dimensionless Local Imperfection (LI)</u>: The local imperfection levels of 0.0%, 2.25% and 4.5% were selected with a fixed wavelength ratio S of 0.1%. Only liners were assumed to have local imperfections (the host pipe was assumed to be circular).

Table 8.2   Summary of Selected Values Used in Parametric Study

	1	2	3
$DR \ (=\dfrac{D}{t})$	30	45	60
$G \ (=100 \cdot \dfrac{g}{D})$	0.1%	0.4%	0.7%
$LI \ (=100 \cdot \dfrac{\Delta_0}{D})$	0.0%	2.25%	4.5%
Ovality $(=100 \cdot \dfrac{IDmajor - IDmean}{IDmean})$	0%	3%	6%

Note: All local imperfections have a fixed length ratio S = 0.1, where $S = \dfrac{L}{\pi \cdot R}$.

8.2.2   Results and analysis

Based on the following considerations, only three levels were chosen for each parameter, and the finite element analyses were run over the 81 combinations:

(1) The dependency of ultimate pressure on each parameter is rather monotonous. Ultimate pressure decreases when any or all of DR, G, OV and LI increases.

(2) The response surface of P_{cr} is smooth enough over the selected region to allow accurate interpolation by employing simple numerical techniques, such as the Lagrangian polynomial.

(3) It is convenient in the design environment if only a few finite element runs will help to set up adequate design criteria.

The short-term buckling analysis procedure as discussed in Chapter 3 was employed to give ultimate pressure predictions. The material properties were from the ovality test (see Table A-5) with E = 459,000 psi and v = 0.3. The 81 ultimate pressure values are listed in Table 8.3 to Table 8.5.

Table 8.3   FEA Predictions of Critical Pressure (LI = 0.0%)

Pipe type	OV = 0%			OV = 3%			OV = 6%		
	G= 0.1%	G= 0.4%	G= 0.7%	G= 0.1%	G= 0.4%	G= 0.7%	G= 0.1%	G= 0.4%	G= 0.7%
DR 30	266	220	190	229	187	160	195	159	135
DR 45	104	77.9	63.4	88.8	66.1	53.7	75.6	55.6	45.2
DR 60	53.6	37.3	29.4	45.9	31.6	24.9	39.1	26.5	20.9

Table 8.4   FEA Predictions of Critical Pressure (LI = 2.25%)

Pipe type	OV = 0%			OV = 3%			OV = 6%		
	G= 0.1%	G= 0.4%	G= 0.7%	G= 0.1%	G= 0.4%	G= 0.7%	G= 0.1%	G= 0.4%	G= 0.7%
DR 30	222	188	165	189	159	139	162	135	118
DR 45	81.8	64.1	54.2	69.5	54	45.7	59	45.6	38.6
DR 60	40.7	29.8	24.8	34.4	25.2	20.9	29.2	21.3	17.6

Table 8.5 FEA predictions of critical pressure (LI = 4.5%)

Pipe type	OV = 0%			OV = 3%			OV = 6%		
	G= 0.1%	G= 0.4%	G= 0.7%	G= 0.1%	G= 0.4%	G= 0.7%	G= 0.1%	G= 0.4%	G= 0.7%
DR 30	187	162	145	158	138	123	136	117	105
DR 45	65.3	53.7	46.9	55.4	45.5	39.8	47	38.5	33.6
DR 60	31.2	24.7	21.3	26.4	20.9	18	22.4	17.7	15.3

8.3   Empirical Model

As mentioned in Chapter 2, Omara *et al.* (1997) suggested that Glock's model for encased pipes (Equation (2.9)) and Bryan's equation (Equation (2.2)) can be expressed in the same form (Equation (2.10)) as a power function of the D/t ratio. Equation (2.10) can be written in the following format

$$\frac{P_{cr} \cdot (1 - \upsilon^2)}{E} = a \cdot (\frac{1}{DR})^m \tag{8.2}$$

In Glock's model, a and m are 1 and 2.2, while in the Timoshenko's equation, a and m are 2 and 3, respectively. Equation (8.1) may be used as an empirical model, with the coefficient a and exponent m to be fitted for various geometric parameters. The value of m should between 2.2 and 3, where 2.2 applies to a round pipe with no gap and 3 applies to a round pipe with an infinitely large gap.

8.3.1   Effect of DR

The effect of DR is visualized by log-log plots for each {G, OV, LI} combination, as illustrated in Figure 8.1. As can be clearly seen from the figure, each curve, corresponding to a specific {G, OV, LI} combination, is very close to a straight line.

$$\lg(\frac{P_{cr} \cdot (1 - \upsilon^2)}{E}) = \lg a - m \cdot \lg(DR) \tag{8.3}$$

which verifies the proposed expression in Equation (8.1).
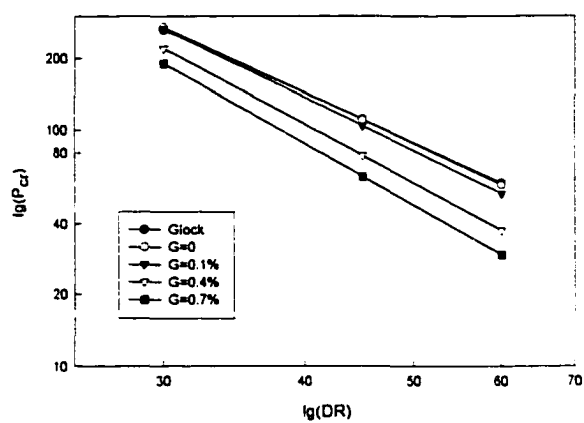
a. OV = 0, LI = 0
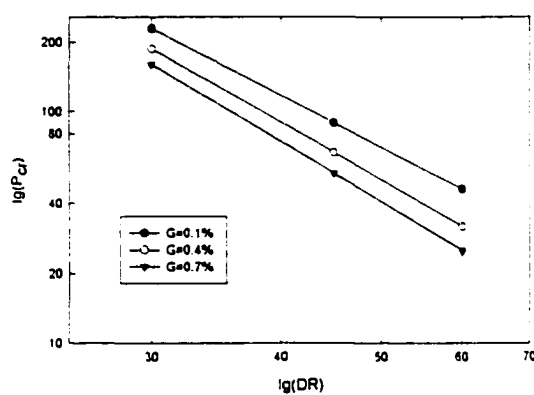
b. OV = 3%, LI = 0
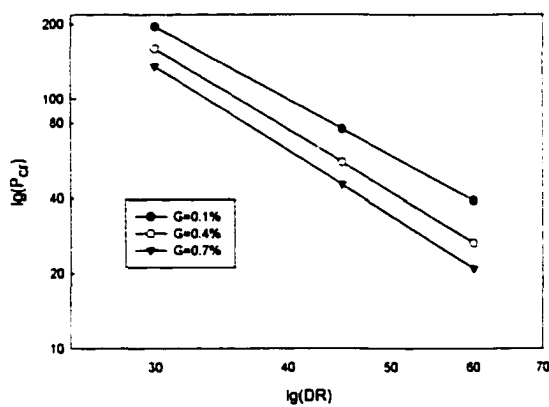
c. OV = 6%, LI = 0

Figure 8.1   Effect of DR
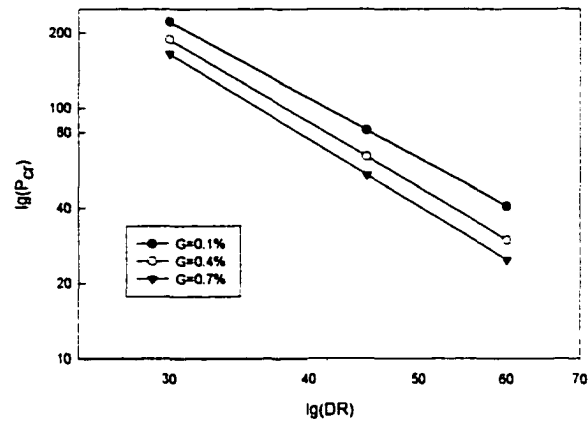
d. OV = 0, LI = 2.25%
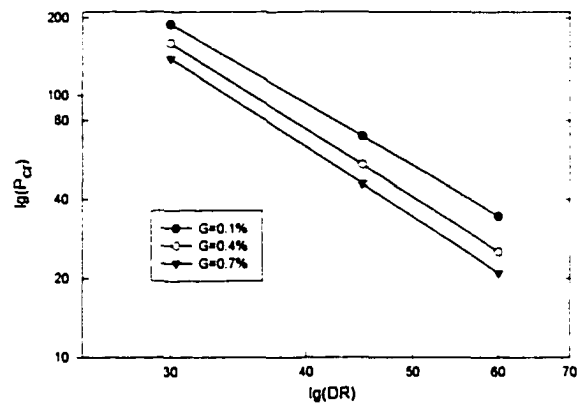
e. OV = 3%, LI = 2.25%
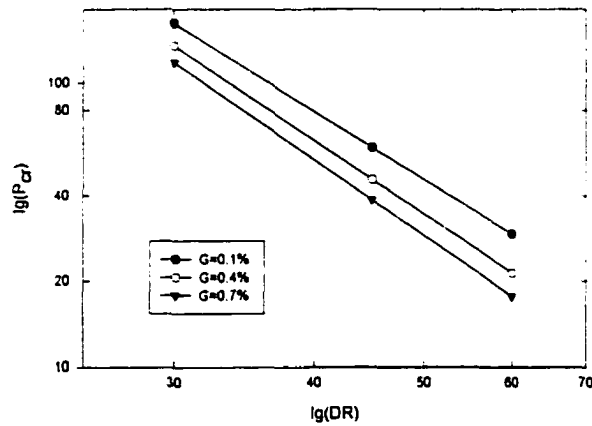
f. OV = 6%, LI = 2.25%

Figure 8.1 Effect of DR (cont'd)
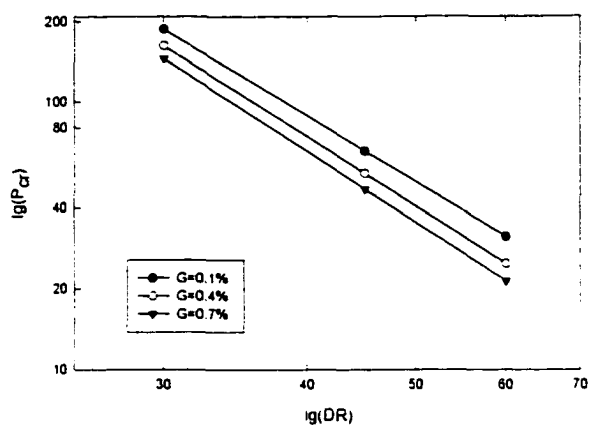
g. OV = 0, LI = 4.5%
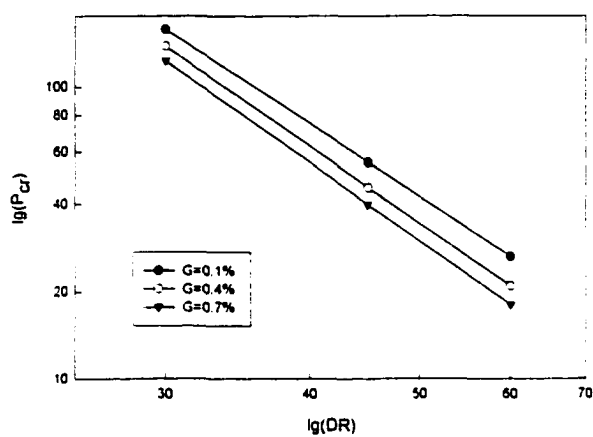
h. OV = 3%, LI = 4.5%
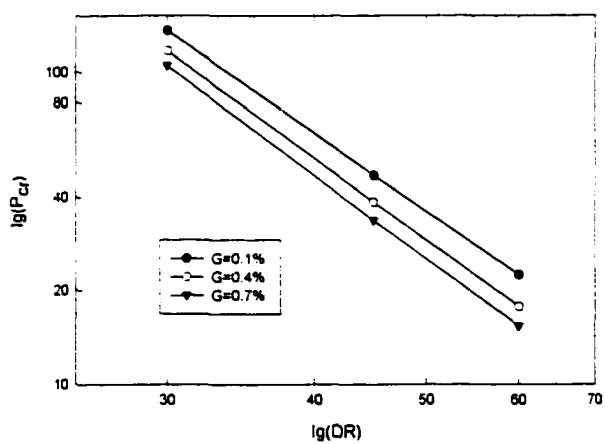
i. OV = 6%, LI = 4.5%

Figure 8.1 Effect of DR (cont'd)

By employing the least-squares regression technique, the a and m values were determined for each of the 27 {G, OV, LI} combinations, as listed in Table (8.6) and Table (8.7). Of the 27 regression analyses, the lowest R-squared value is 0.9995, very close to the highest possible value of 1. This statistical value indicates that Equation (8.1) is a good model for expressing P_{cr} as a function of DR. Results listed in Table 8.6 and 8.7 show that the values vary approximately from 0.992 to 3.447 for a and from 2.311 to 2.781 for m.

As can be seen from Equation (8.2), m is the slope and lga the intercept of the linear regression equation. One feature of the a and m pair is that a smaller m tends to accompany a smaller a, since a less inclined line tends to intercept the vertical axis at a lower point.

Table 8.6   Fitting Constants a

	LI = 0.0%			LI = 2.25%			LI = 4.5%		
	OV=0 %	OV=3 %	OV=6 %	OV=0 %	OV=3 %	OV=6 %	OV=0 %	OV=3 %	OV=6 %
G= 0.1%	1.319	1.167	0.992	1.753	1.545	1.391	2.343	1.964	1.817
G= 0.4%	2.545	2.199	2.002	3.024	2.562	2.226	3.158	2.782	2.372
G= 0.7%	3.447	2.821	2.441	3.452	2.902	2.563	3.396	2.933	2.563

Table 8.7   Fitting Constants m

	LI = 0.0%			LI = 2.25%			LI = 4.5%		
	Oval 0%	Oval 3%	Oval 6%	Oval 0%	Oval 3%	Oval 6%	Oval 0%	Oval 3%	Oval 6%
Gap 0.1%	2.311	2.32	2.319	2.448	2.459	2.473	2.584	2.582	2.603
Gap 0.4%	2.56	2.565	2.585	2.657	2.658	2.665	2.714	2.724	2.726
Gap 0.7%	2.693	2.684	2.692	2.735	2.734	2.746	2.768	2.773	2.781

8.3.2 Effect of Gap

The effect of gap, especially when combined with DR, on the enhancement factor K is investigated by using Equation (8.1) and Bryan's Equation (2.2). Here, K may be expressed as

$$K = \frac{a}{2} \cdot DR^{3-m} \tag{8.4}$$

The a and m for any desired $\{G, OV, LI\}$ within an given region can be interpolated using the Lagrangian technique.

$$y(G, OV, LI) = \sum_{i=1}^{3} \sum_{j=1}^{3} \sum_{k=1}^{3} \{y(G_i, OV_j, LI_k) L_{2,i}(G) L_{2,j}(OV) L_{2,k}(LI)\} \tag{8.5}$$

where y stands for a or m, $L_{2,m(x)}$ is the 2nd order Lagrangian polynomial.

$$L_{2,m}(x) = \prod_{\substack{i=0 \\ i \neq m}}^{2} \frac{(x - x_i)}{(x_m - x_i)} \tag{8.6}$$

The critical pressure P_{cr} can then be obtained by Equation (2.10).

Table 8.8 gives the K values thus obtained for circular pipe and liner over the region of interest, which vary from 4.89652 (for DR = 30 and G = 0.7%) to 14.6449 (for DR = 90 and G = 0.1%). The variation shows that the validity of assuming K = 7 depends on both the dimension ratio DR and liner-pipe fitting condition achieved in a rehabilitation application. The enhancement factor is reduced as the gap increases. The reduction factor is also a function of DR. For example, the enhancement factor K for a DR of 60 is reduced by almost 45% for a gap of 0.7%, while for a DR of 30 it is only reduced by about 28.7%. The accuracy of the predictions for K listed here will be verified shortly in the model validation section.

Table 8.8   Predicted Enhancement Factor K Due to Effect of Gap G

DR	G=0.1%	G=0.2%	G=0.4%	G=0.5%	G=0.7%
30	6.86991	6.62954	5.68318	5.29691	4.89652
35	7.63972	7.26424	6.08202	5.61887	5.13381
40	8.37595	7.86296	6.45007	5.91353	5.34864
45	9.08402	8.4319	6.79315	6.18624	5.54559
50	9.76799	8.97562	7.11549	6.44083	5.7279
55	10.431	9.49762	7.42023	6.68105	5.89797
60	11.0754	10.0006	7.70982	6.90638	6.05764
65	11.7034	10.4869	7.98619	7.12126	6.20834
90	14.6449	12.7195	9.21562	8.06593	6.86063

As illustrated in Figure 8.2, ultimate pressures drops with an increase in G for any given pair of {DR, OV, LI}. It can also be seen from Figure 8.2 and Table 7 that the slope m increases with an increase in G. This trends means that P_{cr} decreases faster with an increase in DR under a large dimensionless gap G.
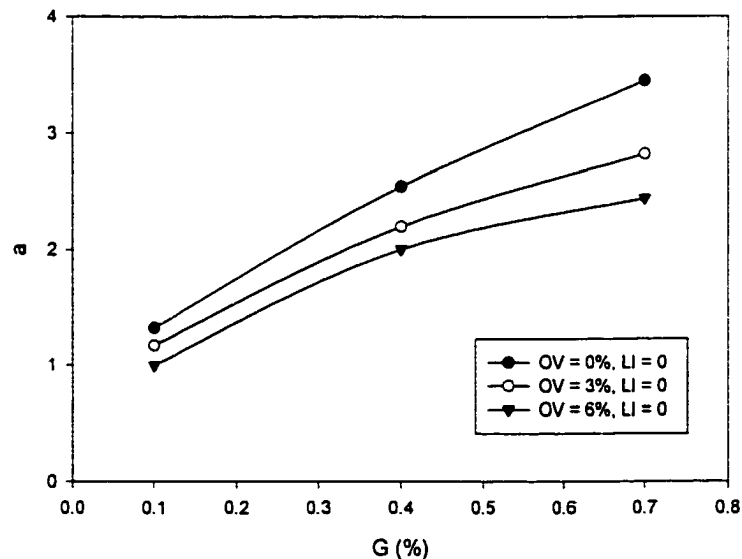
a.   on intercept factor a (LI = 0)

Figure 8.2   Effect of G on Coefficients a and m
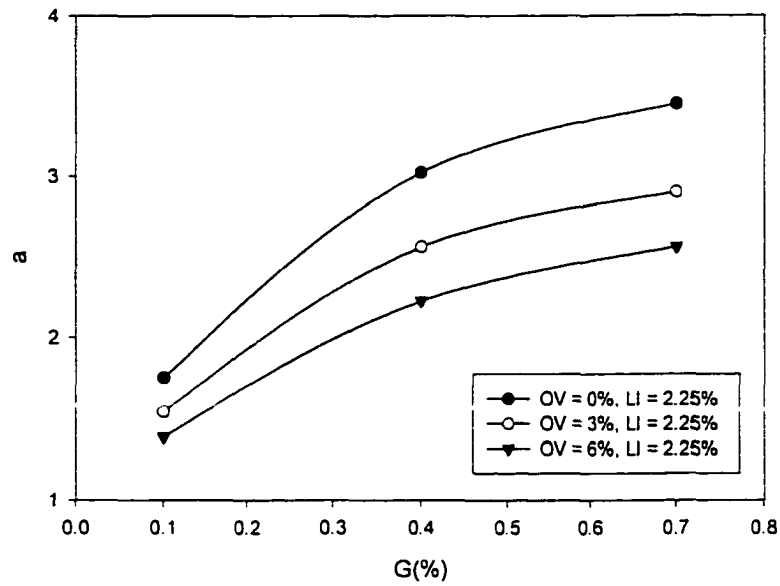
b. on intercept factor a (LI = 2.25%)
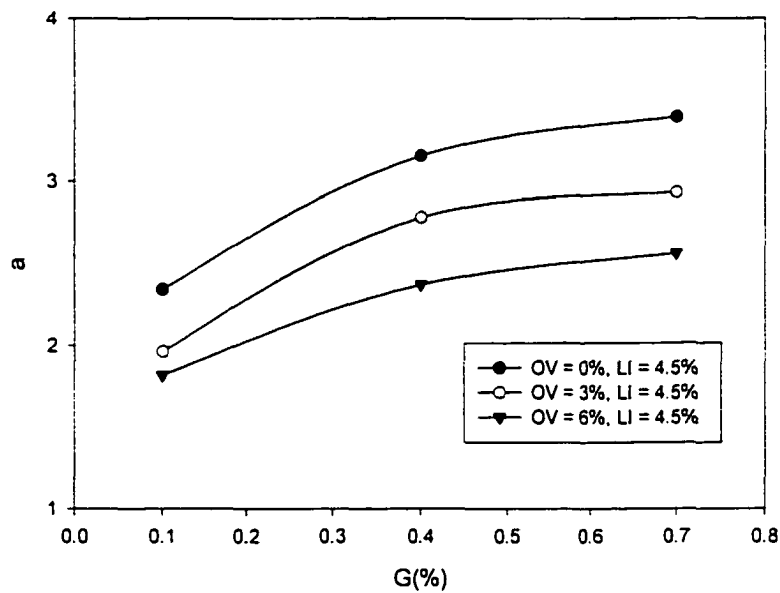
c. on intercept factor a (LI = 4.5%)

Figure 8.2   Effect of G on Coefficients a and m (cont'd)
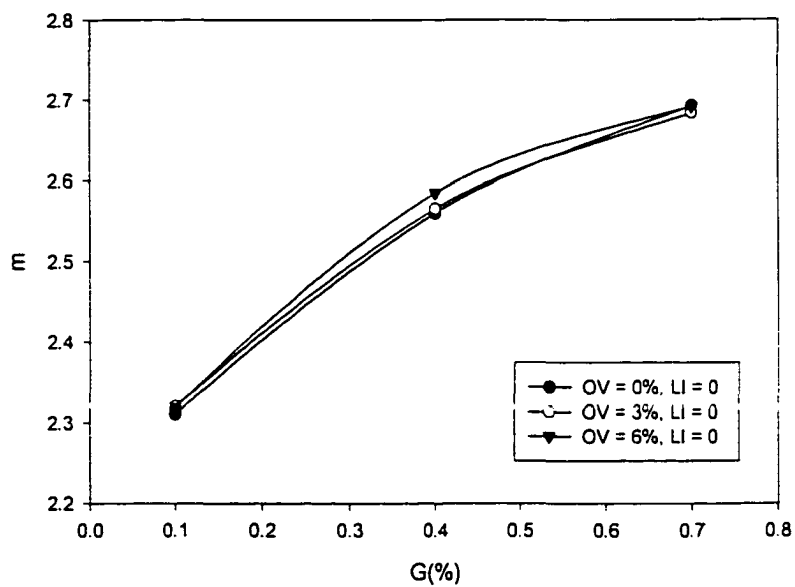
d. on intercept factor m (LI = 0)
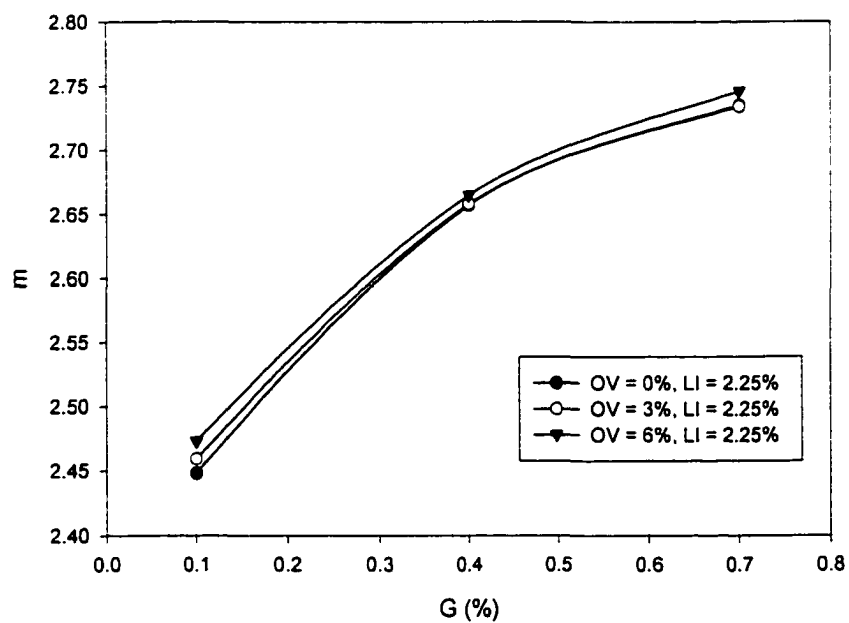
e. on intercept factor m (LI = 2.25%)

Figure 8.2 Effect of G on Coefficients *a* and *m* (cont'd)
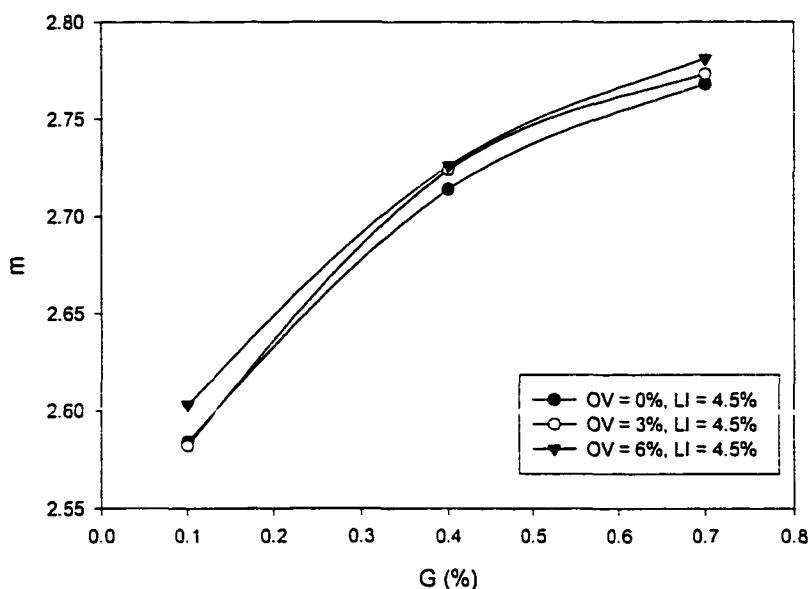
f. on intercept factor m (LI = 4.5%)

Figure 8.2   Effect of G on Coefficients *a* and *m* (cont'd)

8.3.3 Effect of Ovality

As can be seen from Figure 8.2 and Table 8.7, the slope m does not vary much for different ovality levels, meaning that the reduction factors listed in Tables 8.9-8.11 are almost independent of the DR ratio. For example, the reduction factor for a pipe with a DR of 30, a gap of 0.1% and an ovality of 6% is 0.733, which is very close to 0.729 which applies for a DR of 60, a gap of 0.1% and an ovality of 6%. An equation for the reduction factor can be written as:

$$\alpha = e^{-\frac{OV}{17}} \qquad\qquad (8.7)$$

which is a little lower than the equation proposed by El-Sawy and Moore (1997) since their model did not include the effect of gap and local imperfection.

Table 8.9 Reduction Factor Due to Ovality Based on FEA Predictions of Critical Pressure (LI = 0.0%)

Pipe type	OV = 0%			OV = 3%			OV = 6%		
	G=0.1%	G=0.4%	G=0.7%	G=0.1%	G=0.4%	G=0.7%	G=0.1%	G=0.4%	G=0.7%
DR 30	1.0	1.0	1.0	0.861	0.85	0.842	0.733	0.723	0.711
DR 45	1.0	1.0	1.0	0.854	0.849	0.847	0.727	0.714	0.713
DR 60	1.0	1.0	1.0	0.856	0.847	0.847	0.729	0.71	0.711

Table 8.10 Reduction Factor Due to Ovality Based on FEA Predictions of Critical Pressure (LI = 2.25%)

Pipe type	OV = 0%			OV = 3%			OV = 6%		
	G=0.1%	G=0.4%	G=0.7%	G=0.1%	G=0.4%	G=0.7%	G=0.1%	G=0.4%	G=0.7%
DR 30	1.0	1.0	1.0	0.851	0.846	0.842	0.73	0.718	0.715
DR 45	1.0	1.0	1.0	0.85	0.842	0.843	0.721	0.711	0.712
DR 60	1.0	1.0	1.0	0.845	0.846	0.843	0.717	0.715	0.71

Table 8.11 Reduction Factor Due to Ovality Based on FEA Predictions of Critical Pressure (LI = 4.5%)

Pipe type	OV = 0%			OV = 3%			OV = 6%		
	G=0.1%	G=0.4%	G=0.7%	G=0.1%	G=0.4%	G=0.7%	G=0.1%	G=0.4%	G=0.7%
DR 30	1.0	1.0	1.0	0.845	0.852	0.848	0.727	0.722	0.724
DR 45	1.0	1.0	1.0	0.848	0.847	0.849	0.72	0.717	0.716
DR 60	1.0	1.0	1.0	0.846	0.846	0.845	0.718	0.717	0.718
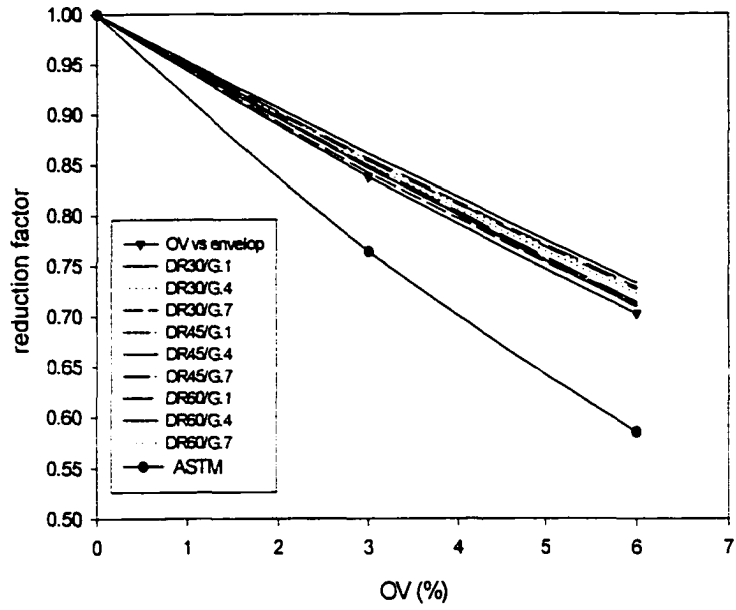
a. local imperfection LI = 0
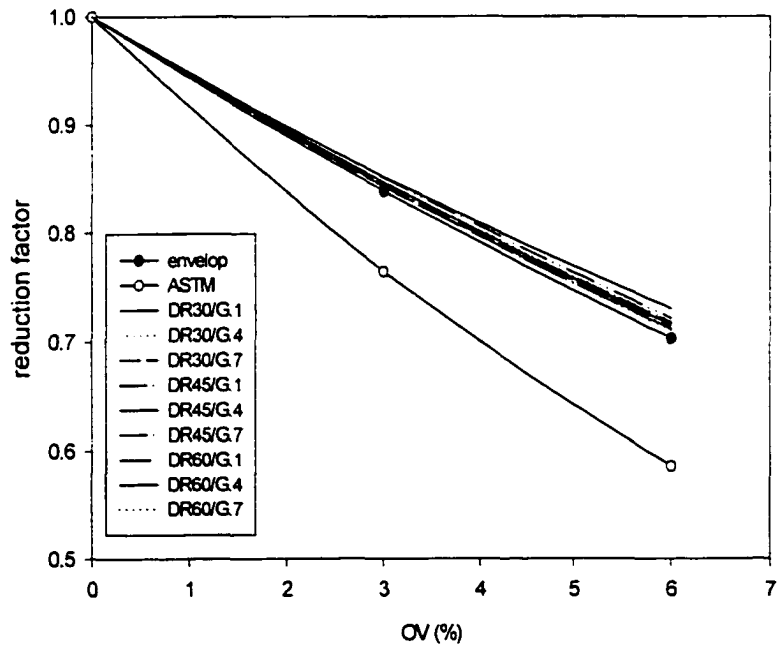
b. local imperfection LI = 2.25%

Figure 8.3   Reduction Factor Due to Pipe Ovality OV
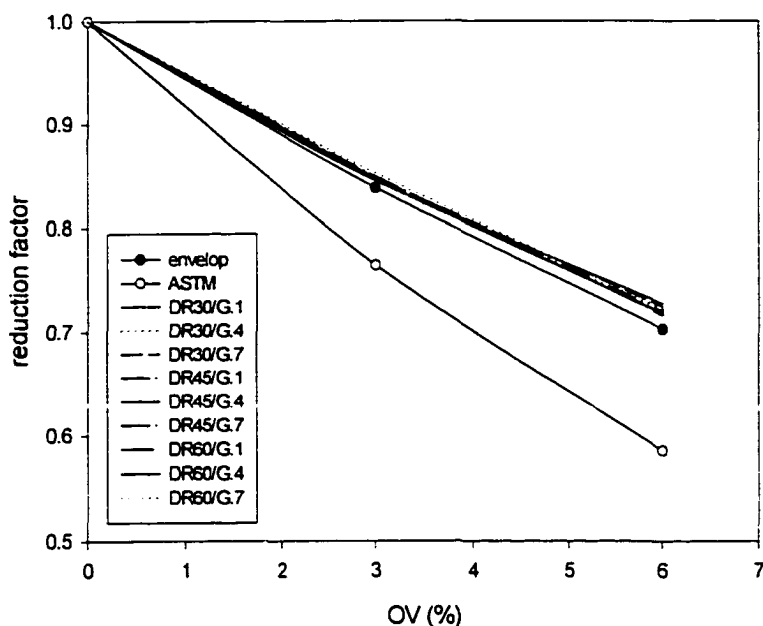
c. local imperfection LI = 4.5%

Figure 8.3 Reduction Factor Due to Pipe Ovality OV (cont'd)

8.3.4 Effect of Local Imperfection

The effect of local imperfection (when combined with DR) on the enhancement factor K is identical to Equation (8.3). The values K varies from 4.82 (for DR = 30, G = 0.1% and LI = 4.5%) to 12.594 (for DR = 90, G = 0.1% and LI = 0). The enhancement factor is reduced as the local imperfection increases. Table 8.12 also shows that reduction factor is also a function of DR. For example, the enhancement factor K for DR = 60 is reduced by almost 40%, with 4.5% of LI and 0.1% of G, while for DR = 30 is only reduced by about 24%.

Table 8.12 Predicted Enhancement Factor K Due to Effect of Local Imperfection LI

DR	LI=1.0%	LI=2.25%	LI=3.5%	LI=4.5%
30	6.31737	5.72958	5.20884	4.82197
35	6.9595	6.23846	5.60569	5.14132
40	7.56826	6.71567	5.97382	5.435
45	8.14928	7.1668	6.31854	5.70793
50	8.70671	7.59597	6.64374	5.96367
55	9.24375	8.0063	6.9523	6.20488
60	9.76291	8.40023	7.2465	6.43359
65	10.2662	8.77971	7.52811	6.65142
90	12.594	10.5074	8.79031	7.61565

8.3.5 Effect of Combination of Gap and Local Imperfection

As discussed in the previous sections, that the existing ASTM design equation for CIPP liners does not account for gap and local imperfections, and the enhancement factor K is recommended as 7 and is assumed to be independent to the DR, gap and local imperfections. But, in Table 8.13, the value of K varies from 3.74 (for DR = 30, G = 0.1% and LI = 4.5%) to 11.07 (for DR = 60, G = 0.1% and LI = 0). And, about 70% of the data in Table 8.13 is less than the value of 7 which is used in the ASTM design model. Additionally, the enhancement factor K for a liner with a DR of 60 (G = 0.1%) is reduced about 60% due to the combined effect of gap (G = 0.7%) and local imperfection (LI = 4.5%), while the enhancement factor K for a liner with a DR of 30 (G = 0.1%) is reduced about 45.6% due to the combined effect of gap (G = 0.7%) and local imperfection (LI = 4.5%).

Table 8.13   Predicted Enhancement Factor Due to Effect of Gap and Local Imperfection LI

Imperfections	DR=30	DR=40	DR=50	DR=60
G=.1%, LI=0%	6.86991	8.37595	9.76799	11.0754
G=.4%, LI=0%	5.68318	6.45007	7.11549	7.70982
G=.7%, LI=0%	4.89652	5.34864	5.7279	6.05764
G=.1%, LI=2.25%	5.72958	6.71567	7.59597	8.40023
G=.4%, LI=2.25%	4.85517	5.35869	5.78494	6.15826
G=.7%, LI=2.25%	4.25087	4.58761	4.86707	5.108
G=.1%, LI=4.5%	4.82197	5.435	5.96367	6.43359
G=.4%, LI=4.5%	4.65289	5.0519	5.38482	5.67306
G=.7%, LI=4.5%	3.73792	3.99591	4.20822	4.39004

8.4   Model Verification

The ultimate pressure predictions given in the previous section will be checked against analytical and experimental results to verify the validity of the proposed model.

8.4.1   FEA Results versus Glock's Model

A number of FEA runs were conducted for the case of G = 0, OV = 0, and LI = 0; that is, a tight-fitting, perfectly round pipe without local imperfection was used for comparison with the analytical solution given by Glock (1977). Only an elastic constitutive relation was used in the finite element runs. Figure 8.1a shows that the elastic solutions agree quite well with Glock's model, as was also observed by El-Sawy and Moore (1997). The slope of the curve (m = -2.198) and the intercept of the curve (a = 0.98) are close to the values of m = 2.2 and a = 1.0 used in Glock's model.

8.4.2 FEA Results versus Experimental Results

The latest physical test data available at TTC were used to validate the FEA results presented in earlier sections. Both the BORSF (1999) and Seemann's (2000) test data will be used. The recorded dimension ratio, ovality, and gap measurements were used to generate the parameters necessary for interpolating the predictions of ultimate pressure from the FEA results given in Figures 8.4 and 8.5. Figure 8.4 shows that most of the test data are greater than the predicted FEM results based on the average experimental measured geometric results. In Seemann's test, the average gap magnitude was around 0.45%. It can be seen that all of the test data are within the predicted critical pressure under effect of 0.1% and 0.7% gap. But most of the test data are larger than the predicted P_{cr} with average gap G = 0.45%. From the test report of Seemann, it was observed that the gap ratio increases with ovality and the buckling lobes of oval pipes always occur across the minor diameter. This could be the reason that the numerical results show better agreement with the experimental results for oval pipes than the results for round host pipes.
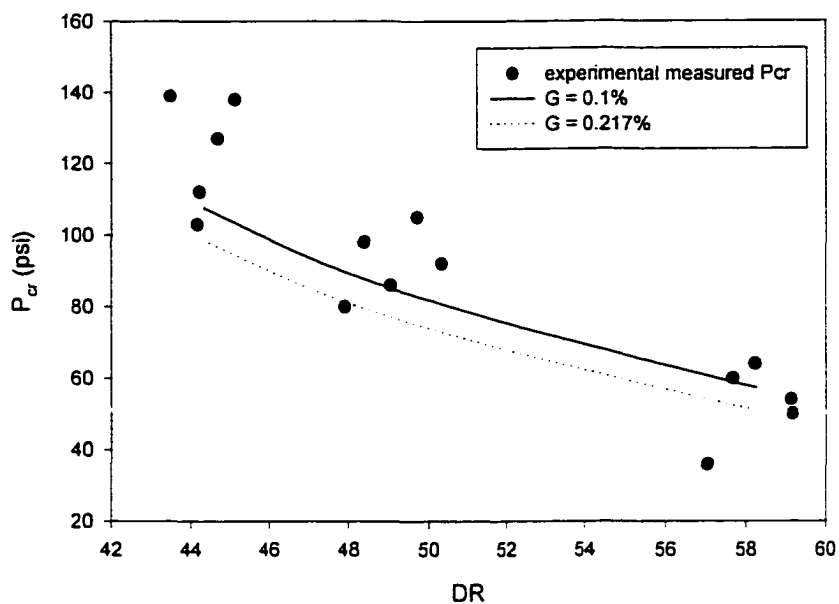
Figure 8.4   Comparison of FEA Results with BORSF Test Data
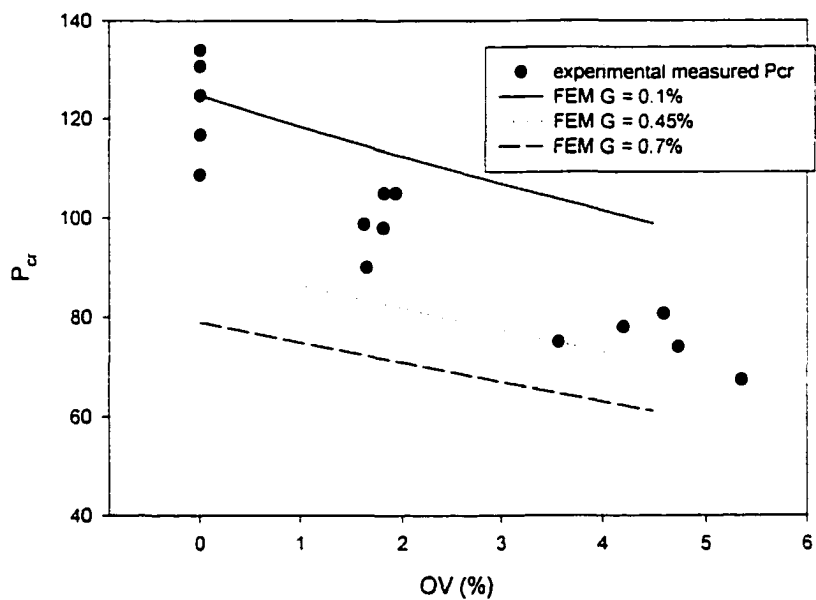
Figure 8.5   Comparison of FEA Results with Seemann's Test Data

8.5 Conclusions

The effect of geometric parameters on the accurate prediction of buckling pressures for CIPP liners was discussed in this chapter. An empirical model was used to relate the one-lobe buckling pressure to the dimension ratio (DR) of liners and to coefficients that depend on the geometric imperfections of the liner-host pipe system. These coefficients can be determined by a small number of finite element runs over a range of the geometric parameters and by numerical analysis techniques such as Lagrangian interpolation and least-squares regression.

From the results presented in this chapter, the following conclusions can be drawn:

(1) The finite element simulations reveal that accurate prediction of the buckling pressure depends heavily on knowledge of the material properties and the geometrical factors of the pipe-liner system.

(2) By using an appropriate finite element approach, the effects of gap, ovality, and local imperfection were determined. Excellent agreement between analytical and test results were found.

(3) The critical pressure at which a liner buckles may be determined by Equation (8.2). The dependency of a and m on the gap, ovality, and local imperfection was determined from finite element runs and interpolation techniques.

(4) The enhancement factor K depends on DR, gap, ovality, and local imperfections. The suggested value of K = 7 may not be suitable for design purposes. Predictions by means of the methodology presented in this paper will lead to more accurate and conservative designs.

(5) For Seemann's test data, the finite element simulations agree better with the experimental data for the oval pipes than for the round pipes.

CHAPTER 9

EFFECT OF MULTIPLE LOCAL IMPERFCTIONS

9.1 Introduction

The distribution of local wavy intrusions and thickness variations around the circumference of a liner is often random and unpredictable. These imperfections can be either symmetrically or asymmetrically distributed. The existing finite element models that have been used to model the buckling of pipe liners can only simulate the symmetric geometric case with prescribed boundary conditions. These models which include the assumption of symmetric deformation do not allow asymmetric multiple local imperfections to be modeled.

Zhao (1999) successfully simulated the transition from two-lobe deformation to one-lobe deformation using a half-symmetry finite element model. However, such two-lobe models may not always be adequate. Welch (1989) discovered a four-lobe deformation mode in his experiments, which cannot be simulated by Zhao's model or any other reported liner buckling finite element model. Consequently, it is constructive to set up a new model that can determine the influence of all types of geometric imperfections on liner response and buckling in a natural way.

The ABAQUS *viscous damping* command can be used overcome the convergence difficulties due to the sudden violation of contact constraints by allowing a viscous

pressure to be transmitted between the contact surfaces as they come into contact or separate. A model which incorporates this ABAQUS command will be employed in this chapter to study the deflection evolution, critical pressure and critical times for liners with symmetric and asymmetric imperfection distributions.

9.2 Deformation Mode of Liner Buckling

Experimental results indicate that encased liners typically deform in a two-lobe mode and collapse in a one-lobe mode. The mode of deformation is strongly related to the geometry of the pipe-liner system, which includes the gap distribution, ovality, local imperfections, and uneven distributed material properties. The deformation mode controls the evolution of stresses and displacements around the circumference of the liner, thereby having a direct effect on the buckling pressure and buckling time of the liner. Higher deformation modes (more lobes) are associated with higher critical pressures and buckling times under the same external pressure. In this section, the emphasis is placed on the effect of multiple local imperfections on the liner buckling mode. A better understanding of the mechanisms of liner buckling will give a solid base for understanding the effect of multiple local imperfections on the critical pressure and time.

9.2.1 Deformation Modes for Perfectly Round Pipes

The geometry of a pipe containing imperfections is shown in Figure 9.1. When a pipe is perfectly round, the deformation mode strongly depends on the gap and distribution of local imperfections. Figure 9.2 shows the deformation history for a liner with four thickness imperfections (located at $\phi = 0°$, $90°$, $180°$, and $270°$) with no

liner/host pipe friction and an evenly distributed gap. As shown, the encased liner initially deforms into four lobes, then transforms to a two-lobe mode, and finally buckles in a one-lobe mode. The thicknesses at the four points are different (2.5% reduction in thickness for $\phi = 0°$, 2.5% for $\phi = 90°$, 5% for $\phi = 180°$, and 3% for $\phi = 270°$), and final buckling occurs at the thinnest location. However, the liner will not necessarily buckle at the thinnest point when the gap is unevenly distributed. The gap will influence the mode transition, and the liner will buckle at the thinner point with larger gap.
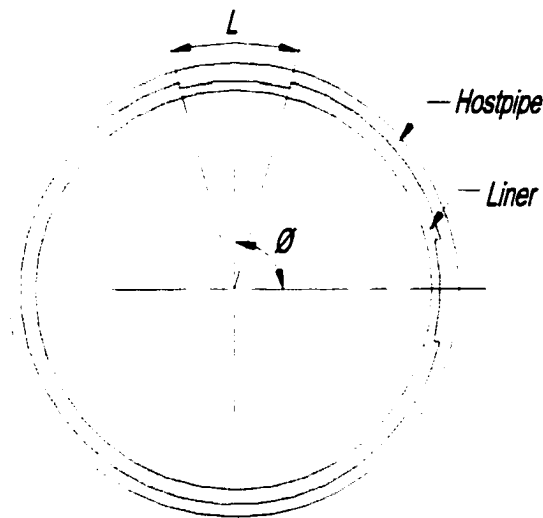
Figure 9.1   Geometry for Multiple Local Imperfection Study.
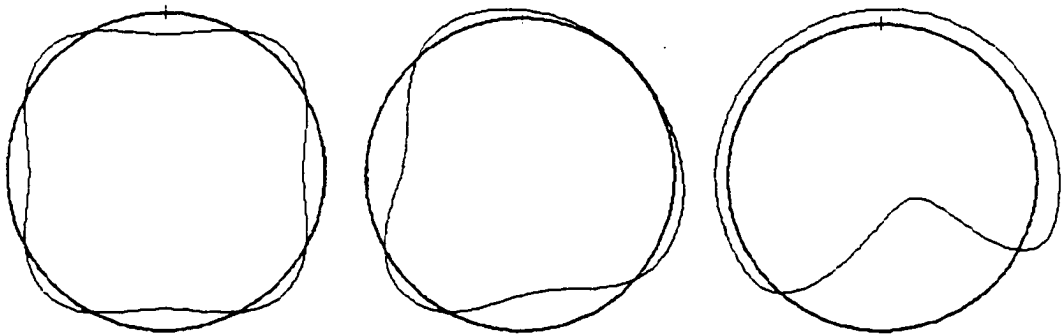
Figure 9.2   Deformation Mode Transition under the Effect of Thickness Variation

9.2.2 Deformation Modes for Oval Pipes

Liners installed in oval host pipes usually deform in a two-lobe mode regardless of the distribution of geometrical parameters. As the level of deformation increases, the lobe with larger deflection will eventually become unstable, resulting in buckling of that lobe. Since existing host pipes commonly have ovalities of 2% to 5%, two-lobe deformation histories are believed to be applicable in field applications. However, any bonding of the liner to the host pipe due to locking or migration of resin into the host pipe could substantially influence this distribution.

9.3 Liner Buckling in Short-term and Long-term Loading

Three types of imperfection combinations were studied for a round pipe with a diameter to thickness ratio of 40, a gap of 0.4% and an ovality of 3%. First, the simultaneous effect of two wavy intrusion imperfections was modeled, where the angle between the two imperfections was taken as 10, 45, and 80 degrees, as listed in Table 9.1. This set of finite element runs was then repeated for thickness imperfections. Finally, an asymmetric case was modeled in which a wavy imperfection is combined with a thickness imperfection. Both short- and long-term analyses were conducted for these geometries, and the coefficient of static friction between the host pipe and liner was taken as 0.2 for these runs.

Table 9.1 Location of Imperfections in Finite Element Models

	Angle Φ_1	Angle Φ_2	Angle Φ_3
Thickness Variation	10	45	80
Local Imperfections	10	45	80
Thickness Variation & Local Imperfections	10	45	80

Note: All local imperfections have a fixed length ratio of $S = \dfrac{L}{\pi \cdot R} = 0.05$ and a fixed

intrusion ratio of $\dfrac{\Delta_0}{D} = 2.25\%$. All thickness variation have fixed length ratio of $S = 0.05$

and a fixed thickness ratio of $\dfrac{t_0}{t} = 0.9$, where t is the average thickness of liner and t_0 is

thinner thickness.

The effect of the multiple local imperfections on short- and long-term liner

buckling as defined in Table 9.1 is given in Table 9.2. Here, the buckling pressures have

been normalized with respect to the buckling pressure for a perfect pipe with same DR,

gap, ovality, and material properties, which turns out to be 87.1 psi for the geometry

modeled. The buckling times in Table 9.2 have been normalized using a critical time of

100 years, which corresponds to the critical time for a perfect pipe with the same

geometry and material properties under 30% of Pcr (0.3 × 87.1 psi = 26.13 psi).

The pairs of normalized buckling pressures and times given in Table 9.2 are

plotted in Figures 9.3 through 9.5. The common thread in all three of these plots is the

dramatic reduction in the buckling time ratio when compared to the buckling pressure

ratio. Also notice that as the distance between the local imperfections increases (e.g., the

angle is increased), the reduction in buckling pressure or time relative to a perfect pipe

factor will decrease. Local imperfections have more impact on the critical pressures and

times than thickness variations in this study because the amplitude of the local imperfection is larger than the thickness variation.

The viscous damping model can also be used study the effect of measured thickness variations on liner response. Stokeld (1999) recorded 24 thickness measurements at even increments around the circumference of a CIPP liner at 7 different locations along the length. These thickness measurements were embedded into a two-dimensional finite element model to simulate the effect thickness variation on the critical pressure and buckling time. Figure 9.6 shows the results of these simulations. Notice that the same trend noticed in Figures 9.3 through 9.5 also apply here: the reduction of critical pressure due to imperfections is amplified when considering long-term liner behavior. This can be used to partially explain why there is more scatter in long-term liner buckling times than in short-term liner buckling pressures. Note that because Figures 9.3 through 9.6 are based on two-dimensional analyses, all of the imperfections are assumed to be infinitely long. Experimental observations show that imperfections that are "short" in the longitudinal direction may have little effect on liner buckling behavior.

Table 9.2   FEA Results for Short-term and Long-term Buckling

	P_{cr} (psi) Angle1	P_{cr} (psi) Angle2	P_{cr} (psi) Angle3	T_{cr} (yrs) Angle1	T_{cr} (yrs) Angle2	T_{cr} (yrs) Angle3
Thickness Variations	74.8	77.6	78.5	33.2	44.5	47.3
Local Imperfections	58.9	60.5	65.4	3.1	4.6	7.9
Thickness Variations & Local Imperfections	63.6	65.7	66.1	6.5	7.9	8.4
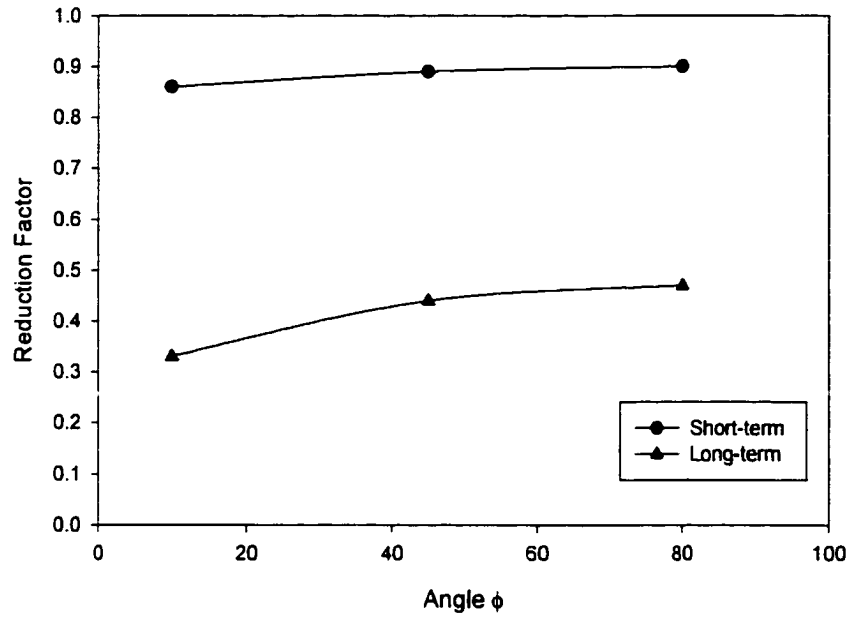
Figure 9.3   Effect of Thickness Variation on Liner Buckling
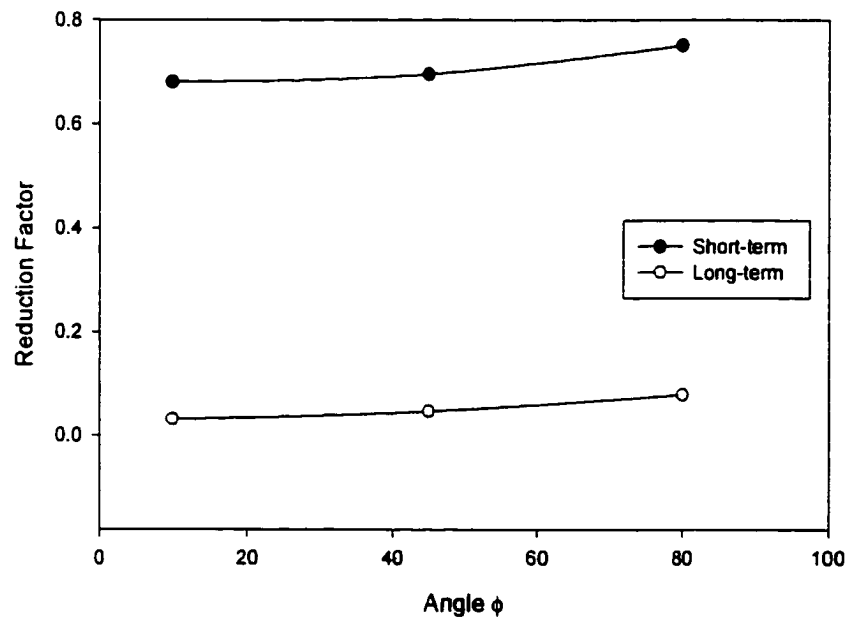
Figure 9.4   Effect of Local Imperfection on Liner Buckling
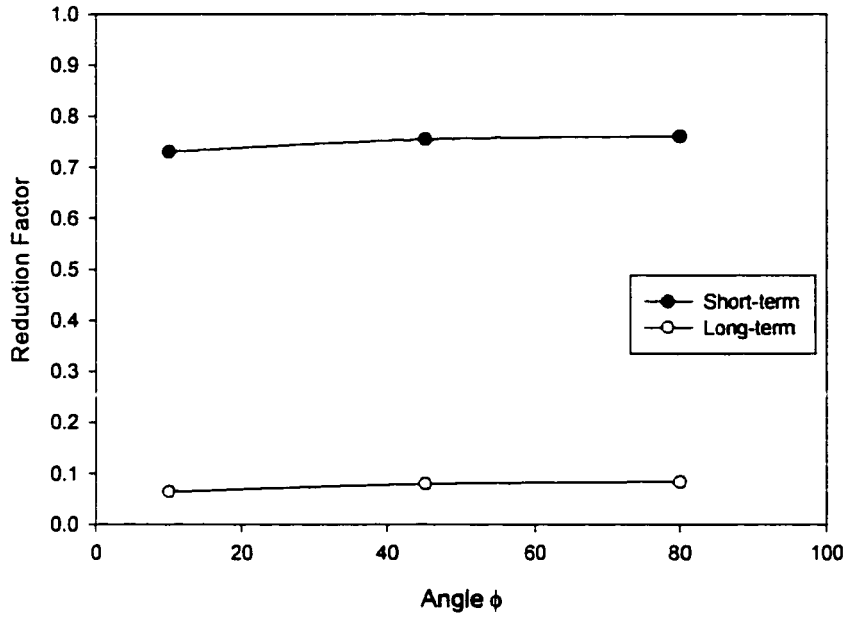
Figure 9.5   Effect of Local Imperfections and Thickness Variations on Liner Buckling
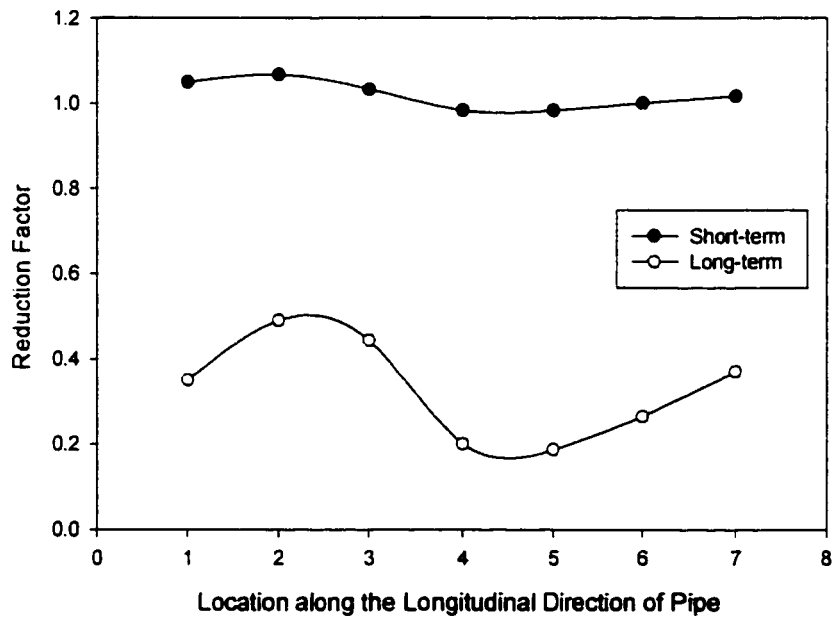
Figure 9.6   Effect of Thickness Variation on Liner Buckling Based on Thickness Measurements for 12 Inch Diameter Host Pipes Lined with CIPP Liners NOTE: This Plot Applies Thickness Variations of Infinite Length

9.4 Conclusions

The deformation mode which develops in an encased liner is influenced by local imperfections, especially for round pipe host pipes. For oval host-pipes, the liner usually deforms in a two-lobe manner, which is followed by single-lobe collapse. As the distance between the local imperfections decreases, the corresponding reduction in the critical pressure or time with respect to a pipe with no local imperfections is increased. Any reduction in the short-term buckling pressure due to local imperfections will be dramatically amplified when liners are subjected to long-term loading.

CHAPTER 10

CONCLUSIONS AND RECOMMENDATIONS

In the present study, the creep-induced liner-buckling problem has been investigated by means of finite element simulation, with emphasis on:

(a) simulation and analysis of experimental buckling results;

(b) stress evolution in for short- and long-term loading;

(c) the effect of contact forces on stress evolution;

(d) analysis of the minimum pipe length-to-diameter ratio for liner buckling specimens;

(e) short-term buckling models accounting for DR, gap, ovality and intrusions; and

(f) the effect of multiple local imperfections on liner buckling.

Conclusions for each of these topics are given below.

10.1 Test Simulation and Analysis

The ABAQUS finite element package was used to simulate the short-term liner buckling results of Seemann (2000) and the BORSF long-term buckling results of Hall et. al (2000), resulting in the following conclusions:

149

(1) Overlooking the effects of imperfections may result in system lifetimes much shorter than predicted when groundwater loading is a significant fraction of P_{cr}..

(2) Unaccounted-for factors which produce scatter in short-term buckling pressures may result in amplified scatter in long-term buckling times, where the amplification increases dramatically as the external pressure level approaches the critical pressure.

(3) Both the short- and long-term finite element models can effectively predict the liner buckling resistance for a given pressure when based on appropriate material properties and liner configurations. The finite element results appear to give conservative estimates of liner buckling pressure and lifetime.

(4) The long-term model suggested by Zhao (1999) as described in Equation (4.2) has a good agreement with finite element results.

10.2 The Effect of Contact on Pipe-Liner Systems

Short-term liner buckling simulations were completed for a variety of DRs, ovalities and gaps to examine their influence on the evolution of contact conditions, deflections and stresses, resulting in the following conclusions:

(1) The larger contact force and area associated with thinner liners is associated with the higher enhancement factors (K) that have been observed experimentally. The larger contact area for thinner liners results in a shorter span for the lobe, thus decreasing deflections and stresses and increasing the buckling pressure.

(2) The contact force results in a reverse moment that decreases the stress level at the lobe, especially prior to the time that inverse curvature at the lobe is formed.

(3) Gap appears to result in larger decreases in the critical pressure than ovality for conditions likely to be experienced in the field, since the available contact area decreases more significantly with increasing gap.

(4) The stress state across the wall of a liner can be decomposed into flexural and compressive components, and the ratio of these stresses determines the dominance of either flexural or compressive stresses.

(5) The flexural to compressive stress ratio increases with increasing DR, ovality and gap.

(6) Flexural stress is dominant at the time of buckling for short-term tests, indicating that flexural material properties should be used for short-term buckling predictions.

10.3 Stress Evolution

Finite element simulations of the evolving stress states under long-term loading were completed for various DRs, ovalities, gaps and material creep constant, resulting in the following conclusions:

(1) When the flexural stress to compressive stress ratio is less than or equal to 2, inverse curvature has not yet occurred at the lobes, and the liners behaves more like an arch than a beam.

(2) When the flexural stress to compressive stress ratio is less than or equal to 2, a compressive stress state exists over 75% of the cross section at the critical point.

(3) For most liners, the flexural to compressive stress ratio is less than 2 over the 50-year design life when the external pressure is less than 30% of the critical pressure,

indicating that compressive material properties are most appropriate for design calculations.

(4) By choosing an appropriate DR during design, such that the groundwater pressure is less than 30% of the critical pressure, inverse curvature and buckling can be prevented during the first 50 years of a liner's life.

(5) If a liner forms inverse curvature within 50 years, it will buckle within 100 years. The deformation, contact force, and flexural stress will increase much faster after the formation of inverse curvature.

(6) It is common to find significant stress relaxation at the critical point of a liner when the external pressure is small. When the rate of stress relaxation can no longer keep pace with the rate of stress increase due to inward radial deflections, the formation of inverse curvature and buckling is imminent.

10.4 The Critical Length of Liner Specimens

Two and three dimensional finite element simulations were completed to examine the influence of host pipe length on the liner buckling pressure, resulting in the following conclusions:

(1) Three-dimensional finite element results for a liner with clamped ends show that end effects become unimportant after length to diameter (L/D) ratios of approximately 5.

(2) Since L/D values of six or more were used for all liner buckling tests at the TTC, with the location of buckling varying along the length and frequently occurring near a clamped end, the clamped ends used in the liner buckling tests at the TTC are believed to result in conservative estimates of the critical buckling pressure.

10.5 Short-term Liner Buckling Design Model

The short-term liner buckling model of Zhao (1999) was extended to include intrusion imperfections, resulting in a model that incorporates the fully coupled effects of DR, ovality, gap, and imperfections on short-term liner buckling. The model uses least squares fitting and Lagrangian interpolation to relate the results of a relatively small number of finite element runs to accurately predict liner buckling over the range of the geometric parameters. The enhancement factor K was shown to depend on DR, gap, ovality, and local imperfections. The suggested value of K of 7 in ASTM F1216 may not be suitable for design purposes.

10.6 The Effect of Multiple Local Imperfections

The deformation mode which develops in encased liners is influenced by local imperfections, especially for round pipe host pipes. For oval host-pipes, the liner usually deforms in a two-lobe manner, which is followed by single-lobe collapse. As the circumferential distance between the local imperfections increased, the corresponding reduction in the critical pressure or time with respect to a pipe with no local imperfections is increased. Any reduction in the short-term buckling pressure due to local imperfections will be dramatically amplified when liners are subjected to long-term loading.

10.7 Recommendations for Future Studies

The implications of short-term and long-term liner buckling simulations on liner buckling experiments and on liner design were explored in this thesis. Recommendations for further study are given below:

(1) The two dimensional solutions presented for intrusion and thickness imperfections apply only to imperfections of infinite length. Three dimensional finite element analyses should be completed to explore the effect of imperfection length on liner behavior.

(2) The end conditions in liner buckling experiments apparently lower the buckling pressure. Three-dimensional finite element simulations of the end conditions should be completed to understand the origin of this decrease in critical pressure.

(3) The finite element simulations presented here were completed for a homogeneous and isotropic material. Numerical experimentation to examine the influence of fibers or other composite structures on liner behavior should be completed to point the way to the development of more advanced and economical liner systems.

(4) No closed form long-term liner buckling models which incorporate measured long-term material properties exist. Finite element simulations should be completed to link liner geometry and the creep properties determined from creep deformation testing to the lifetime of a liner.

(5) The numerical model presented in this paper accounts only for permanent creep deformation with no possibility of strain recovery when the stresses are relaxed. A constitutive relation incorporating both creep and recovery should be embedded into the finite element model.

(6) Present liner buckling studies are all based on the assumption that the deformation mode of an encased liner is either one-lobe or two-lobe. Experimental results indicate a two-lobe deformation history followed by single lobe collapse. Long-term liner buckling simulations to predict the possible transition from two-lobe to one-lobe should be completed.

APPENDIX A

RELATED LINER BUCKLING TEST RESULTS

APPENDIX A

RELATED LINER BUCKLING TEST RESULTS

Table A-1   Short-Term Buckling Test Summary (BORSF)

Name	Thickness (in)	ID (in)	Mean Diameter (in)	OD (in)	SDR	Buckling Pressure (psi)
8" Diameter 4.5 mm Liners						
A	0.1478	7.6835	7.8313	7.9792	53.9741	80
B	0.1507	7.6670	7.8177	7.9683	52.8872	86
C	0.1497	7.6965	7.8462	7.9958	53.4243	80
D	0.1455	7.6265	7.7720	7.9175	54.4158	88
E	0.1537	7.7095	7.8632	8.0168	52.1703	78
AVG	0.1495	7.6766	7.8261	7.9755	53.3743	82.4
8" Diameter 5.0 mm Liners						
A	0.1602	7.6335	7.7937	7.9538	49.6597	92
B	0.1622	7.5805	7.7427	7.9048	48.7451	105
C	0.1652	7.6465	7.8117	7.9768	48.2957	110
D	0.1592	7.6785	7.8377	7.9968	50.2419	115
E	0.1587	7.6475	7.8062	7.9648	50.1985	112
AVG	0.1611	7.6373	7.7984	7.9594	49.4282	106.8
8" Diameter 5.5 mm Liners						
A	0.1822	7.6120	7.7942	7.9763	43.7859	113
B	0.1763	7.6550	7.8313	8.0077	45.4121	115
C	0.1755	7.6145	7.7900	7.9655	45.3875	133
D	0.1742	7.6180	7.7922	7.9663	45.7397	115
E	0.1770	7.5960	7.7730	7.9600	44.9153	113
AVG	0.1770	7.6191	7.7961	7.9732	45.0481	117.8

157

Table A-1 Short-Term Buckling Test Summary (continued)

Name	Thickness (in)	ID (in)	Mean Diameter (in)	OD (in)	SDR	Buckling Pressure (psi)
12" Diameter 5.5 mm Liners						
A	0.2	11.4435	11.6435	11.8435	59.2175	64
B	0.202	11.4480	11.65	11.852	58.6733	60
C	0.1972	11.4585	11.6557	11.8528	60.1158	54
D	0.1973	11.477	11.6743	11.8717	60.1605	50
E	0.2048	11.476	11.6808	11.8857	58.026	36
AVG	0.2003	11.4606	11.6609	11.8611	59.2386	52.8
12" Diameter 6.5 mm Liners						
A	0.2437	11.429	11.6727	11.9163	48.9042	80
B	0.238	11.434	11.672	11.91	50.042	86
C	0.2317	11.4265	11.6582	11.8898	51.323	92
D	0.2348	11.4335	11.6683	11.9032	50.6877	105
E	0.2408	11.4085	11.6493	11.8902	49.3709	98
AVG	0.2378	11.4263	11.6641	11.9019	50.0656	92.2
12" Diameter 7.5 mm Liners						
A	0.2588	11.4180	11.6768	11.9357	46.1133	138
B	0.2612	11.4045	11.6657	11.9268	45.6675	127
C	0.2633	11.36	11.6233	11.8867	45.1392	103
D	0.2623	11.3315	11.5938	11.8562	45.195	112
E	0.2665	11.3195	11.5860	11.8525	44.4747	139
AVG	0.2624	11.3667	11.6291	11.8916	45.318	123.8

Table A-2 Material Flexural Modulus Summary (BORSF)

Pipe Type	1255 (psi)	1265 (psi)	1275 (psi)	845 (psi)	850 (psi)	855 (psi)
F1	453030	540810	423910	370660	477920	385090
F2	449800	385570	523610	390620	589100	427030
F3	462040	488240	493080	415280	490340	537480
F4	429780	502280	457530	380650	533230	330960
F5	497520	478420	536530	450080	510090	476250
AVG	459210	476090	486950	400640	477920	385090

Table A-3   Material Tensile Modulus Summary (BORSF)

Pipe Type	1255 (ksi)	1265 (ksi)	1275 (ksi)	845 (ksi)	850 (ksi)	855 (ksi)
F1	363.1	471.7	465.2	448.5	514.8	396.4
F2	387.8	511.7	484.5	549.9	559.9	443.9
F3	500	496.9	470.5	483.4	551.6	394.3
F4	362.2	439.7	466.4	551.2	503.5	458.1
F5	503.4	476.3	401.6	510.7	424	597.1
AVG	423.3	479.26	457.64	508.74	510.76	457.96

Table A-4   Long-term Test Results Summary (BORSF)

Pipe No.	845				850				855			
	SDR	P	Time (hours)	Test Valid	SDR	P	Time (hours)	Test Valid	SDR	P	Time (hours)	Test Valid
1	55.19	39	2826.5	Good	47.59	51	2656.5	Good	44.90	56	6819.0	Bad
2	52.99	39	1051.1	Good	48.46	51	2875.5	Good	44.65	56	2012.8	Bad
3	52.99	39	51.7	Bad	49.68	51	1995.6	Good	45.42	56	1938.8	Good
4	54.44	41	4581.8	Bad	50.95	53	3831.3	Bad	44.40	58		Bad
5	56.77	41	13220.8	Bad	49.99	53	13066.0	Bad	45.16	58	942.6	Good
6	56.37	41	3449.2	Bad	47.88	53	6306.9	Bad	46.75	58	6306.9	Bad
7	54.44	43		Bad	51.28	55	147.0	Bad	46.21	60	804.6	Good
8	53.34	43	304.7	Good	47.88	55	6691.6	Bad	46.21	60	540.2	Good
9	54.07	43	22.3	Bad	51.28	55	901.5	Bad	45.42	60	880.7	Bad
10	51.28	43	13196.8	Bad	51.95	55	3424.5	Bad	45.16	60	963.3	Good
11	55.58	45	2521.4	Bad	49.68	57	488.3	Good	46.48	63	155.0	Bad
12	55.97	45	476.4	Good	47.59	57	488.8	Good	47.03	63	2711.6	Bad
13	55.19	45	419.2	Good	49.06	57	802.5	Good	46.48	63	4486.5	Bad
14	55.97	48	672.3	Good	52.64	60	219.4	Good	44.90	67	184.8	Good
15	55.97	48	881.1	Bad	50.30	60	488.8	Good	46.21	67	727.4	Good
16	54.44	48	314.1	Good	48.17	60	655.8	Good	44.90	67	15.0	Bad
17	54.81	52	25.3	Bad	46.75	64	422.0	Good	45.94	73	211.8	Good
18	55.58	52	854.3	Bad	47.03	64	629.0	Good	45.42	73	515.5	Good
19	54.44	52	209.3	Good	49.06	64	329.2	Good	45.16	73	353.9	Good
20	54.07	55	333.2	Good	48.76	70	329.2	Good	46.48	80	244.7	Good
21	53.70	55	2545.6	Bad	49.37	70	96.0	Good	46.48	80	144.3	Good
22	54.07	55	74.8	Good	50.95	70	92.7	Good	46.75	80	140.3	Good
23	52.64	58	3.0	Good	47.88	77	143.3	Good	48.17	87	46.0	Good
24	54.07	58	253.3	Good	51.95	77	210.8	Good	45.68	87	141.4	Good
25	56.37	58	8.3	Good	49.68	77	0.1	Bad	44.16	87	35.5	Good
AVG	54.59				49.43				45.78			

NOTE: All pressures are in psi.

Table A-4   Long-term Test Results Summary (Continued)

Pipe No.	1255				1265				1275			
	SDR	P	Time (hours)	Test Valid	SDR	P	Time (hours)	Test Valid	SDR	P	Time (hours)	Test Valid
1	59.20	25	3701.5	Good	50.19	41	2150.7	Good	42.75	56	7313.4	Good
2	55.86	25	1058.4	Good	48.35	41	583.7	Bad	43.53	56	3301.0	Good
3	63.63	26	8070.3	Good	49.77	43	7088.7	Good	42.45	58	10105.8	Good
4	60.40	26	4752.3	Good	48.95	43	782.0	Good	46.25	58	5415.8	Good
5	57.48	27	1198.3	Good	51.49	45	1789.4	Bad	44.02	61	406.5	Bad
6	60.71	27	503.7	Good	49.56	45	668.3	Good	43.69	61	3697.2	Good
7	60.71	27	3694.7	Bad	46.65	45	139.3	Bad	42.60	61	1827.2	Good
8	56.93	29	423.3	Good	51.05	47	692.2	Good	43.06	64	1438.1	Good
9	60.71	29	4693.3	Good	46.83	47	241.5	Good	43.86	64	2895.1	Good
10	58.62	29	2950.7	Good	50.40	47	1840.5	Good	45.36	64	1662.0	Bad
11	60.40	31	1034.5	Good	49.15	50	759.5	Good	43.06	67	1588.0	Good
12	58.33	31	2786.5	Good	47.20	50	434.4	Good	42.30	67	522.4	Good
13	61.02	31	112.8	Good	49.36	50	800.1	Good	43.86	67	2729.4	Good
14	53.36	33	453.3	Good	49.98	53	2528.8	Good	45.36	71	1619.4	Good
15	57.21	33	481.2	Good	50.19	53	794.1	Good	46.25	71	1124.4	Good
16	55.60	33	554.5	Good	49.56	53	103.6	Bad	44.85	71	965.6	Good
17	58.62	35		Bad	46.46	57	145.8	Good	43.38	75	1188.1	Good
18	58.91	35	462.0	Good	48.35	57	117.6	Good	47.35	75	1940.0	Good
19	56.39	35	285.0	Good	47.58	57	107.7	Good	40.98	75	1821.1	Good
20	58.04	37	121.2	Good	47.77	61	379.8	Good	44.18	80	41.8	Good
21	60.10	37	42.6	Good	47.02	61	31.8	Good	45.36	80	255.8	Good
22	60.10	37	82.1	Good	50.19	61	44.8	Good	41.56	80	932.8	Good
23	58.91	41	1.9	Good	48.75	66	23.2	Good	42.91	90	185.7	Good
24	58.33	41	49.2	Good	47.77	66	45.8	Good	43.22	90	99.3	Good
25	55.60	41		Bad	49.36	66	368.8	Good	42.75	90	123.8	Good
AVG	58.61				48.88				43.80			

NOTE: All pressures are in psi.

Table A-5   Material Modulus Summary (Ovality Test)

Pipe Type	Tensile		Flexural	
	5% (ksi)	0% (ksi)	5% (ksi)	0% (ksi)
F1	538	557	463.6	448.5
F2	452.6	512	452.1	497.8
F3	546.9	547	431.7	435.6
F4	474	462	484.2	448.3
F5	492.7	577.0	446.1	485.8
AVG	500.8	531.0	455.5	463.21

Table A-6   Geometry of the Test Specimens (Oval Liner Tests)

Name	Host Pipe		Calculated	volume-based		Liner		
	ID (Minor)	ID (Major)	Ovality	Gap	Gap	Thickness	Mean OD	
	(inches)	(inches)	(%)	(in^3)	(inches)	(inches)	(inches)	SDR
0% Ovality 12" Diameter Liners								
1	11.953	N/A	0	149.5	0.056	0.3077	11.842	40.46
2	11.935	N/A	0	137.3	0.051	0.2925	11.833	42.64
3	12.059	N/A	0	128.2	0.047	0.2937	11.965	42.93
4	11.958	N/A	0	N/A*	0.051	0.295	11.877	42.42
5	11.995	N/A	0	140.4	0.052	0.3017	11.891	41.48
AVG	11.980	N/A	0	138.8	0.051	0.2981	11.877	41.98
2% Ovality 12" Diameter Liners								
1	11.703	12.165	1.936	146.5	0.055	0.2957	11.825	42.13
2	11.756	12.191	1.817	140.4	0.052	0.2927	11.869	42.74
3	11.769	12.163	1.646	149.5	0.055	0.3127	11.855	39.82
4	11.742	12.129	1.621	134.3	0.050	0.3058	11.836	40.70
5	11.747	12.180	1.810	143.4	0.053	0.2812	11.857	44.54
AVG	11.743	12.166	1.766	142.8	0.053	0.2976	11.848	41.99
5% Ovality 12" Diameter Liners								
1	11.557	12.411	3.563	129.4	0.048	0.3037	11.888	41.18
2	11.403	12.499	4.585	146.5	0.054	0.2933	11.842	42.55
3	11.362	12.646	5.348	170.9	0.063	0.2908	11.877	43.07
4	11.393	12.523	4.725	152.6	0.057	0.2933	11.845	42.56
5	11.425	12.425	4.193	140.4	0.052	0.3017	11.820	41.23
AVG	11.428	12.501	4.483	147.9	0.055	0.2966	11.855	42.12

Table A-7   Geometry and Buckling Pressure for Each Specimen (Oval Liner Tests)

	specimen	SDR	computed Ovality (%)	volume-based gap (inches)	buckling pressure (psi)
0% ovality	1	40.457	0	0.056	134.0
	2	42.641	0	0.051	116.7
	3	42.930	0	0.047	124.7
	4	42.700	0	0.051	130.7
	5	41 476	0	0.052	108.7
	STD DEV	1.050	0	0.003	10.3
	AVG	42.041	0	0.051	123.0
2% ovality	1	42.127	1.94	0.055	105.0
	2	42.742	1.82	0.052	105.0
	3	39.822	1.65	0.055	90.0
	4	40.700	1.62	0.050	98.7
	5	44.542	1.81	0.053	98.0
	STD DEV	1.834	0.13	0.002	6.2
	AVG	41.987	1.77	0.053	99.3
5% ovality	1	41.178	3.56	0.048	75.0
	2	42.552	4.59	0.054	80.7
	3	43.066	5.35	0.063	67.3
	4	42.561	4.72	0.057	74.0
	5	41.229	4.19	0.052	78.0
	STD DEV	0.859	0.66	0.006	5.0
	AVG	42.117	4.48	0.055	75.0

APPENDIX B

ABAQUS INPUT FILE

163

APPENDIX B

ABAQUS INPUT FILE

```
*HEADING
(oval = 3%), (gap = 0.4%) RING BUCKLING ANALYSIS, CPE4, Long-term
*NODE,INPUT=liner1.inp
*NODE,INPUT=liner3.inp
*NODE,INPUT=liner5.inp
*Ngen,NSET=SYM1
1,4001,1000
*NGEN,NSET=sym2
161,4161,1000
*NSET,NSET=MID,GEN
2001,2161,1
*ELEMENT,TYPE=CPE4
1,1,2001,2002,2
320,320,2320,2001,1
1320,2320,4320,4001,2001
*ELGEN,ELSET=EALL
1,2,2000,1000,319,1,1
*elset,elset=eall
eall,320,1320
*ELSET,GENERATE,ELSET=LOAD
1001,1320
*elset,elset=a
160,1160
*elset,elset=b
120,1120
*elset,elset=c
80,1080
*orientation,name=or,system=cylindrical
0.,0.,0.,0.,0.,10.
3,0.
*MATERIAL ,NAME=A1
*ELASTIC
459000,0.3
*plastic
8080
```

```
*creep,law=strain
1.00788e-8,1.14585,-.76
*SOLID SECTION,MATERIAL=A1,ELSET=EALL,orientation=or
*NODE,input=hostpipe.inp
*ELEMENT,TYPE=R2D2
10001,50001,50002
*ELGEN,ELSET=HOSTPIPE
10001,320
*RIGID BODY,ELSET=HOSTPIPE,REF NODE=50001
*SURFACE DEFINITION,NAME=ASURF
load,S2
*SURFACE DEFINITION,NAME=BSURF
HOSTPIPE,spos
*CONTACT PAIR,INTERACTION=damp
ASURF,BSURF
*surface interaction,name=damp
1.
*surface behavior, viscous damping
.4,.088,.8
*BOUNDARY
50001,ENCASTRE
*RESTART,WRITE,FREQ=5
*STEP,NLGEOM,INC=1000
*STATIC
0.2,1.,1.E-20,1.E-1
*DLOAD
load,P2,26.13
*NODE PRINT,FREQ=30
U
*EL PRINT,ELSET=eall,FREQ=30
S
*contact print,slave=asurf,master=bsurf,freq=30
*contact print,slave=asurf,freq=30
CFN
*END STEP
*step,nlgeom,inc=500
*visco,cetol=1.e-4
1.e-7,52560000,1.e-30
*node print,freq=500
u
*el print,elset=eall,freq=500
s
*contact print,slave=asurf,master=bsurf,freq=500
*contact print,slave=asurf,freq=500
CFN
*end step
```

APPENDIX C

FITTING PLOTS

APPENDIX C

Fitting Plots
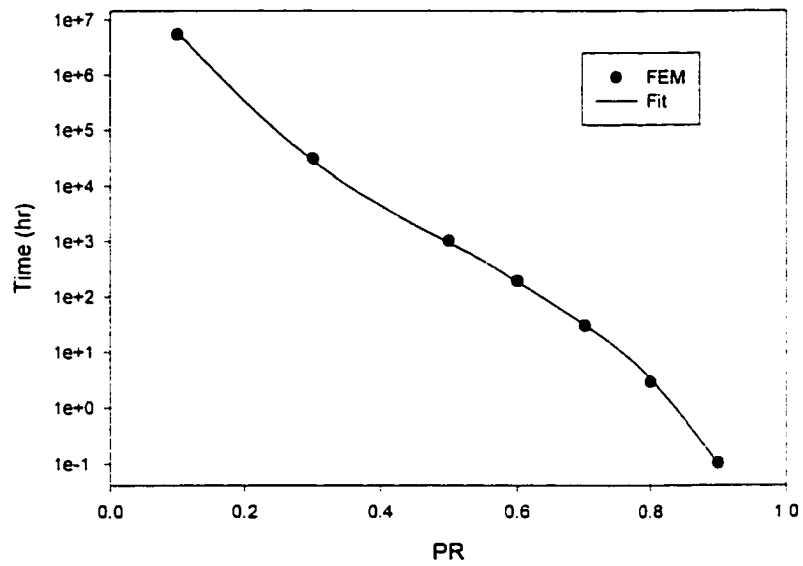
Figure C.1   Typical Critical Time Pressure Ratio Fitting Curve for Simulation of BORSF Long-term Test Results (1265 series of pipe)
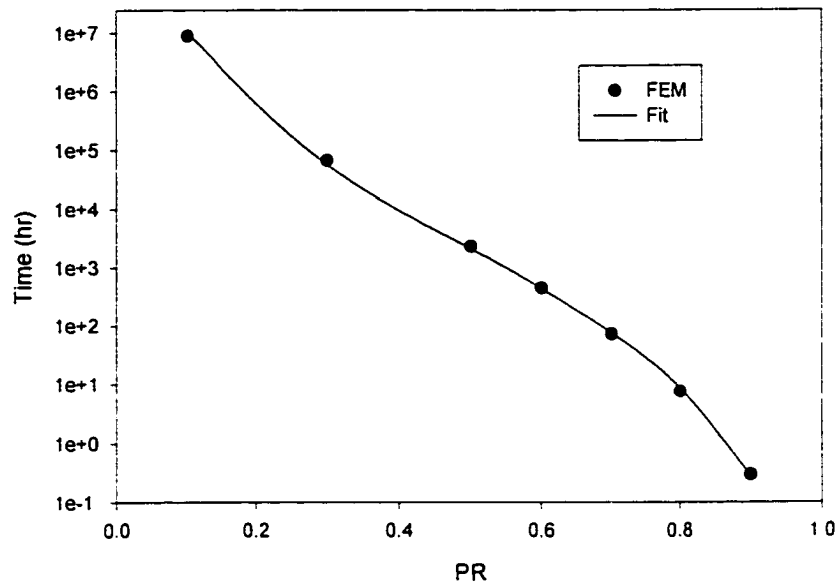
Figure C.2   Typical Critical Time Pressure Ratio Fitting Curve for Simulation of BORSF Long-term Test Results (1275 series of pipe)
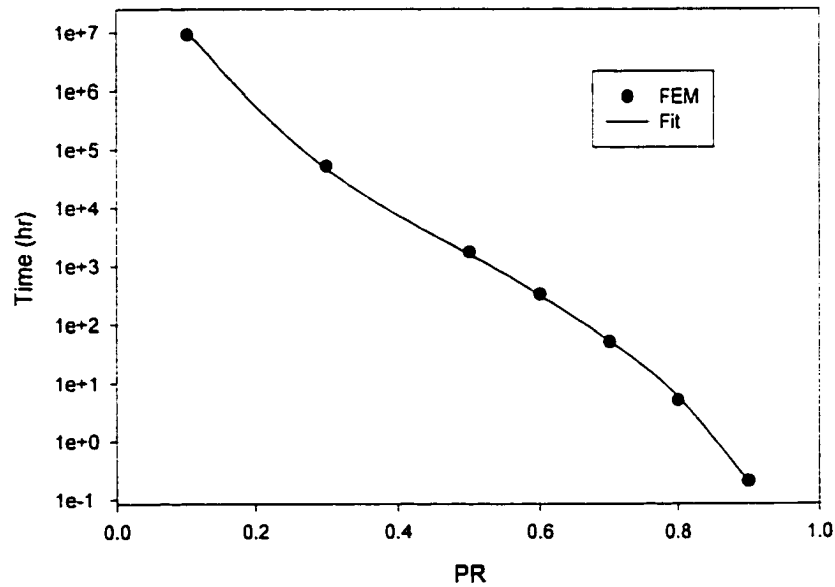
Figure C.3   Typical Critical Time Pressure Ratio Fitting Curve for Simulation of BORSF Long-term Test Results (855 series of pipe)
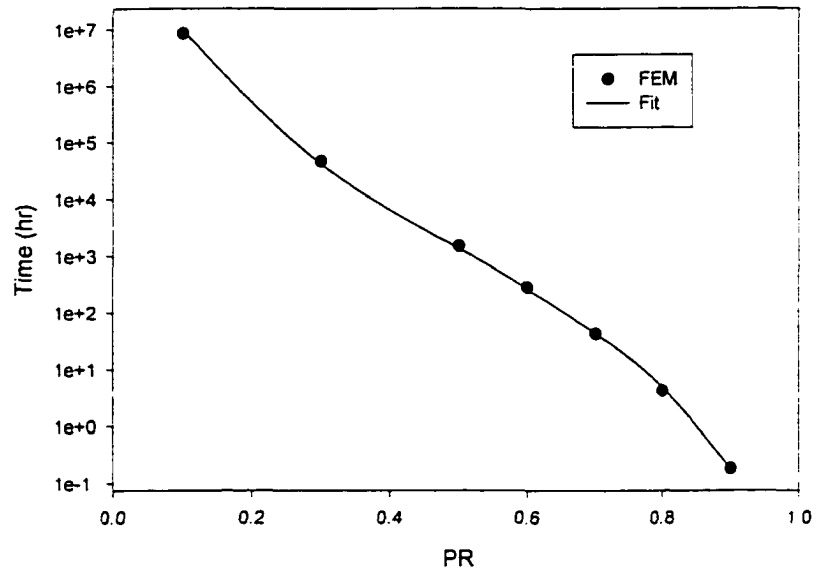
Figure C.4   Typical Critical Time Pressure Ratio Fitting Curve for Simulation of
BORSF Long-term Test Results (850 series of pipe)
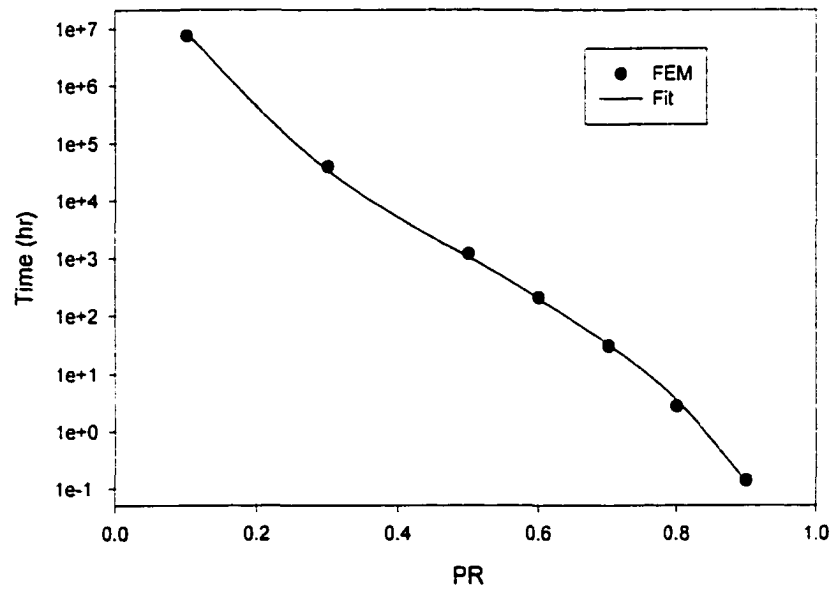
Figure C.5   Typical Critical Time Pressure Ratio Fitting Curve for Simulation of
BORSF Long-term Test Results (845 series of pipe)

REFERENCES

ABAQUS, (1998). *User's Manual*. Hibbitt, Karlsson & Sorensen, Inc.

ASTM F1216-93 (1989) *Standard Practice for Rehabilitation of Existing Pipelines and Conduits by the Inversion and Curing of a Resin-Impregnated Tube*, ASTM, Philadelphia, PA, USA.

Aggarwal, S.C. & M. J. Cooper (1984) " *External Pressure Testing of Insituform Lining,*" Internal Report

Amstutz, E. (1969). *"Das Einbeulen von Schaecht- und Stollenpanzerungen,"* Shweizeriche Bauzeitung, vol. 87, 541-549.

Bryan, G.H.(1888) *"Application of the Energy Test to the Collapse of a Long Pipe under External Pressure,"* Proceeding of the Cambridge Philosophical Society, vol. 6, 287 – 292

Carmen, A.P. (1917) *"The Collapse of Short, Thin Tubes,"* Illinois, University of Illinois Engineering Experiment Station, June, Bulletin No. 99.

Cheney, J. A. (1971) *"Buckling of Soil-Surrounded Tubes,"* ASCE Journal of the Engineering Mechanics Division, 97, EM4, 1121-1132, ASCE, USA.

Chicurel, R. (1968) *"Shrink Buckling of Thin Circular Rings,"* ASME Journal of Applied Mechanics, vol. 35, 608-610.

Cook, G. (1914) *"The collapse of Short Tubes by External Pressure,"* Philosophical Magazine, Sept, 502 – 511.

El-Sawy, K. & Moore, I. D. (1997) *"Parametric Study for Buckling of Liners: Effect of Liner Geometry and Imperfections,"* Proceedings of 1997 ASCE Conference on Trenchless Pipeline Projects, 416-423, Boston, MA, USA.

Findley, W. N. (1987) *"26-Year Creep and Recovery of Poly and Polyethylene,"* Polymer Engineering and Science, vol. 27, No. 8, 582-585, SPE.

Glock, D. (1977) *"Behavior of Liners for Rigid Pipeline Under External Water Pressure and Thermal Expansion,"* Der Stahlbau, vol. 7, 212-217.

170

Guice, L. K. (1994) *Long-Term Structural Behavior of Pipeline Rehabilitation Systems*, Trenchless Technology Center, Louisiana Tech University, Ruston, LA, USA.

Hoff, N.J. (1959) *"A Study of Creep Collapse of a Long Circular Cylindrical Shell Under Uniform External Pressure,"* Journal of the Aero/Space Sciences, 663-669.

Hoff, N.J. (1958) *"A Survey of the Theories of Creep Buckling,"* Proc. 3rd US National Congress of Applied Mechanics, Brown University, RI.

Lo, K. H. & Zhang, J. Q. (1994) *"Collapse Resistance Modeling of Encased Pipes,"* Dave Eckstein (ed.) Buried Plastic Pipe Technology: 2nd Volume, ASTM STP 1222, ASTM, Philadelphia, PA, USA.

Moore, I. (1998) *"Tests for pipe liner stability: what we can and cannot learn,"* Proceedings of North American No-Dig' 98, NASTT, Albuquerque, NM, 443-457.

Nishiguchi, I. et al (1990) *"A Simplified Method for Predicting Creep Collapse of a Tube Under External Pressure,"* Journal of Pressure Vessel Technology, vol. 112, 8, 233-239.

Omara, A.M. (1996) *Analysis of Cured-In-Place Pipes (CIPP) Installed in Circular and Oval Deteriorated Host Pipes*, D.E. Dissertation, Louisiana Tech University, Ruston, LA, USA.

Seemann, R.K., Hall, D.E. and Straughan, W.T. (2000) *"Buckling Experiments for CIPP Liners Installed in Ovalized Host Pipes,"* Trenchless Technology Center Internal Report, Louisiana Tech University, Ruston, LA.

Slocum, S.E.(1909) *"The Collapse of Tubes under External Pressure,"* Engineering, vol. 9, 35-37

Southwell, R.V. (1913) *"On the Collapse of Tubes by External Pressure,"* Philosophical Magazine, May, 687-698

Welch, A.J. (1989) *Creep Buckling of Infinitely Long Constrained Cylinders Under Hydrostatic Loading*, Ph.D. Dissertation, University of Bradford, England.

Whittle, G. L. and Schrock, B.J. (1999). *"Long-Term Moduli Values of Pipeliner Materials,"* Paper presented at a Pipe Rehabilitation Council meeting on April 20, 1999 in Seattle, Washington, 27-32.

Yamamoto, Y. & Matsubara, N. (1981) *"Buckling Strength of Steel Cylindrical Liners for Waterway Tunnels,"* Theoretical and Applied Mechanics, vol. 30, 225-235, University of Tokyo Press. Japan.

Zhao, Q. (1999) "Finite Element Simulation of Creep Buckling of Constrained CIPP Liners Subject to External Pressure," Ph.D. Dissertation, Louisiana Tech University, Ruston, LA, USA.